Applied Physics Reviews

REVIEW ARTICLE | OCTOBER 16 2020

Robust non-Pt noble metal-based nanomaterials for electrocatalytic hydrogen generation

Jie Yu; Yawen Dai; Qijiao He; ... et. al

Applied Physics Reviews 7, 041304 (2020)
https://doi.org/10.1063/5.0021578

Applied Physics Reviews REVIEW scitation.org/journal/are

Robust non-Pt noble metal-based nanomaterials for electrocatalytic hydrogen generation

Cite as: Appl. Phys. Rev. 7, 041304 (2020); doi: 10.1063/5.0021578
Submitted: 20 July 2020 · Accepted: 24 September 2020 ·
Published Online: 16 October 2020

Jie Yu,[1] Yawen Dai,[1] Qijiao He,[1] Chun Cheng,[1] Zongping Shao,[2,3,a)] and Meng Ni[1,4,a)]

AFFILIATIONS

[1]Department of Building and Real Estate, The Hong Kong Polytechnic University, Hung Hom, Kowloon, Hong Kong 999077, China
[2]State Key Laboratory of Materials-Oriented Chemical Engineering, College of Chemical Engineering, Nanjing Tech University, No. 5, Xin Mofan Road, Nanjing 210009, People's Republic of China
[3]Department of Chemical Engineering, Curtin University, Perth, Western Australia 6845, Australia
[4]Environmental Energy Research Group, Research Institute for Sustainable Urban Development (RISUD), The Hong Kong Polytechnic University, Hung Hom, Kowloon, Hong Kong 999077, China

[a)]Authors to whom correspondence should be addressed: shaozp@njtech.edu.cn and meng.ni@polyu.edu.hk

ABSTRACT

Currently, the electrocatalytic hydrogen evolution reaction (HER) has been a key point of focus for developing sustainable hydrogen economy, but it is hampered by sluggish reaction kinetics. Despite the fact that various non-noble metal-based materials as electrocatalysts toward the HER are gaining considerable attention, noble metal-based nanomaterials (NMNs) for catalyzing the HER still have advantageous features, i.e., wide pH applicability, high intrinsic activity, and good stability. Considering a high chemical similarity to HER-benchmark Pt metals, various non-Pt NMNs with high atom utilization, super efficiency, and durability for HER catalysis are engineered through various structural/electronic tailoring strategies, which has become a significant trend in this research field. Herein, a panoramic review about recent representative efforts and progress in the design of non-Pt NMNs is presented. It first introduces the HER fundamentals and then generally describes the structural and electronic characteristics of non-Pt noble metals matching the HER. Followed on, different tuning strategies for fabricating effective non-Pt NMN catalysts, including composition optimizing by constructing alloys or novel compounds, morphological tuning via decreasing the particle size or designing unique nanostructures, and hybrid engineering as well as crystalline structure/facet controlling, are systemically summarized, with a special focus on the underlying structure–activity relationship for different catalysts. The features of pH universality and bifunctionality for these non-Pt NMN catalysts are also highlighted. At the end, existing challenges and future perspectives awaiting this emerging research field are discussed.

TABLE OF CONTENTS

I. INTRODUCTION

Energy plays a crucial role in our daily life, which also drives the rapid advancement of our society. As we all know, ever since the industrial revolution, modern society has relied more and more

heavily on exhaustible fossil fuels.[1,2] It is roughly estimated that over 79.5% consumption of energy in the whole world comes from traditional fossil fuels.[3] However, fossil fuels are non-renewable and emit a lot of pollutants and greenhouse gas during their utilization. Actually, the excessive use of fossil fuels based on low-efficiency combustion technology has caused many negative effects on the earth's environment, such as the formation of haze, acid rain, and extreme climate.[3] It is well accepted that in order to realize a sustainable development of our society, clean and sustainable energy systems should be adopted. Wind, tidal, and solar energies are renewable, abundant, and carbon-neutral, which are ideal energy resources to replace traditional fossil fuels for the future.[4] However, these renewable energies are intermittent and site-specific, which hamper their wide application.[5] To reliably utilize renewable energies, effective energy storage is essential, such as electrochemical energy storage by batteries, pumped hydro-energy storage, flywheel energy storage, compressed gas energy storage, etc. However, large scale electrical energy storage using batteries is costly as large-scale batteries are needed. The pumped hydro and compressed gas storages are inexpensive, but are site-specific. Flywheel energy storage suffers from significant self-discharge and is not suitable for long-term energy storage. Alternatively, the excess renewable power can be stored as chemical energy by driving an electrolysis cell for generating hydrogen (H_2) gas, which can be converted back to electricity using a fuel cell when the renewable power is insufficient. As H_2 can be stored, transported, and converted without much difficulty, as depicted in Fig. 1, it is considered as a promising energy carrier for energy storage.[6] H_2 has the largest gravimetric energy density among various available fuels and is carbon-free.[7] Moreover, hydrogen production based on water electrolysis is also regarded as a highly clean and sustainable approach due to water as the sole starting raw material and high-purity hydrogen as the product.

In such a typical electrochemical water-splitting system, two half-cell reactions, i.e., oxygen evolution reaction (OER) at the anode and hydrogen evolution reaction (HER) at the cathode, are involved. The occurrence of these two reactions requires additional energy input to overcome the reaction energy barrier, known as a dynamic overpotential.[8,9] Certain catalysts are needed to minimize this overpotential and hence save the energy. As to the HER, considerable research studies have been conducted to develop various efficient electrocatalysts in recent years, including noble-metal nanomaterials (NMNs), transition metals (TMs), their corresponding oxides (TMOs), phosphides (TMPs), chalcogenides (TMDs), nitrides (TMNs), and carbides (TMCs), as well as metal-free composites.[10] Compared to noble metals (NMs), these transition metal-based or metal-free materials feature earth abundance, low cost, and certain electrocatalytic performances. However, they also show some inherent drawbacks, mainly of poor conductivity, limited pH applicability, low intrinsic activity, and weak durability, which can hinder their practical applications.[11–13] At least, in the near future, it is still a big challenge for the widespread application of these noble metal-free electrocatalysts in large scale water electrolysis for hydrogen production. Consequently, the noble-metal nanomaterials, with super activity and robust stability in a wide range of pH, are still the most attractive electrocatalysts for the HER to ensure an energy-efficient water-splitting procedure.

As always, platinum (Pt) is considered as the benchmark electrocatalyst for the HER in all ranges of pH, which expresses nearly zero overpotential, low Tafel slope, and superior long-term durability. With regard to other platinum-group noble metals, like Ru, Rh, Pd, and Ir, they possess a high similarity to Pt metal in chemical inertness and thus theoretically are also promising HER catalysts.[13,14] More importantly, the HER activity of Pt in basic media is approximately two or three orders of magnitude inferior to that in acidic media due to slow water-dissociation kinetics, while there is only one order of magnitude performance variation between basic and acidic solutions for other noble metals, i.e., Ru or Rh.[15] Accordingly, much attention has been paid to these non-Pt noble metal electrocatalysts with great success in the last years. Furthermore, taking the scarce reserve for noble metals into consideration concurrently, researchers mainly employed various tuning strategies to rationally design non-Pt noble metal-based nanomaterials (NMNs) with high utilization amounts of noble metals, well-exposed active sites, enhanced intrinsic activity of each active center, and excellent electronic conductivity in the past 5 years.[16–20] These tuning methods, as summarized in Fig. 2, include optimizing element composition by forming alloys or constructing novel compounds, downsizing the particle dimension to a few nanometers or developing a unique morphology, and building up hybrids with another

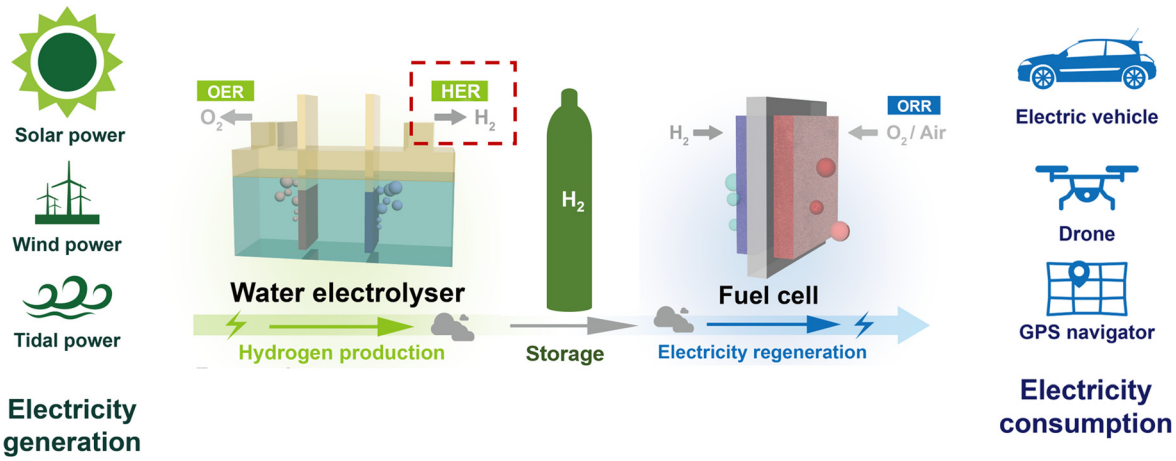

FIG. 1. An overall ideal route toward distributed power generation based on stable and sustainable hydrogen renewable energy supply.

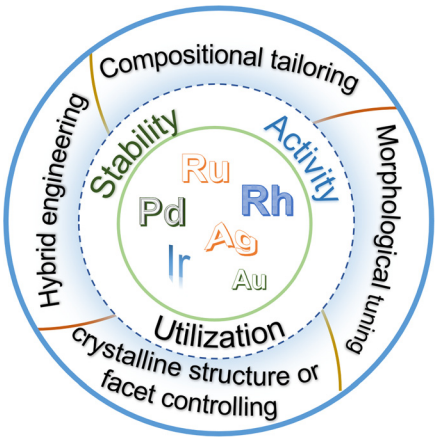

FIG. 2. Illustration of the tuning strategies for rationally designing non-Pt NMNs toward an efficient HER.

inexpensive but useful component as well as controlling crystalline structures or exposed facets. Following these substantial achievements, here we provide a comprehensive and timely summary about the recent advances in the design and synthesis of non-Pt NMNs (Ru, Rh, Pd, Ag, Ir, and Au) for HER electrocatalysis, which starts with a brief discussion on the general catalytic mechanisms of the HER and the proposed "volcano"-type plots toward electrocatalytic activity. Then, we also simply review several structural and electronic characteristics matching the HER for these non-Pt noble metals. Subsequently, fruitful achievements of non-Pt NMN catalysts in the past 5 years are introduced with a key emphasis on the state-of-the-art engineering strategies, as mentioned above, for tailoring the catalytic activity. Meanwhile, light will be shed on the underlying structure–activity relationship and mechanism. Additionally, a particular focus on these non-Pt NMN catalysts with pH universality and bifunctionality is given in the fourth section. Lastly, we propose the major challenges for the non-Pt NMN HER catalysts and offer perspectives on future research work.

II. FUNDAMENTALS OF THE HER

A. General reaction mechanisms

The HER undergoes a two-step two-electron reduction process under any pH condition, which has been suggested as three possible principal reactions.[21] In the first step, i.e., the electrochemical adsorption/reduction process (the Volmer reaction), a proton adsorbed on the electrode material surface couples with an electron to form an adsorbed hydrogen intermediate (H_{ads}) [Eqs. (1) and (2)]. With different electrolytes, the proton exists in different forms. Hydrogen ions (H^+) work as the proton source in acid, while the protons stem from the cleaving of H–O–H bonds in basic solution.

Volmer reaction:

$$H^+ + e^- \rightarrow H_{ads} \ (\text{in acidic media}), \quad (1)$$

$$H_2O + e^- \rightarrow H_{ads} + OH^- \ (\text{in neutral or basic media}). \quad (2)$$

Subsequently, the second step shows two different pathways for the production of H_2 molecules. One is known as the Heyrovsky reaction, which occurs at low H_{ads} coverage. In this way, an as-formed H_{ads} species combines with another proton and a new electron to evolve H_2 [Eqs. (3) and (4)].

Heyrovsky reaction:

$$H^+ + H_{ads} + e^- \rightarrow H_2 \ (\text{in acidic media}), \quad (3)$$

$$H_2O + H_{ads} + e^- \rightarrow H_2 + OH^- \ (\text{in neutral or basic media}). \quad (4)$$

However, when the coverage of H_{ads} is relatively high, two adjacent H_{ads} species prefer to directly react with each other to give a H_2 molecule, which is named as the Tafel reaction [Eq. (5)].

Tafel reaction:

$$H_{ads} + H_{ads} \rightarrow H_2 \ (\text{in pH} - \text{universal media}). \quad (5)$$

Theoretically, a Tafel slope, attained by experimental results, can suggest the dominant reaction mechanism during a HER process.[21] When a Tafel slope of 118 mV dec^{-1} is observed, the rate-determining step is the electrochemical adsorption/reduction step and the corresponding mechanism is called the Volmer mechanism. If the Tafel value is 39 or 28 mV dec^{-1}, the first step is fast and the Heyrovsky or Tafel reaction is the rate-determining step, respectively, corresponding to the Volmer–Heyrovsky or Volmer–Tafel mechanism, respectively.

B. Proposed volcano-type curves

Electrochemical hydrogen adsorption and desorption on the active sites of the material surface essentially belong to a couple of competitive reactions. Thus, a suitable bonding strength, neither too weak nor too strong, between catalysts and hydrogen species is of critical significance for a desired HER catalyst. From a physicochemical point of view, the free energy of hydrogen adsorption (ΔG_{H^*}) can synchronously disclose both the abilities of H_{ads} adsorption and H_2 desorption during a HER process.[22] Based on the well-acknowledged Sabatier principle, ideally, the largest HER j_0 (j_0 refers to the exchange current density) can be achieved at $\Delta G_{H^*} = 0$.[23] Later, a volcano model was built up by correlating the j_0 value with ΔG_{H^*} obtained from the quantum chemistry. In this model, ΔG_{H^*} equals to zero at the peak point of the volcano. The positive or negative ΔG_{H^*} values, respectively, mean too weak or too strong adsorption of H_{ads} on the catalyst surface, thus contributing to a weakened HER performance, i.e., a decreased j_0 [Fig. 3(a)].[24] Furthermore, Trasatti *et al.* proposed a similar volcano-like curve to associate the log j_0 values to the metal–hydrogen (M–H) bond energy, as described in Fig. 3(b).[25,26] Recently, with the rapid advancement of this computational science field, the updated volcano-shaped trend was presented with these experimental j_0 values as a function of the density functional theory (DFT)-derived ΔG_{H^*}, typically the one proposed by Nørskov *et al.*, as seen from Fig. 3(c).[27,28]

III. BRIEF OVERVIEW OF THE HER ELECTROCATALYSTS BASED ON NON-PT NMNs

Non-Pt noble metals with appropriate surface properties have already emerged as attractive and promising catalytic materials for their super catalytic behaviors in various chemical reactions, e.g., CO oxidation, methanol reforming/decomposition, hydrodesulfurization, OER, HER, etc.[29–33] In a catalyzing HER, the principle shown in Fig. 3 well guides the design of the electrocatalysts, which presents the observations from theoretical and experimental investigations. Remarkably, these non-Pt noble metals, mainly including Pd, Rh, and Ir, position

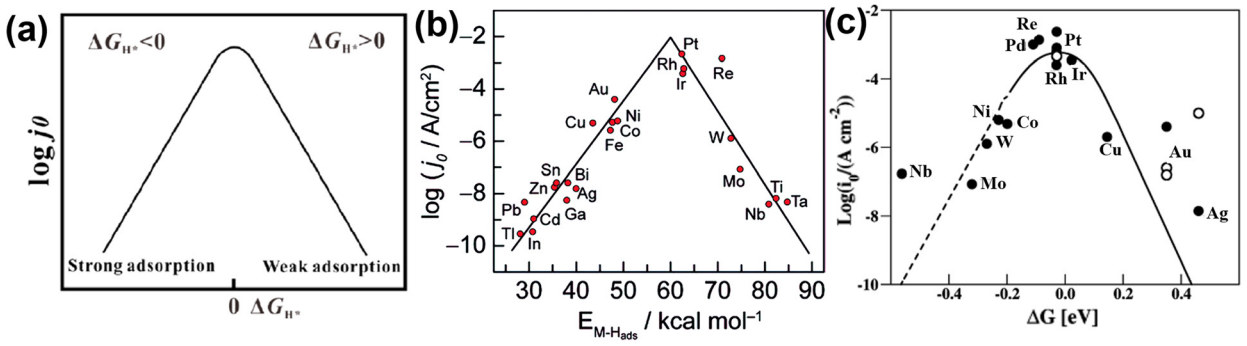

FIG. 3. Proposed volcano-type curves (a) based on HER activity (log j_0) vs adsorption energies (ΔG_{H*}), (b) between log j_0 and M–H binding energy on the surface of several metals, or (c) based on the relationship of log j_0 and ΔG_{H*} of various metals. (a) Reproduced with permission from Parsons *et al.*, Trans. Faraday Soc. **54**, 1053–1063 (1958). Copyright 1958 Royal Society of Chemistry. (b) Reproduced with permission from Cook *et al.*, Chem. Rev. **110**(11), 6474–6502 (2010). Copyright 2010 American Chemical Society. (c) Reproduced with permission from Skúlason *et al.*, J. Phys. Chem. C **114**(42), 18182–18197 (2010). Copyright 2010 American Chemical Society.

close to Pt, that is, approximately at the apex of this volcano-like diagram.[27,28] Thus, they own the most appropriate ΔG_{H*}, approaching zero, which makes them the most efficient catalysts for the HER.[27,28] As the principle proposed by Trasatti *et al.* explains, the suitable hydrogen adsorption/desorption at the metal surface can be well indicated by the moderate M–H bond energy (~65 kcal mol^{-1}).[25,26] Ru metal has this analogous Ru–H bond strength of about 65 kcal mol^{-1}, which enables a super catalytic behavior of Ru as a HER electrocatalyst.[12] For the other two noble metals, i.e., Au and Ag, their much weak adsorption energy of hydrogen suggests their relatively low HER catalytic efficiency. However, the satisfactory performance on them is sometimes caused by the structural and electronic optimization. To be noted, based on the catalyst design strategies shown in Fig. 2, these outstanding nanostructured non-Pt noble metal-based materials have unique electronic configuration, versatile composition, novel micromorphology, tailorable chemical valence, etc., which are substantially associated with the number of active sites and the reaction energy barrier of catalytic reactions. Eventually, the admirable catalytic properties are achieved on these non-Pt NMNs. Aiming at these great outcomes, the next section focuses on the discussion of various electronic modulation and structural design tactics to propel the catalytic performance.

IV. CONSTRUCTING ROBUST NON-PT NOBLE METAL-BASED ELECTROCATALYSTS TOWARD THE HER

A. Element composition optimization

1. Noble-metal-based alloys

Incorporation of other alien metals into the lattice of a given metal has been identified to be a versatile and impactful pathway in boosting the HER electrocatalytic performance owing to the ligand effects and cumulative strain from the changed bond energy and bond length, endowing favorable electronic structure and adsorption energy of hydrogen intermediates.[16,17,34–48] Therefore, plenty of alloy materials have been developed.

a. Noble metal–noble metal alloys. Noble–noble metallic alloys have been proven to express highly enhanced catalytic activity for the HER.[34–38] Zhu *et al.* explored the hollow Ir–Ag alloy nanotubes (NTs) as the HER catalysts in acidic media and demonstrated a considerable catalytic activity, showing an overpotential of only 20 mV at a 10 mA cm^{-2} current density in the acidic environment.[34] Yao and his co-workers illustrated that Ag doping in the Pd–Ag alloy surface well regulated the electronic structure of the monometallic Pd surface, which in turn balanced the reaction rates of water-dissociation and hydrogen-formation steps toward boosting the HER performance.[35] The strength of Pd–H against the H_{ad} combination into H_2 in the HER was largely mitigated to an appropriate value after the incorporation of Ag atoms, as shown in Fig. 4(a), that was, at the Pd–Pd–Ag hollow sites, the value of hydrogen binding energy (HBE) (−0.49 eV) was very close to that of Pt (111). Meanwhile, Qin *et al.* also confirmed the optimization of HER performance in basic media by devising alloyed Pd_3Ru nanoparticles with several Ru segregations on the surface.[39] They elucidated the effect of Ru dopants in HBE and the adsorption of OH^-, which consequently lowered the energy barrier of the reaction-determining step in the HER process. As reported by Choi and his co-workers, the atomically Pd or Pt-doped MAu_{24} and M_2Au_{36} nanocrystals further helped reintroduce the effect mechanism of metal doping.[36] The authors found that upon introducing Pd/Pt atoms into Au_{25} or Au_{38} nanoclusters (NCs), their electrochemical redox potentials were altered to enable an efficient electron transfer and hence controlled the onset potentials. Furthermore, through theoretical simulations, they offered a trend on the basis of ΔG_H for varied metal-doped Au nanoclusters. In line with the calculated ΔG_H values, electrochemical experiments evidenced that the doping impact on HER catalytic activity, reflected by the catalytic current density and turnover frequency (TOF), followed this order of Pt > Pd > undoped counterpart.

Among the noble-metal-based combinations, alloying with Pt shows a particular interest. Besides the as-referred Pt–Au alloy, alloyed Pt–Ag, Pt–Pd, Pt–Rh, and Pt–Ir materials also have been extensively studied for the HER catalysis.[40–44] According to Chao *et al.*, atomically dispersed Cu metal on Pd nanorings (NRs) was used as seeds for introducing Cu–Pt dual sites into Pd NRs, in which the atom ratio of Pt is about 1.5%.[41] The trimetallic alloy, namely Pd/Cu–Pt NRs, achieved exceptional HER performance [Fig. 4(b)] because of atomically Cu–Pt active sites that were confirmed by the presence of Cu–Pt coordination bonds as well as the absence of Pt–Pt and Cu–Cu bonds from extended x-ray absorption fine structure (EXAFS) results shown

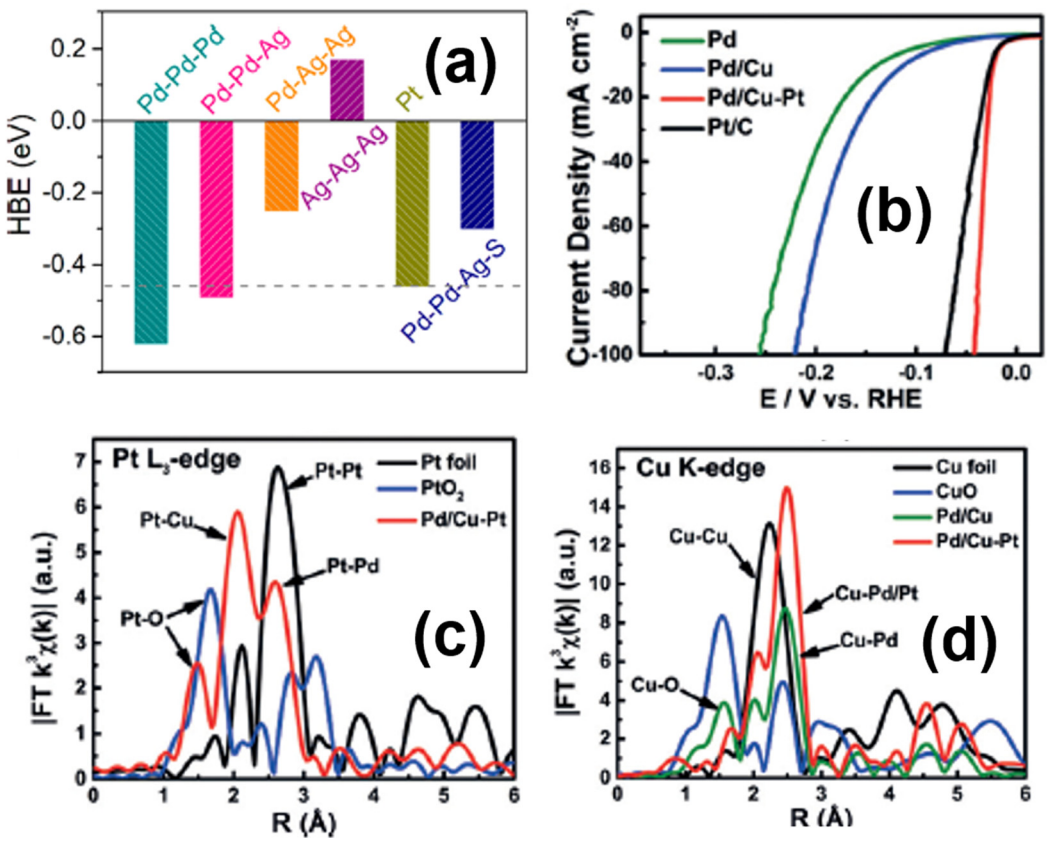

FIG. 4. (a) HBE values on different active sites obtained through DFT calculations. Reproduced with permission from Yao *et al.*, ACS Energy Lett. **4**(6), 1379–1386 (2019). Copyright 2019 American Chemical Society. (b) Linear-sweep-voltammetry (LSV) curves toward the HER for various samples, including Pd nanosheets, Pd/Cu NRs, Pd/Cu–Pt NRs, and benchmark Pt/C, under acidic conditions. (c) and (d) The k^3-weighted c(k)-function of EXAFS spectra for (c) Pt L_3-edge and (d) Cu K-edge. Reproduced with permission from Chao *et al.*, Angew. Chem., Int. Ed. 129(50), 16263–16267 (2017). Copyright 2017 Wiley-VCH.

in Figs. 4(c) and 4(d). The comparison among H adsorption energies of different metals, based on theoretical calculations, strongly supported the experimental analysis. Most recently, Yang's group considered a Pt–Ru bimetallic nanoalloy as the extraordinary HER catalyst in a broader pH range.[44] To control the Pt/Ru amount and realize a homogeneous metal distribution, a novel simple electrochemical deposition (ECD) technique was applied with RuO_2 loaded on carbon cloth as the working electrode and Pt mesh as the counter electrode, where trace Pt ions can be electrochemically dissolved from the counter electrode and then were electrochemically deposited on the working electrode. Owing to a synergistic influence between Pt and Ru that resulted in boosted hydrogen desorption and accelerated H_2O dissociation, Pt–Ru bimetals supported on carbon cloth with an optimum Pt amount presented a super good catalytic efficiency with the η_{10} of only 8, 19, and 25 mV and the Tafel slopes of 25, 28, and 36 mV dec^{-1} in 0.5 M H_2SO_4, 1 M KOH, and 1 M PBS, respectively. Analogously, Pt–Ru nanoalloys embedded in porous spherical carbon were reported in a previous study by Xing's group.[43] A precisely controlled polycondensation reaction was employed for the production; but, several performance indices, such as overpotential (19.7 mV in 0.5 M H_2SO_4 electrolytes), Tafel slope (27.2 mV dec^{-1} in 0.5 M H_2SO_4 electrolytes), etc., significantly differed in view of the discrepancies in the catalyst nanostructure and metal loading amounts.

For further increasing the alloy atom utilization efficiency, single-atom alloys (SAAs) have been elaborately fabricated. However, such a single-atom form is relatively difficult to obtain because of the metastable nanostructures and fast crystallization growth rate.[45,46] Chen and his co-workers put forward a rapid synthesis of alloyed RuAu single-atom catalysts using laser ablation in liquid.[46] During the preparation process, a Ru target was first submerged in the mixed solution with $HAuCl_4$ and HCl, followed by irradiation using a nanosecond laser [Fig. 5(a)]. This treatment caused the Ru target vaporization and thermal decomposition of $HAuCl_4$, thus producing RuAu single-atom alloys after subsequent fast quenching. Various types of RuAu single-atom alloys (SAAs), Ru, RuAu-0.1, RuAu-0.2, RuAu-0.3, and RuAu-0.5, were synthesized by varied concentrations of $HAuCl_4$. It was found that there was an upper limit dissolution for Au atoms in these nanoalloys here, i.e., RuAu-0.2. To create a current density of 10 mA cm^{-2} under basic conditions, the required HER overpotential for the optimal RuAu-0.2 was only 24 mV, which was 34 and 22 mV smaller than the data of Ru and Pt/C, respectively [Fig. 5(b)]. Moreover, compared to Pt/C, RuAu-0.2 exhibited a threefold higher TOF, being as

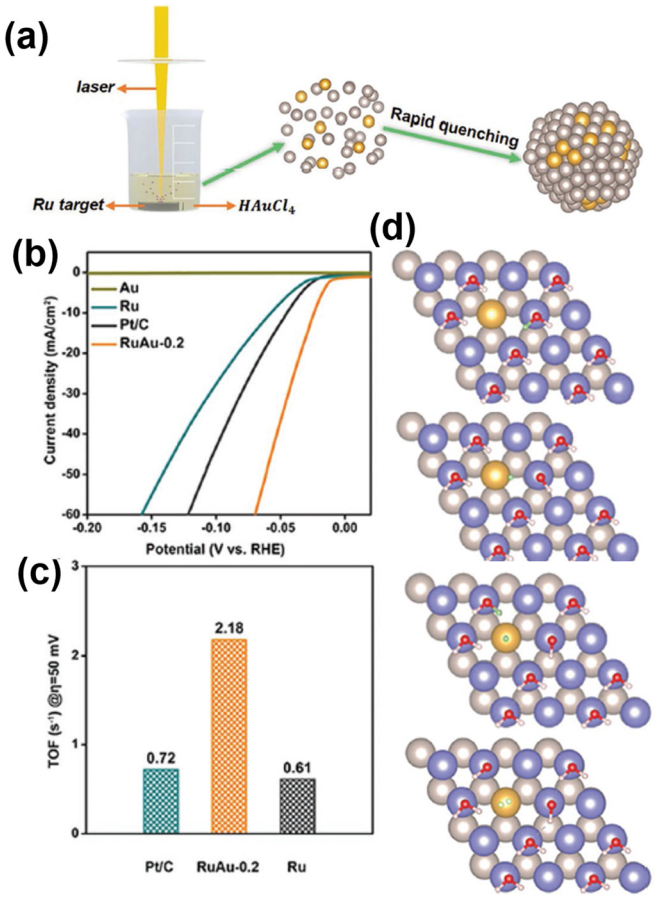

FIG. 5. (a) The preparation process of RuAu SAAs. (b) HER polarization curves of the pure Au, Ru, and RuAu-0.2 electrocatalysts, in comparison with commercial Pt/C, in 1 M KOH. (c) The corresponding TOF results at the overpotential of 50 mV. (d) A schematic illustrating the hydrogen-evolution process on RuAu SAAs. These deep blue, silver gray, golden, red, and white and green balls indicate the top layer of Ru, the bottom layer of Ru, Au, O, and H atoms, respectively. Reproduced with permission from Chen *et al.*, Adv. Energy Mater. **9**(20), 1803913 (2019). Copyright 2019 Wiley-VCH.

high as 2.18 s^{-1} [Fig. 5(c)]. X-ray photoelectron spectroscopy (XPS) and DFT calculations were carried out to unveil the origins of such high activity. As illustrated in Fig. 5(d), RuAu SAAs promoted the HER in the basic environment through the relay catalysis of Ru and Au active centers, namely, water molecules were adsorbed and dissociated on Ru atoms, and then Au atoms captured the released protons and accelerated the generation of molecular hydrogen, as such, an ultrahigh catalytic activity for the alkaline HER was attainable in the RuAu SAAs. Impressively, this synthesis method can be generalized, even for the immiscible Ru and Ag in the solid state. Almost at the same time, Zhang *et al.* deposited the trace Pt atoms on the Pd nanoparticles for the surface formation of Pt–Pd single-atom alloys.[45] The SSA nanostructure owned the highly unoccupied density of states (DOSs) in the 5d character and greatly diminished the H_2 adsorption energy, correspondingly giving rise to a Pt-outperformed HER catalytic performance in acidic media.

b. Noble metal-transition metal alloys. As to these high-performance noble–noble metallic alloys, the high cost is still an obstacle for wide commercial adoption. Aiming to handle this issue, the precious metals, i.e., Ru, Rh, Pd, Ag, Ir, and Au, can form alloys with some cheaper transition metals (TMs), with the dosage of these precious metals even down up to an order of magnitude.[16,17,47,48] Particularly, 3d TMs, such as Ni, Co, Fe, Cu, and Mn, have been mixed with noble metals for upgrading the HER activity.[16,17,47–49] The electronegativity difference between noble metals and TMs could lead to the d-band filling of noble metals, accompanied by a negative shift in the d-band center, sequentially generating a favorable electronic configuration that substantially accelerates performance amelioration. Pi *et al.*, using a facile wet-chemical method, prepared various monodispersed IrM (M = Ni, Co, and Fe) nanoclusters (NCs) with mean sizes of 1.5–2 nm and systematically studied their catalytic performances.[50] It was revealed that both HER and OER activities increased in this trend, i.e., Ir NCs < IrFe NCs < IrCo NCs < IrNi NCs, with IrNi NCs unleashing the best catalytic properties in acidic solutions ($\eta_{onset} = 210$ mV for OER and $\eta_{20} = 19$ mV for HER) among these samples. Nonetheless, there was no coverage of the underlying origins about such results in this work. Afterwards, another case by Guo's group further supported the boosting order on the catalytic activity for IrM (M = Ni and Co) alloys (Ir < IrCo < IrNi) and found that the decreased hydrogen binding energy (HBE) should be accountable for this trend.[51] Figure 6(a) described the potential values of H sorption peaks through the CV curves in the H_{upd} (under potential deposited H) region, which could mirror HBE. The obtained potentials followed this sequence of IrNi < IrCo < Ir that was in accordance with the variation tendency in their downshift of Ir 4f XPS peaks [Fig. 6(b)] and had an absolute reciprocal relationship with their catalytic activities. Notwithstanding relative to IrNi and IrCo, alloying Fe with Ir metal exhibited a minimum activity enhancement; a regulated electronic structure along with d electron couplings in IrFe still appeared to heavily raise HER activity in comparison with pure Ir metal.[16] Likewise, alloyed RhFe catalysts with shortened Rh–Rh bonds also maneuvered the superior HER activity to the pure Rh counterpart, announced by Golvano-Escobal *et al.*[52] and Zhang *et al.*[53] Very lately, Majee and colleagues further emphasized the impacts of the doped-Ag proportion on HER activities of AgNi alloys with decahedral geometry.[54] The optimal ratio, of about 5 at. % Ag (AgNi-5), in the decahedral AgNi alloys rationalized the site-specific element distribution on the surface, where its faces were Ni-rich and Ag predominantly resided at the apex and edges, and thereby gained maximum charge transport. Toward HER, to arrive at a 10 mA cm^{-2} current density in 1 M KOH, AgNi-5 required a low overpotential of ~24 mV, which was comparable to that of Pt/C. In addition, there was no noticeable current change at the fixed potential of −0.15 V for 5 days. It is also worth to mention that the relative adsorption capability of H species at the Ni centers was identified as a function of their proximity to Ag atoms. In addition, annealing noble metal cations (Ru, Ir, or Pd)-permeated Ni/Co-based metal-organic frameworks (MOFs) were broadly demonstrated to yield the noble-transition metallic nanoalloy core implanted in graphene-like carbon cages (nanoalloy@NC).[55–59] These nanoalloy@NC samples synthesized in this way contained a very low noble metal loading (less than 2 wt. %) and yet exhibited extraordinary catalytic behavior toward the HER.[55–59] A reasonable interpretation for the high performance was proposed to be that the near-optimal

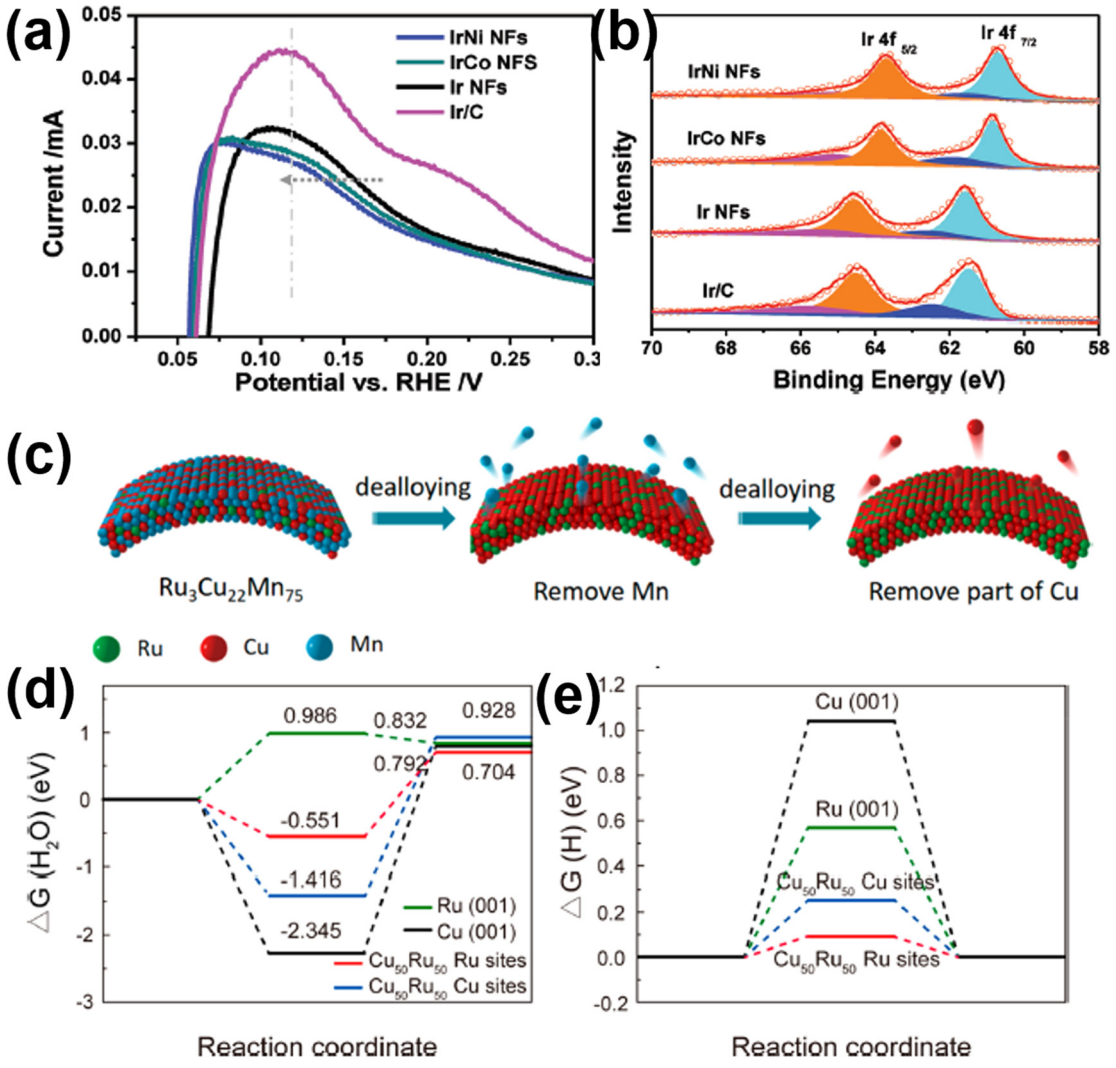

FIG. 6. (a) H sorption peaks in the H_{upd} region for different reported samples in acidic media. (b) Ir 4f XPS peaks for different materials. Reproduced with permission from Lv *et al.*, Small Methods **4**(6), 1900129 (2020). Copyright 2020 Wiley-VCH. (c) Diagrammatic illustration of the synthesis route of nanoporous CuRu alloys. (d) The calculated water-splitting barriers and (e) hydrogen adsorption energy results. Reproduced with permission from Wu *et al.*, ACS Energy Lett. **5**(1), 192–199 (2019). Copyright 2019 American Chemical Society.

adsorption energies for H-related intermediates were achieved in these electrocatalysts based on the modification of charge distribution on the N-doped graphene (NG-x) layer by modulating metal cores.[55,56] For Cu-noble metal alloys, Li *et al.* observed that a volcano relationship matched the HER catalytic activity trend with increasing Cu content from x:y = 3:1 to 1:3 in Pd_xCu_y.[48] Pd_1Cu_1 stood out to be the best one in 0.5 M H_2SO_4. Similarly, Wang *et al.* synthesized Au–Cu alloy nanoparticles with altered Cu proportion as prominent HER catalysts.[60] The particle sizes ranged from 5 to 30 nm and there were few morphology distinctions depending on the Cu content; but the escalating Cu ratio transferred the homogeneous $AuCu_3$ alloy phase to Au_3Cu alloy wrapped by a Cu coating. CuRu alloy was also a high-performance catalytic material for the HER.[49,61] A little while ago, Wu *et al.* identified the actual electrocatalytic sites of the HER in nanoporous CuRu alloys that were manufactured by a simple dealloying process [Fig. 6(c)].[61] In the dealloying route, a single-phase ternary $Ru_3Cu_{22}Mn_{75}$ alloy was treated in $(NH_4)_2SO_4$ solution to remove all Mn and partial Cu, so then to obtain the nanoporous CuRu alloys. *In situ* x-ray absorption spectroscopy (XAS) measurements in conjunction with theoretical calculations elucidated that the combination of Cu and Ru reinforced the Cu–H interaction whilst weakened the strength of the Ru–H bond to dramatically enhance the HER efficiency, of which the water-splitting barrier and hydrogen adsorption energy were reduced to −0.551 eV and 0.092 eV, respectively [Figs. 6(d) and 6(e)]. Here, these, together with accelerated charge/ions migration in the interconnected porous structure, were thought to be

dominant reasons for a remarkable HER catalytic behavior in terms of small η_{10} (~15 and ~41 mV) and Tafel slopes (~30 and ~35 mV dec^{-1}) in both basic and neutral solutions, respectively.

Mo and W also have been introduced into the noble metal structures and their impacts on electrocatalysis have been investigated.[62,63] Guo's group reported a nanodendritic-like Ir–W alloy (IrW ND), prepared by a colloidal–chemical approach with $IrCl_3{\cdot}xH_2O$ and $W(CO)_6$ as metal sources, cetyltrimethylammonium chloride (CTAC) as the surfactant, glucose as a reducing agent, and oleylamine as the solvent.[62] The raw materials were first mixed under ultrasonication and underwent heat treatment in a capped vial. When compared to the monometallic Ir, the IrW ND sample offered a strengthened HER efficiency in both the acid and base, with $\eta_{10} = 12$ and 29 mV and the TOF values of 3.75 and 2.16 s^{-1} at the 10 mV overpotential, respectively [Figs. 7(a) and 7(b)]. Moreover, this hydrogen generation rate was even twice better than that obtained from the Pt catalyst [Figs. 7(a) and 7(b)]. The theoretical analysis based on DFT pointed out the key factors in improvement of HER performance in different electrolytes [Figs. 7(c) and 7(d)]: a stronger H adsorption of the surface Ir site in IrW relative to Ir facilitated hydrogen evolution in acid, while the higher alkaline HER activity was due to a higher affinity to OH to the W site toward accelerating the dissociation of water. Additionally, the authors also found a remarkable increase in OER electrocatalytic activity and stability upon W doping, and they ascribed such a phenomenon to the weakened binding energy of oxygen intermediates and the stabilized active iridium oxides formed in the course of the OER. Later, Zhang and his co-workers verified that heteroatom Mo doping positively modified the hydrogen adsorption energy in the hcp-structured Ru metal and resulted in considerable promotion on the HER activity.[63]

For the sake of extending the combination of metals, several ternary alloy systems have also been exploited.[64–68] For example, an IrNiTa metallic glass (MG) nanofilm with low iridium content was studied as an intrinsically highly active catalyst for producing hydrogen.[65] The author suggested that a synergy between the suitable alloy composition and amorphous nanostructure brought about the high performance. Shan and colleagues added different transition metals (Co, Ni, or Fe) into the RuIr alloy nanostructure.[67] The dependency of OER and HER catalytic properties on the dopant types was subsequently established in detail [Figs. 7(e) and 7(f)]. The optimal Co doping induced the creation of more low-coordinated oxygen species and altered the surface valence states of Ru and Ir that give rise to the modified binding strength of oxygen/hydrogen intermediates [Figs. 7(g) and 7(h)]. Thus, following Co doping of the RuIr alloy, the Co–RuIr sample significantly expedited the HER and OER rates in 0.1 M $HClO_4$ electrolytes, leading to low overpotentials of 14 mV for HER and 235 mV for OER at 10 mA cm^{-2} [Figs. 7(e) and 7(f)]. Eventually, a cell voltage of only 1.52 V at a current density of 10 mA cm^{-2} was observed for total water electrolysis. Analogously, a series of different transition metals (Ni, Co, and Fe) doped-RuPd alloys with ultrathin nanosheet (NS) structures were reported in a recent work by Zhang *et al.*, which gave excellent HER catalytic activities in basic solutions.[68] As to the optimized $Ru_{38}Pd_{34}Ni_{28}$ NSs, the overpotential was just 20 mV at a current density of 10 mA cm^{-2} and the mass activity at −0.07 V vs reversible hydrogen electrode (RHE) was up to 6.15 A $mg^{-1}_{noble\ metal}$. Good cycling stability was also obtained. Note that this mass activity was 9.6 folds and 88 folds higher than the results in Pt/C and Pd/C catalysts, respectively, becoming the largest one among various non-Pt materials studied so far. From DFT results, a significant electronic structure regulation by incorporating the transition metals (Fe, Co, and Ni) to RuPd NSs was uncovered, specifically showing a linear upshifting of d-band center from −2.5 eV to −1.5 eV. In particular, continuous electron replenishment from metal Ni ensured a fast electron transfer toward adsorbates. Simultaneously, stable Pd active sites strengthened p–d coupling in the initial water dissociation with a facile activation barrier.

2. Noble-metal-based compounds

The electrocatalytic properties of noble metal-based materials could often be manipulated by constructing novel compounds, containing metal oxides, phosphides, dichalcogenides, borides, carbides, and the like.[69–73] Generally, every compound inherited distinctive properties that tempted diverse catalytic active sites.

a. Noble-metal-based oxides (NMOs). Noble-metal-related oxides, especially IrO_2 and RuO_2, which are proverbially used as benchmark OER catalysts, also have been applied to catalyze the HER in some studies.[74–78] As stated by our previous report, several ruthenium-based oxides, including RuO_2 nanorods, hydrous RuO_2, heteroatom (Fe, Co, Ni, Cu, etc.)-doped RuO_2, Ruddlesden–Popper-type Sr_2RuO_4, etc., were highly efficient for HER catalysis.[12] Besides, Kundu *et al.* disclosed that Rh_2O_3 provided stronger adsorption of OH^-, thus facilitating adsorptive dissociation of water and in turn HER activity.[79] Very recently, Li's group successfully synthesized hollow $RuIrO_x$ nanonetcages by using a dispersing-etching-holing multistep strategy.[69] Specifically, as illustrated in Fig. 8(a), with MOF ZIF-8 as an etchable parent material, initially an ion exchange readily occurred between Zn^{2+} in it and free Ru^{3+}/Ir^{4+}; subsequently, through a solvothermal reaction, these $Ru^{3+}/Ir^{4+}/Zn^{2+}$ cations underwent hydrolysis along with a gradual etching of the ZIF-8 internal core, which yielded nanosized hollow boxes followed by a further calcination to achieve the homogeneous $RuIrZnO_x$ oxides; lastly, an electrochemical *in situ* etching treatment was implemented to remove amphoteric ZnO from $RuIrZnO_x$, yielding the final $RuIrO_x$ nanonetcage structures. Figures 8(b)–8(d) exhibited the representative high-angle annular dark-field scanning transmission electron microscopy (HAADF-STEM) images of $RuIrO_x$ nanonetcages, which attested the highly porous walls with the pore size of 1–4 nm constituted by interconnected ultrathin nanowires (NWs) (2–4 nm in width). This synthetic protocol endowed the porous netcage-like nanoframework with a plethora of exposed active centers and a three-dimensional accessibility toward substrate molecules. Accordingly, there was a threefold or fivefold larger electrochemically active surface area (ECSA) in the $RuIrO_x$ nanonetcages with respect to commercial Ir/C and Ru/C particulates, respectively. Moreover, on the basis of DFT analysis and operando XAS results, two attractive features were observed for this $RuIrO_x$ material. First, the energy barriers for the potential limiting steps in HER and OER processes were remarkably lowered, in which the H adsorption energy was just −0.07 eV [Figs. 9(a) and 9(b)]. Second, electrons were migrated from Ir atoms to Ru atoms, inhibiting Ru from overoxidation [Figs. 9(c) and 9(d)] and high valence state Ir was believed to help to oxygen evolution. All these permitted this nanonetcage catalyst to deliver a superior HER/OER activity (HER: 13 mV at pH = 14

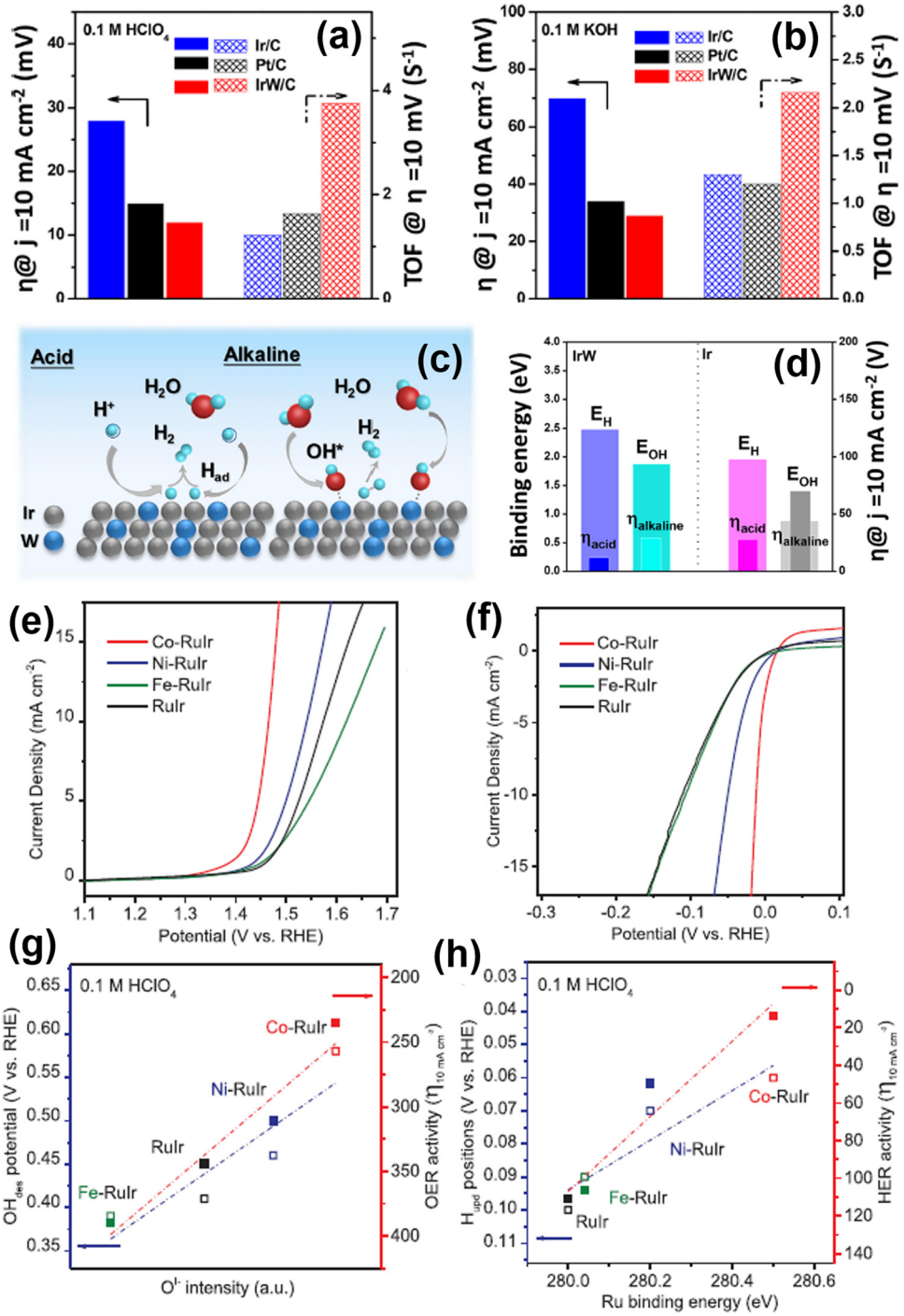

FIG. 7. The overpotentials at a current density of 10 mA cm^{-2} and TOF values at 10 mV overpotential of this IrW/C sample and the commercial Ir/C and Pt/C catalysts in both the (a) acid and (b) base. (c) Diagram showing the HER mechanism under acidic and alkaline conditions on the surface of IrW NDs. (d) Relationship between HER activity and H or OH binding energies on IrW and Ir electrocatalysts. Reproduced with permission from Lv *et al.*, ACS Cent. Sci. **4**(9), 1244–1252 (2018). Copyright 2018 American Chemical Society. (e) OER and (f) HER polarization curves of these Co–RuIr, Ni–RuIr, Fe–RuIr, and RuIr samples in 0.1 M $HClO_4$ electrolytes. Dependence of (g) OH^- desorption potential and OER activity on intensity of O^{I-} species and (h) H_{UPD} potential and HER activity on Ru binding energy. Reproduced with permission from Shan *et al.*, Adv. Mater. **31**(17), 1900510 (2019). Copyright 2019 Wiley-VCH.

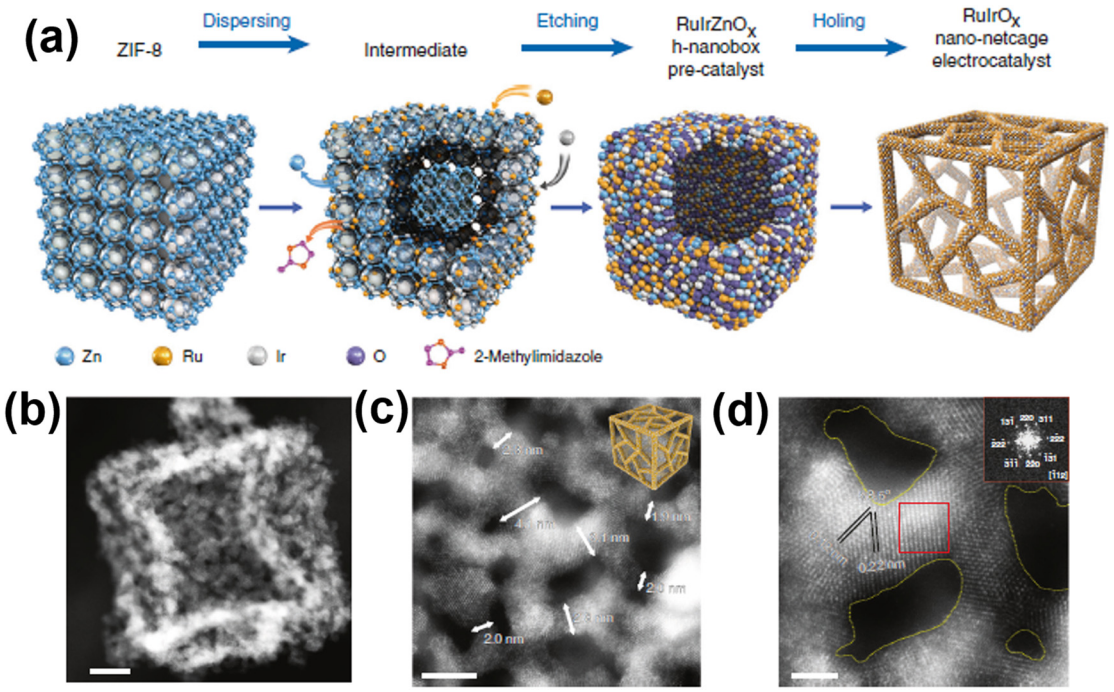

FIG. 8. (a) The synthetic procedure of hollow $RuIrO_x$ nanonetcages. (b)–(d) The representative HAADF-STEM images of $RuIrO_x$ nanonetcages. The scale bar is 10, 5, and 2 nm, respectively. Reproduced with permission from Zhuang *et al.*, Nat. Commun. **10**, 4875 (2019). Copyright 2019 Nature Publishing Group.

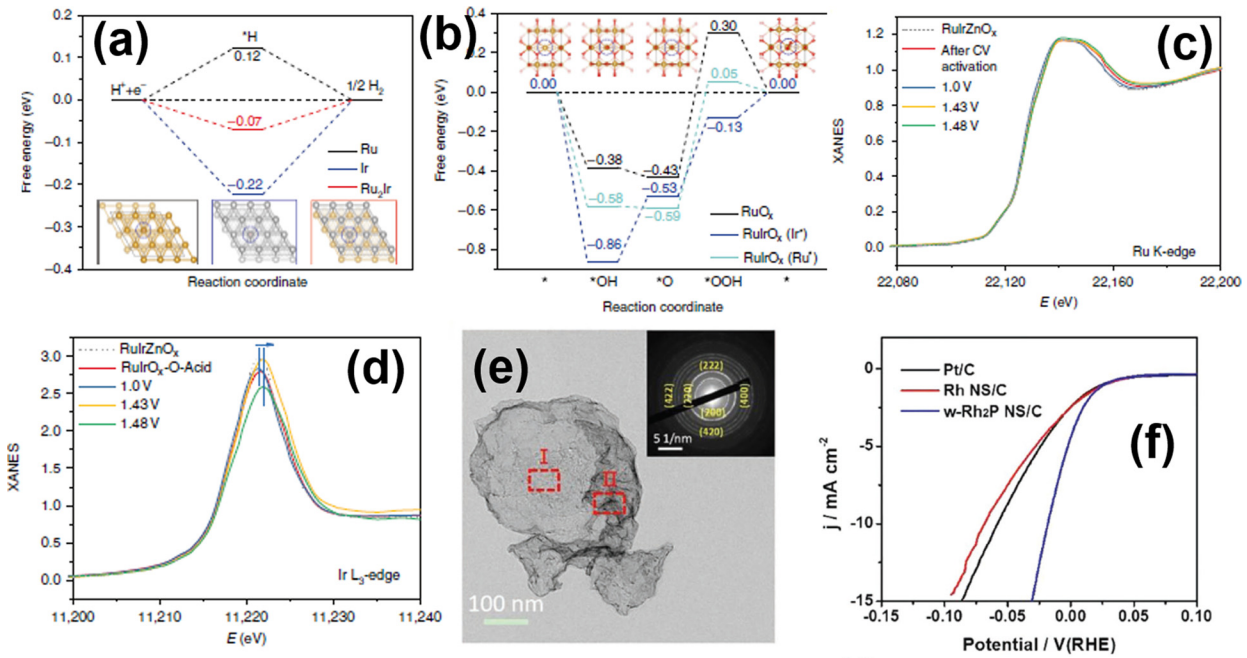

FIG. 9. The free energy diagrams of the (a) HER and (b) OER on the surface of various catalytic materials. The H, O, Ir, and Ru atoms are represented by pink, red, gray, and gold balls, respectively. Normalized *in situ* x-ray absorption near-edge structure (XANES) spectra for (c) Ru K-edge and (d) Ir L_3-edge of the RuIrOx sample, which were obtained at different OER operating potentials in the acidic media. Reproduced with permission from Zhuang *et al.*, Nat. Commun. **10**, 4875 (2019). Copyright 2019 Nature Publishing Group. (e) TEM image of w-Rh_2P NS. The inset is its selected area electron diffraction (SAED) image. (f) LSV curves of the as-prepared w-Rh_2P NS, Rh NS, and commercial Pt/C for HER in 0.1 M KOH. Reproduced with permission from Wang *et al.*, Adv. Energy Mater. **8**(27), 1801891 (2018). Copyright 2018 Wiley-VCH.

and 12 mV at pH = 0 and OER: 250 mV at pH = 14 and 233 mV at pH = 0.) and stability (all: negligible fluctuation in activity after a 3000 cycling test) in both alkaline and acidic environments. Meanwhile, there are nearly no studies on silver/gold/palladium oxides for the application toward HER catalysis, most presumably owing to their relatively low activities.

b. Noble-metal-based phosphides. Since 2017, when Li's group and Mu's group pronounced that Rh_2P and RuP_2-based materials featured a suitable hydrogen adsorption energy and hence granted superior HER activities in a wide range of pH,[80,81] ample efforts have been made on noble metal phosphides, especially rhodium phosphides (RhP_x, i.e., Rh_2P, RhP_2, etc.) and ruthenium phosphides (RuP_x, i.e., RhP_2, RuP, Ru_2P, etc.), for hydrogen evolution.[82–87] In 2018, Guo's group put forward the design of wrinkled Rh_2P nanosheets (w-Rh_2P NS) with an ultrathin thickness of ∼ 3.3 nm [Fig. 9(e)] based on a two-step chemical solvothermal procedure, in which Rh nanosheets were first obtained by heating the mixture of rhodium acetylacetonate [$Rh(acac)_3$], nickel acetylacetonate [$Ni(acac)_2$], L-ascorbic acid (AA), hexacarbonylmolybdenum [$Mo(CO)_6$], and oleylamine (OAm) at 180 °C in an oil bath and then these nanosheets were phosphorized at 300 °C with the help of tri-n-octylphosphine (TOP) in the N_2 environment.[84] Such resultant w-Rh_2P NS recorded a decent HER behavior in 0.1 M KOH with a η_{10} of 18.3 mV, which was 40.1 and 50.6 mV lower than those of commercial Pt/C and Rh NS, respectively, [Fig. 9(f)] and a relatively low Tafel slope of 61.5 mV dec^{-1}. With the support from theoretical calculations on density of state (DOS) and free energies, the in-depth catalytic mechanism in base was revealed, in which the P-3p orbital with the active open-shell property boosted up Rh-4d for augmented proton–electron charge exchange via orbital Coulombic interactions and also the lower-lying 3p-σ bonding level ensured the anchoring of O-related species as an excellent distributary center, so as to avail HER performance under alkaline conditions. Moreover, the w-Rh_2P NS sample was also highly efficient for HER catalysis in acidic and neutral environments. Similarly, around the same time, the remarkable electrocatalytic activity for pH-universal HER in Rh_2P was further verified by Yang *et al.* using monodisperse Rh_2P nanoparticles, which was prepared by a colloidal method with $Rh(acac)_3$ and TOP as Rh and P sources.[85] In our group, the RuP nanoparticles, obtained by a simple phosphidation of $RuCl_3$ in PH_3 from NaH_2PO_2, demonstrated a phenomenal catalytic performance in all pH media.[87] Surprisingly, we found that bigger RuP nanoparticles exhibited larger intrinsic activity and stability compared to the small ones, which might be derived from the stabilization of P species due to a lowered surface energy in large nanoparticles. It is noteworthy that, with a controllably equivalent nanostructure, the RuP catalyst performed more excellent than RuP_2 in terms of HER activity, as a result of more catalytically active centers and higher electric conductivity of RuP.[88,89] Additionally, several mixed RhP_x or RuP_x phases, acting as catalytic materials, were also reported with remarkable HER properties at all pH ranges.[82,86,90] Under the identical synthesis conditions, it was claimed that RhP_2 was more active for catalyzing the HER than RuP_2 in acidic media, while this trend was reversed in alkaline electrolytes.[70]

Other noble-metal phosphides, like IrP_2, PdP_2, etc., were also proven to deliver a splendid HER performance.[91,92] However, so far, it is very rare to find reports on them compared with that on RhP_x or RuP_x. Encouraged by a close-to-zero proton adsorption energy in PdP_2, Luo *et al.* developed a material of palladium phosphides deposited on carbon black (PdP_2@CB) by a facile phosphorization pathway to study the HER properties.[92] A 10 mA cm^{-2} current density toward the HER was reached by applying tiny overpotentials of 27.5, 35.4, and 84.6 mV in 0.5 M H_2SO_4, 1 M KOH, and 1 M PBS, all of which were comparable to that of Pt/C (30.1, 46.6, and 122.7 mV, respectively) and much better than the Pd@CB under the same conditions, manifesting the superb activity. Besides, PdP_2@CB could be *in situ* converted to Pd oxides/hydroxides under anodic oxidation voltage for efficiently catalyzing the OER. According to the same research group that first proposed the RuP_2-based electrocatalyst, a novel iridium diphosphide (IrP_2) catalyst encapsulated in an ultrathin N-doped carbon substrate (NC), denoted as IrP_2@NC, was further produced by direct calcination of mixed $IrCl_4$, phytic acid (PA), and melamine under Ar atmosphere.[91] The as-synthesized IrP_2@NC sample afforded a vitally low HER overpotential of 8 and 28 mV at 10 mA cm^{-2} in the acidic and basic environments, respectively, far below those of commercial Pt/C (18 and 42 mV, respectively), along with a highly stable activity. The exceptional activity was mainly attributed to the lowered H adsorption strength resulting from the combination of Ir and P and NC introduction. To further extend the synthesis, the author also adopted this method to obtain the two samples, RhP_2@NC and Pd_5P_2@NC, showing the η_{10} of 29 and 249 mV in acid, respectively. Above all, cases stated that noble-metal phosphides held great promise for HER applications.

c. Noble-metal-based chalcogenides. Noble-metal chalcogenides, a kind of novel HER catalytic material with relatively low intrinsic electrical resistivity, have also been widely investigated in the past few years, which mimicked the catalytic behavior of benchmarking Pt almost over a whole pH range.[93–103] The initially exploited $Ru_{0.33}Se$ nanoparticles loaded on TiO_2 nanotube arrays actualized an efficient activity for the HER in basic media with a η_{10} of 57 mV.[93] Soon afterwards, our group fabricated high-crystalline and sphere-shape RuS_2 particles on reduced graphene oxides (rGOs) by a facile solvothermal approach followed by calcination treatment.[71] Along with a high intrinsic catalytic property in RuS_2, the as-made material delivered a remarkable HER catalytic performance over a wide pH range, comparing favorably to the Pt/C sample. Also, recently, the amorphous structure of RuS_2 nanoparticles was found to possess high Pt-like activities for catalyzing the HER in pH-universal media by Li and co-workers, as elaborated below.[94] In another recent report, through tuning the sulphuration temperature, both disorder and defects were synchronously engineered in RuS_2 nanoparticles.[100] Benefiting from these controlled disorder and defects, the electrochemically active surface area was enlarged and the electronic structure was well modulated in a low-crystalline RuS_2 material, rendering an extraordinary catalytic activity for both the OER and HER in alkaline solutions. DFT calculations unveiled that Ru vacancies drove the d-band center of surface Ru upshift from −0.93 eV to −0.77 eV, which could reinforce the H adsorption to an optimum level.

Toward other noble-metal chalcogenides, a pioneering work in 2014 by Singh *et al.* demonstrated that Rh_3S_4 and $Rh_{17}S_{15}$ showed better HER activity than Rh_2S_3 and RhS_2 phases.[101] The active sites for HER on these rhodium sulfides have been determined to be Rh rather than S atoms through CO poisoning experiments coupled with DFT calculations. In 2016, Yoon *et al.* engineered highly exposed edge sites

in Rh_2S_3 by constructing hollow hexagonal nanoprism shapes with well-defined facets and controlled size.[95] In light of this, an outstanding catalytic performance for the HER was endowed with achieving a current density of 10 mA cm^{-2} by a small overpotential of 122 mV and high stability under harsh acidic conditions. Shokhen *et al.* conducted electrochemical activation on Ag_2S to produce mesoporous silver covered by a silver oxo-sulfide layer, which was highly active for hydrogen generation in 0.5 M H_2SO_4 and electrochemically or chemically stable over several days.[102] Taking the merits of first-principle calculation theory, Huang and his co-workers obtained this finding that on monolayer $PdSe_2$ and $PdTe_2$, creating a double vacancy (DV_{Se} and DV_{Te}) and boron-doping could appropriately regulate the interaction between the basal plane and H_{ads} species and upgraded the electrocatalytic hydrogen-evolving activity of these metal dichalcogenides.[98] Intrinsically, $IrSe_2$ is a quite ordinary HER electrocatalyst, displaying the η_{10} of 225, 371, and 298 mV in these electrolytes with pH = 0, 7, and 14, respectively.[99] These values were decreased by as much as around 200 mV using the intercalation of Li atoms, which could root in abundant Se vacancies and high porosities. Besides, this tactic was also applicable to reform the poor OER activity of $IrSe_2$, evidenced by the η_{10} overpotential change from above 470 mV to below 320 mV at all pH ranges.

Simultaneously introducing sulfur and phosphorus into the palladium lattice created a layered palladium thiophosphate ($Pd_3P_2S_8$) material.[103] Its crystalline phase is electrochemically inert toward the HER. Zhang's group successfully applied an electrochemical Li^+ intercalation in a controllable galvanostatic lithiation process to continuously alter the phase transition from crystal to amorphization and introduced a plethora of P/S vacancies as well as heightened electrical conductivity in the $Pd_3P_2S_8$ sample, so as to gain the optimal atomic configuration and electronic state toward HER performance [Figs. 10(a)–10(d)].[103] Thereupon, a significant promotion in HER catalysis was achieved. Specifically, at the identical electrocatalyst loading, this onset overpotential value in 0.5 M H_2SO_4 was substantially reduced from 175 mV of crystalline $Pd_3P_2S_8$ to 52 mV of amorphous Li-incorporated $Pd_3P_2S_8$ (Li-PPS), approaching to the value of Pt/C [Fig. 10(e)].

d. Noble-metal-based borides, carbides, or others. Similar to phosphides or chalcogenides, recently, noble-metal borides, carbides, and silicides, have gained immense interests as potential HER electrocatalysts.[104–108] For instance, Li and his co-workers presented an innovative ruthenium diboride (RuB_2) catalyst, that owned an appropriate *d*-band center and a high density of superb active sites, thereby efficiently catalyzing the HER process under pH-universal conditions.[72] Based on a simple two-step solvothermal route with Pd acetylacetonate [$Pd(acac)_2$] and dimethylamine borane (DMAB) as Pd and B sources, respectively [Fig. 11(a)], Chen *et al.* fabricated Pd_2B nanosheets (NSs) as an acidic HER catalyst.[104] Pd and B could form the bulk alloy with atomic structure evolution from the fcc phase to hcp phase through varying the B content, and Pd_2B with a hcp structure was the thermodynamically most stable phase [Fig. 11(b)], in which B lay at the octahedral interstitial sites (Oh) of the Pd lattice [Fig. 11(c)]. This Pd_2B sample achieved a η_{10} as small as 15.3 mV with a low Tafel slope of 22.5 mV dec^{-1} and a large exchange current density of 2.84 mA cm^{-2}, all of which significantly exceeded the Pd NS material and benchmarking Pt catalyst. Besides, a long-term durability test revealed that Pd_2B NS could retain 97.6% activity after 12 h while the activities

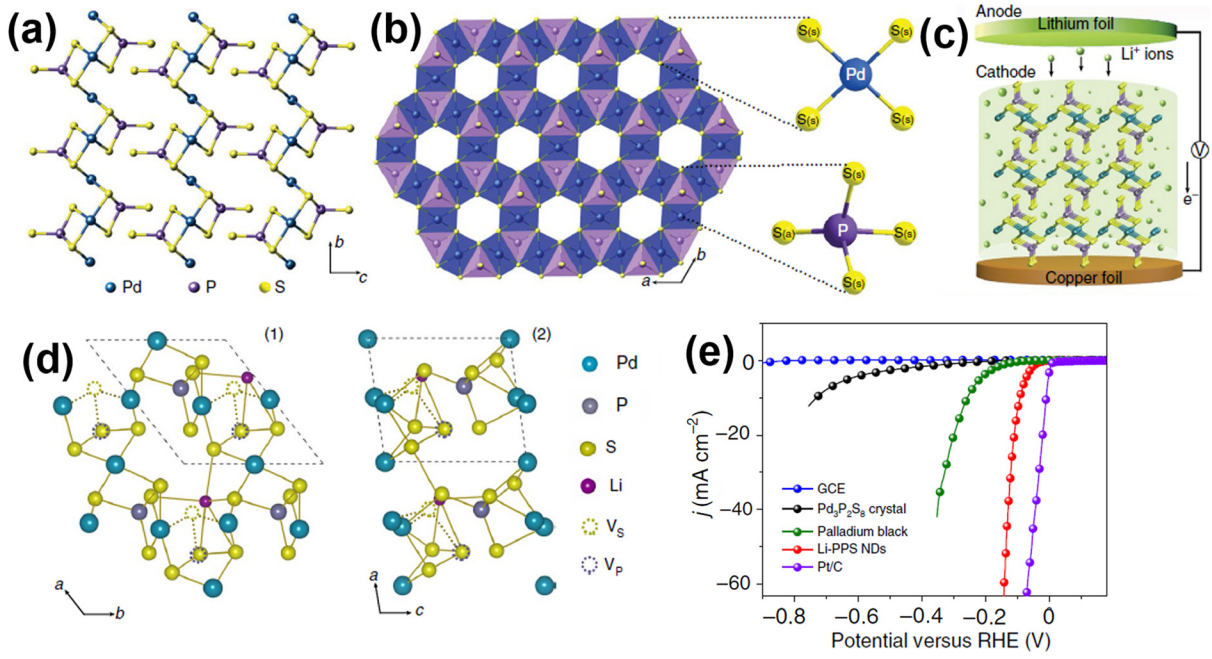

FIG. 10. (a) Atomic configuration (three-layer units) of $Pd_3P_2S_8$ along the *a* axis. (b) Coordination polyhedral structure of $Pd_3P_2S_8$ along the *c* axis. (c) The schematic of synthesis of the phase transition from crystal to amorphization based on an electrochemical Li^+ intercalation. (d) The atomic structure of the resultant amorphous form along the *c* axis (left) and *b* axis (right). (e) HER polarization curves of different as-obtained samples and commercial Pt/C in 0.5 M H_2SO_4. Reproduced with permission from Zhang *et al.*, Nat. Catal. **1**(6), 460–468 (2018). Copyright 2018 Nature Publishing Group.

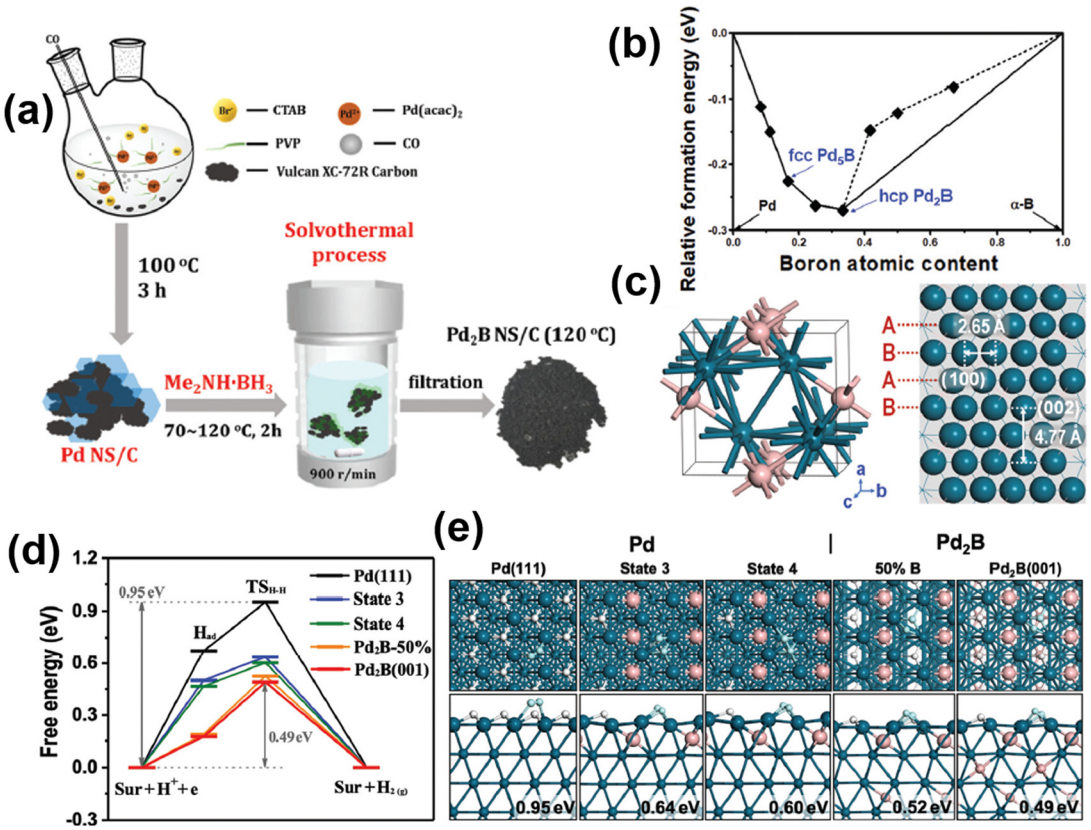

FIG. 11. (a) Schematic illustration of producing Pd_2B nanosheets. (b) The formation energy of Pd–B alloy with varying B content through DFT calculations. (c) Representative hcp Pd_2B crystal structure. (d) The free energy profiles for the HER process on different surfaces. (e) The structure change and free energy barriers of the located transition states. Cyan: Pd atoms; pink: B atoms; white: H atoms; light cyan: the reacting H atoms. Reproduced with permission from Chen *et al.*, Energy Environ. Sci. **12**(10), 3099–3105 (2019). Copyright 2019 Royal Society of Chemistry.

in Pd NS and commercial Pt/C after 12 h were damped to 39.9% and 68.7%, respectively. As analyzed from Figs. 11(d) and 11(e), the presence of subsurface B and the lattice expansion after the hcp phase generation due to the B insertion, toward promoting the H–H coupling, played pivotal roles in improving the HER performance. Zou's group experimentally and theoretically validated that RuSi was electrocatalytically active in producing hydrogen under acidic conditions.[106] Thanks to its proper electronic state administrated by a good balance of ligand and strain influence, this material achieved 10 mA cm^{-2} by an overpotential of 19 mV and a small Tafel slope of 28.9 mV dec^{-1}. Most recently, a new and simple chemical–reduction approach utilizing an organic oxidant, tetracyanoethylene (TCNE) as the carbon source and inhibitor of Rh ion reduction, was engaged to evoke the formation of Rh_2C, which actualized marvelous efficiency in the HER due to a suitable H adsorption energy, leading to a 13 mV overpotential at 5 mA cm^{-2}.[73] Together with these intermetallic compounds, intermetallic MH_x (M = precious metals) created by H intercalation have also been investigated as catalytic materials for the HER and demonstrated pronounced performance. In the RhPd alloy, interstitial H atom introduction could tune the hydrogen adsorption energy to a desirable value by modulating the surface electronic structure, bond length, and coordination numbers of Rh and Pd, consequently resulting in a prominently enhanced alkaline HER activity.[107]

e. Heterometallic coordination compounds. It has been reported that some heterometallic coordination compounds, with an intriguing cooperative effect between the metal ions and molecule ligands, were also a class of promising candidates for HER catalysis.[109–113] Li *et al.* constructed one polyoxometalate (POM)-encapsulated twenty-nuclear silver-tetrazole nanocage architecture, named as HUST-100, which exhibited a moderate H_2-evolving activity with $\eta_{10} = 234$ mV in 0.5 M H_2SO_4, arising from the combination of the porosity of metal–organic nanocages and the redox activity of POM moieties.[109] Eguchi *et al.* experimentally found that the introduction of porphyrin on the Au surface triggered charge transfer from porphyrin to the internal Au cluster, causing a shift in the 5d state of Au that boosted hydrogen-generating behavior.[110] At the same time, Hu *et al.* using first-principle calculation, predicated that the $Au_{22}(L^8)_6$ clusters [$L^8 = 1$, 8-bis(diphenylphosphino) octane] could be a distinguished catalyst for the HER, even better than metallic Pt. They observed that up to six hydrogen atoms could adsorb onto the surface of this cluster and had a close-to-zero adsorption free energy [Figs. 12(a) and 12(b)].[111]

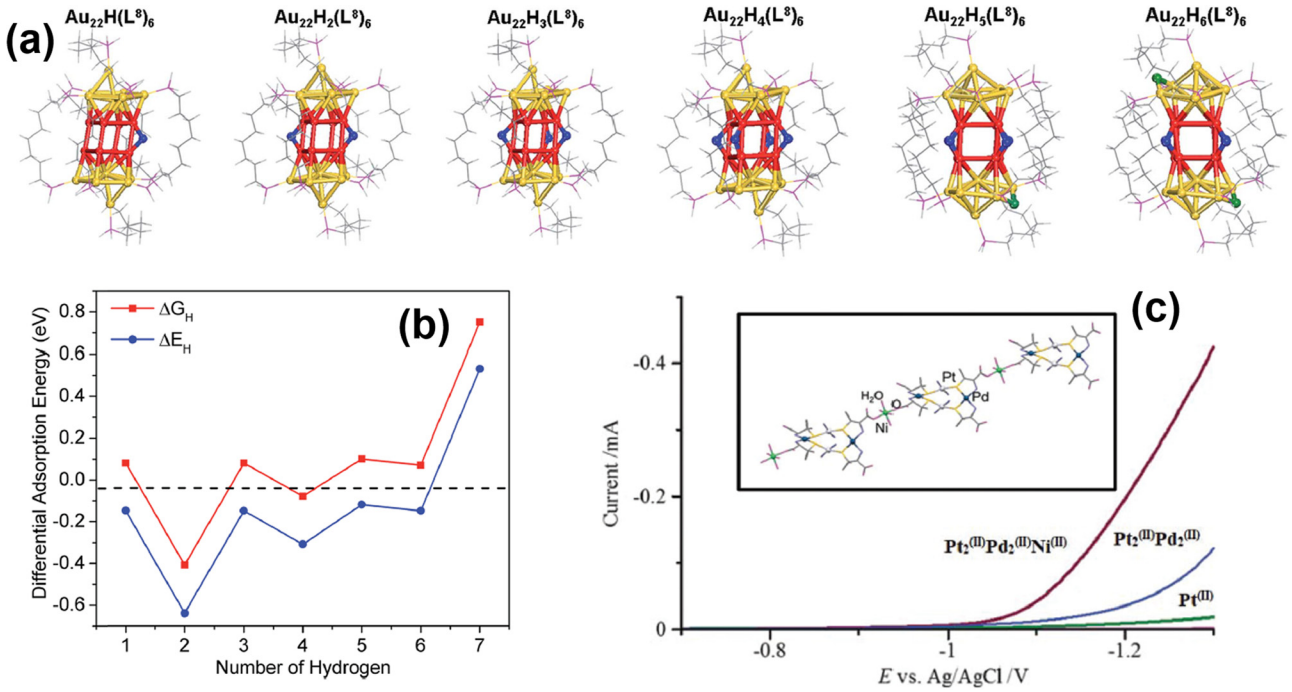

FIG. 12. (a) The structures of the $Au_{22}(L^8)_6$ cluster with different numbers of adsorbed H. The red, yellow, blue, green, light gray, magenta, and gray balls represent coordinatively unsaturated (cus) Au, other Au, H at cus Au, H at non-cus Au, other H, P, and C atoms, respectively. (b) The adsorption free energy (ΔG_H) and differential adsorption energy (ΔE_H) depending on the adsorbed-H number on the surface of $Au_{22}(L^8)_6$. Reproduced with permission from Hu *et al.*, J. Mater. Chem. A **6**(17), 7532–7537 (2018). Copyright 2018 Royal Society of Chemistry. (c) LSV curves of the $Pt_2^{(II)}$–$Pd_2^{(II)}$–$Ni^{(II)}$, $Pt_2^{(II)}$–$Pd_2^{(II)}$, and $Pt^{(II)}$ for the HER in a mixed solution of H_2O–CH_3CN. The inset is the 1D chain heterotrimetallic structure of $Pt_2^{(II)}$–$Pd_2^{(II)}$–$Ni^{(II)}$. Reproduced with permission from Kuwamura *et al.*, Chem. Commun. **53**(5), 846–849 (2017). Copyright 2017 Royal Society of Chemistry.

Konno's group synthesized a $Pt_2^{(II)}$–$Pd_2^{(II)}$–$Ni^{(II)}$ trimetallic coordination polymer, i.e., $[\{Ni(H_2O)_4\}\text{–}\{Pd_2Pt_2(NH_3)_4(D\text{-pen})_4\}]Cl_2$ (D-H_2pen = D-penicillamine) and explored a cooperative effect on HER catalysis. Relative to $[Pd_2Pt_2(NH_3)_4(D\text{-pen})_4]$ (denoted as $Pt_2^{(II)}$–$Pd_2^{(II)}$) and trans-$[Pt(NH_3)_2(D\text{-pen})_2]^{2-}$ (denoted as $Pt^{(II)}$), a considerable augmentation in HER catalytic properties was gained in this trimetallic coordination polymer [Fig. 12(c)], owing to containing all 10-group metal elements.[112] $Pt^{(II)}$ reacted with the Pd^{II} center to create a $Pt_2^{(II)}$–$Pd_2^{(II)}$ complex, and in $Pt_2^{(II)}$–$Pd_2^{(II)}$, two NH_3-based ligands could strongly bind to each $Pt^{(II)}$ site that exerted non-bonding steric and NH···S hydrogen bonding interactions [Fig. 12(c)]. The $Pt_2^{(II)}$–$Pd_2^{(II)}$ in this $Pt_2^{(II)}$–$Pd_2^{(II)}$–$Ni^{(II)}$ polymer worked as an O-donating metalloligand to the Ni^{II} center. With a stepwise combination of $Pt^{(II)}$ with $Pd^{(II)}$ and $Ni^{(II)}$ centers, the electrocatalytic hydrogen evolution was greatly improved through a heterogeneous activity, which corroborated a conspicuous synergism because of all metal cations belonging to the same family.

3. Noble metal dopants

Noble metals, acting as dopants, could be introduced into sundry typical catalytic materials and they have shown a huge promise for triggering new active sites and ameliorating the intrinsically catalytic capacity of original active centers in these materials.[114–123] As proven cases for this strategy, noble metal (i.e., Au, Ir, Rh, Ru, etc.)-inserted Ni/Co/Fe hydroxides were successfully synthesized, which remarkably exceeded their pristine undoped counterparts in HER catalysis.[18,114–117] Chen *et al.* claimed that the introduction of Ru dopants in the lattice of NiFe-layered double hydroxide (NiFe-LDH) could well adjust the water-dissociation active centers on the NiFe-LDH and subsequently improved the HER electrocatalytic performance in base, together with remained superior OER activity.[117] From a similar perspective, a handful of Rh species was also integrated with NiFe-LDH to realize a high-efficiency bifunctional catalysis toward the OER and HER in alkaline environments.[18] However, the difference between Ru–NiFe-LDH and Rh–NiFe-LDH was due to that Rh in Rh–NiFe-LDH existed with two states, i.e., oxidized dopants and ultrafine metallic clusters (less than 1 nm). The doped Rh ions by replacing Fe centers worked as the dominant OER active sites while there was a strong interaction between NiFe-LDH and metallic Rh clusters that was responsible for the improvement of the HER. Li and his co-workers also reported the synchronous enhancement of HER and OER activities in the NiV LDH material by partially substituting Ni sites with Ir atoms (NiVIr LDH) that resulted in the construction of Ir–O–V active groups.[115] The NiVIr LDH material was prepared via employing a one-step hydrothermal route, in which Ni foam was immersed into a mixed solution of $Ni(NO_3)_2{\cdot}6H_2O$, VCl_3, $IrCl_3{\cdot}xH_2O$, and urea, and then the system was heated at 120 °C for 12 h. In this Ir–O–V group, the Ir atom played multiple roles in efficient catalysis [Figs. 13(a) and 13(b)]: first, it helped dissociate water molecules and then it tailored

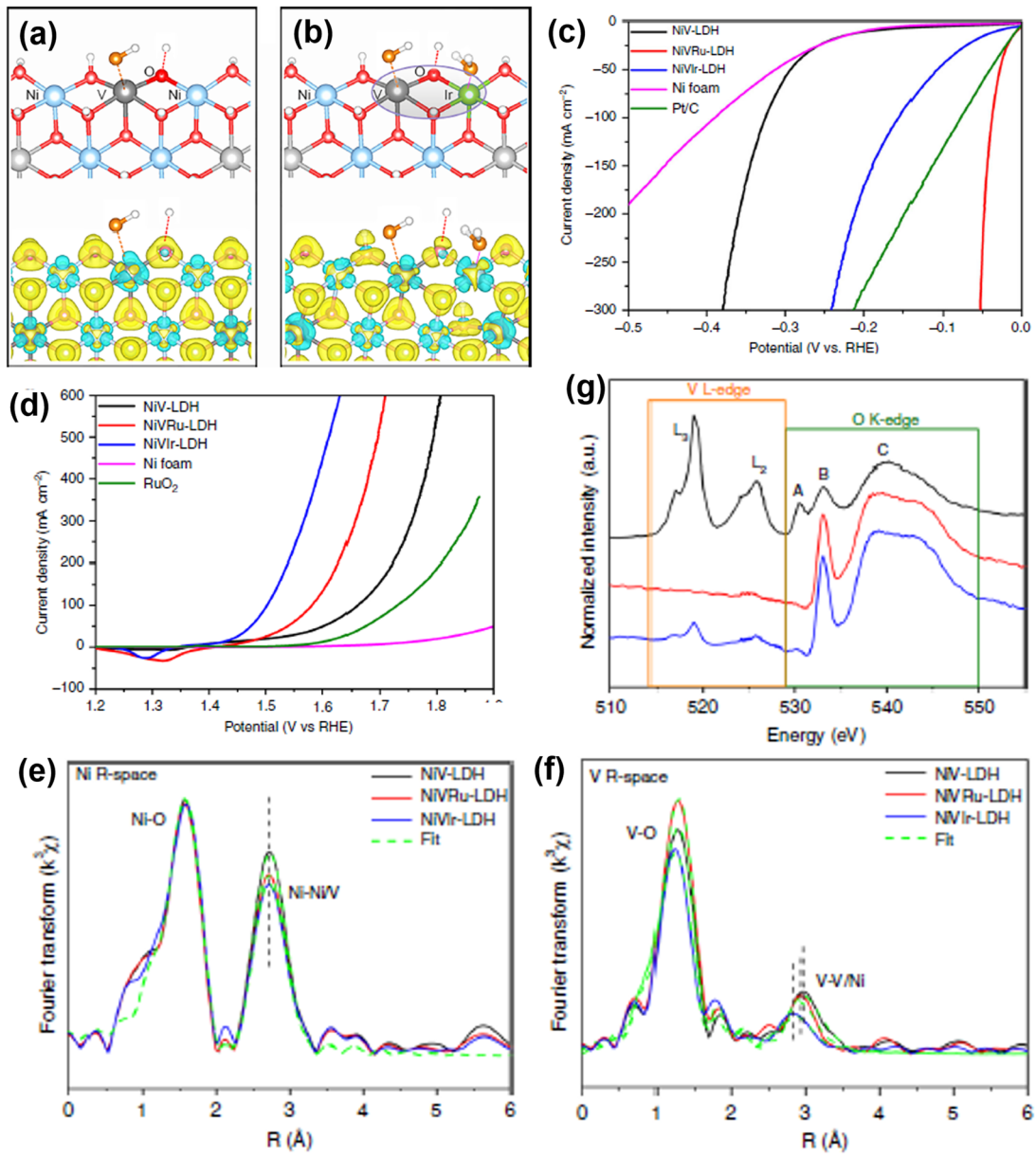

FIG. 13. Active sites (top) and charge density distribution (down) for the overall water splitting of the (a) NiV LDH and (b) NiVIr LDH samples. Reproduced with permission from Li *et al.*, ACS Energy Lett. **4**(8), 1823–1829 (2019). Copyright 2019 American Chemical Society. LSV curves for (c) HER and (d) OER in various samples of NiV LDH, NiVIr LDH, NiVRu LDH, bare Ni foam, and the benchmark catalysts, i.e., Pt/C (for HER) and RuO_2 (for OER). The extended XANES oscillation functions of (e) Ni K-edge and (f) V K-edge. (g) XANES spectra of the V L-edge and O K-edge. Reproduced with permission from Wang *et al.*, Nat. Commun. **10**, 3899 (2019). Copyright 2019 Nature Publishing Group.

the charge density of neighboring bridge O and V atoms (the charge density at O site and V site was decreased and increased, respectively), hence simultaneously optimizing the adsorption energies of hydrogen and oxygen intermediates, which in turn facilitated HER and OER, respectively. The resultant NiVIr LDH achieved outstanding catalytic properties in 1 M KOH with HER and OER overpotentials of 41 and 203 mV when sustained at 10 mA cm^{-2}, which were 107 and 116 mV lower than that of the pristine NiV LDH counterpart. Around the same time, Wang *et al.* conducted an identical study, where Ir or Ru-doped NiV LDH (NiVIr LDH or NiVRu LDH) were explored as HER ad OER catalysts in alkaline electrolytes, which displayed unrivalled activity (the HER η_{10} of 47 and 12 mV and the OER η_{10} of 180 and 190 mV, respectively) and lifetime [200-h (HER) or 400-h (OER) long-term operation at a ultrahigh current density of 200 mA cm^{-2}

without obvious attenuation], as obtained from Figs. 13(c) and 13(d).[118] With the assistance of the advanced XANES and EXAFS spectroscopy methodology, the detailed electronic structure and local atomic coordination environments were revealed to clarify the doping effect of Ru or Ir atoms, namely, severely distorted octahedral structure at V sites and an abundance of V vacancies were formed in the NiVIr LDH or NiVRu LDH. When compared to the NiV LDH, the coordination number of Ni-Ni/V and V-V/Ni in NiVIr LDH and NiVRu LDH was diminished, from 5.1 and 5.3 to 4.2/4.6 and 2.8/3.8, respectively [Figs. 13(e) and 13(f)]. Meanwhile, there was a larger Debye–Waller factor for the V-Ni/V after the introduction of Ir or Ru (0.0186 for NiVIr LDH and 0.0172 for NiVRu LDH vs 0.0123 for NiV LDH), suggesting high octahedral structure distortion. The absence of the L_2 and L_3 peaks in Fig. 13(g) strongly proved that V vacancies did exist in NiVRu-LDH and NiVIr-LDH. In further theoretical investigations, it was revealed that the energy barrier of each elementary step for the HER and OER was reduced after Ru or Ir doping, particularly noting Ru for HER and Ir for OER. Hence, together with this optimized reaction energy of each step, the electronic and atomic modulation of NiV LDH contributed to the favorable HER and OER catalysis.

Following the manifested positive effect of noble metal dopant on hydroxides, several optimization researches in the metal phosphides have also been performed.[119,120] Qu *et al.* replaced a small fraction of catalytic Ni sites in the NiFe phosphide (NiFe–P) by Ru atoms and evaluated their influence on the HER catalytic behavior.[119] The addition of Ru reduced the H adsorption free energies on original P sites and raised additional active sites on Ru atoms, simultaneously accompanied by the optimization of the electronic properties with heightened conductivity. Thus, Ru-incorporated NiFe–P speed up the HER dynamics in 1 M KOH, which only needed 44 mV overpotential to drive a 10 mA cm^{-2} current density and displayed a small Tafel slope of 80 mV dec^{-1}. Additionally, prior to this study, Yan *et al.* underscored the role of Ag dopants on the HER activity of Ru-incorporated Fe–Co_2P. The enhanced conductivity and electron-donating ability from Ag doping accounted for the amelioration of the HER activities.[120]

Another sort of host materials for noble-metal doping are 2D layered metal chalcogenides, especially the classical MoS_2 with the stable 2H phase, in which the edge S atoms are generally deemed as active sites toward hydrogen evolution.[121–124] The introduction of Ru atoms in 2H-MoS_2 has been successfully reported to upgrade the HER catalytic performance. Wang's group utilized the systematic experimental and theoretical tools to give a reasonable explanation for this performance enhancement. The in-plane S atoms adjacent to Ru atoms turned into new active centers, which further not only substantially accelerated water adsorption and dissociation, but also favored hydrogen adsorption/desorption.[121] Noteworthily, it was widely accepted that metastable 1T-MoS_2 with basal-plane S atoms as active centers was more conductive and catalytically active for the HER than 2H-MoS_2. In a recent published work proposed by Zhang *et al.*, a phase transition from 2H to 1T and rich S vacancies induced by single-atom Ru doping for concurrently decreasing the energy barrier of water-dissociation and hydrogen-adsorption steps was believed to be the essential origin of phenomenal activity for the HER in MoS_2 [Figs. 14(b) and 14(c)].[122] The MoS_2 inserted with Ru single atoms (denoted as SA-Ru-MoS_2) was obtained by simple adding and stirring of MoS_2 nanosheets in a $RuCl_3$ solution, along with subsequent vacuum drying [Fig. 14(a)]. Energy dispersive spectrometer (EDS) quantitative analysis unveiled an atomic ratio of 1:1.64 for Mo and S, suggesting the presence of plentiful S vacancies (Sv). A dark-field scanning TEM image of the SA–Ru–MoS_2 sample, shown in Fig. 14(b), exhibited visibly distinguished structural regions, where Mo and S atoms were represented by red and green spheres, respectively. The common honeycomb lattice framework corresponded to a 2H-MoS_2 phase while the trigonal lattice region referred to 1T-MoS_2 structure. Toward hydrogen production in basic electrolytes, the current density of 10 mA cm^{-2} was reached at the overpotential of 76 mV for the best SA–Ru–MoS_2 sample, which approached to Pt/C (51 mV). Correspondingly, DFT results confirmed that at the 1T-Ru-MoS_2-Sv site, a spontaneous water dissociation occurred and the adsorption/desorption energy of H_{ads} species was much closer to ideal value, i.e., 0 [Fig. 14(c)]. This finding was also in good agreement with a previous study by Xing's group, in which the Mo sites in MoS_2 were substituted with trace amounts of Pd (only 1 wt. % of Pd).[123] The resultant Pd-doped MoS_2 afforded the overpotential of 78 mV at 10 mA cm^{-2} and an 805 μA cm^{-2} exchange current density, as well as a good matrix stability. Impressively, Wang *et al.* and Huang *et al.* uncovered that the doping of a small quantity of Pd could powerfully activate this otherwise non-electroactive TaS_2 and NbS_2 as highly excellent HER electrocatalysts.[125,126]

Table I summarizes the HER performance in the different media for various representative non-Pt NMN electrocatalysts with different element compositions.

B. Size control and morphological tuning

Modulating the size and shape of noble-metal nanocrystals with high surface area can efficiently improve the atomic utilization and expose more active centers, resulting in a gain in the HER catalytic activity.[20,74,127–141] In this regard, the ultrafine nanoparticle is the most common nanostructure. Generally, the nanoparticles could be fabricated by *in situ* growth or low-temperature reduction on various supports.[20,127,128] One kind of typical cases is to carbonize metal salt/organic molecule precursors that are tailorable in nanostructure and composition.[20,129] In this study from Nanda's group, a composite of ultrafine Ru nanocrystals loaded on N-doped graphene (Ru@NG-x) was prepared by employing dicyanamide (DCA) and $RuCl_3$ as the carbon precursor and metal source, respectively, and its micromorphology was effectively manipulated by the mass ratio of these raw materials (x).[129] The high-resolution TEM (HRTEM) images revealed that when x was equal to 2 or 4, the Ru nanocrystals in the Ru@NG samples had the average size of ~2 nm, while increasing x to 10 could cause a double increment in the diameter of Ru nanocrystals, approximately 4–5 nm. Through the electrochemical experiments in both acidic and alkaline electrolytes, it was confirmed that the catalytic activity for HER in the three samples (i.e., Ru@NG-2, Ru@NG-4, and Ru@NG-10) followed a sequence of Ru@NG-2 $\approx$ Ru@NG-4 $>$ Ru@NG-10, which was inversely in accordance with the trend of the Ru nanocrystal size: Ru@NG-2 $\approx$ Ru@NG-4 (~2 nm) $<$ Ru@NG-10 (4–5 nm). Further summary or analysis about this part is presented in Sec. IV C. Facile solvothermal synthesis was also developed to generate well-dispersed nanoparticles in the absence of supports. For example, Fu *et al.* designed monodispersed IrNiFe nanoparticles (NPs) with a mean size of 2.2 nm.[64] Benefitting from the ultrasmall monodispersed nanostructure and the strong electronic synergy

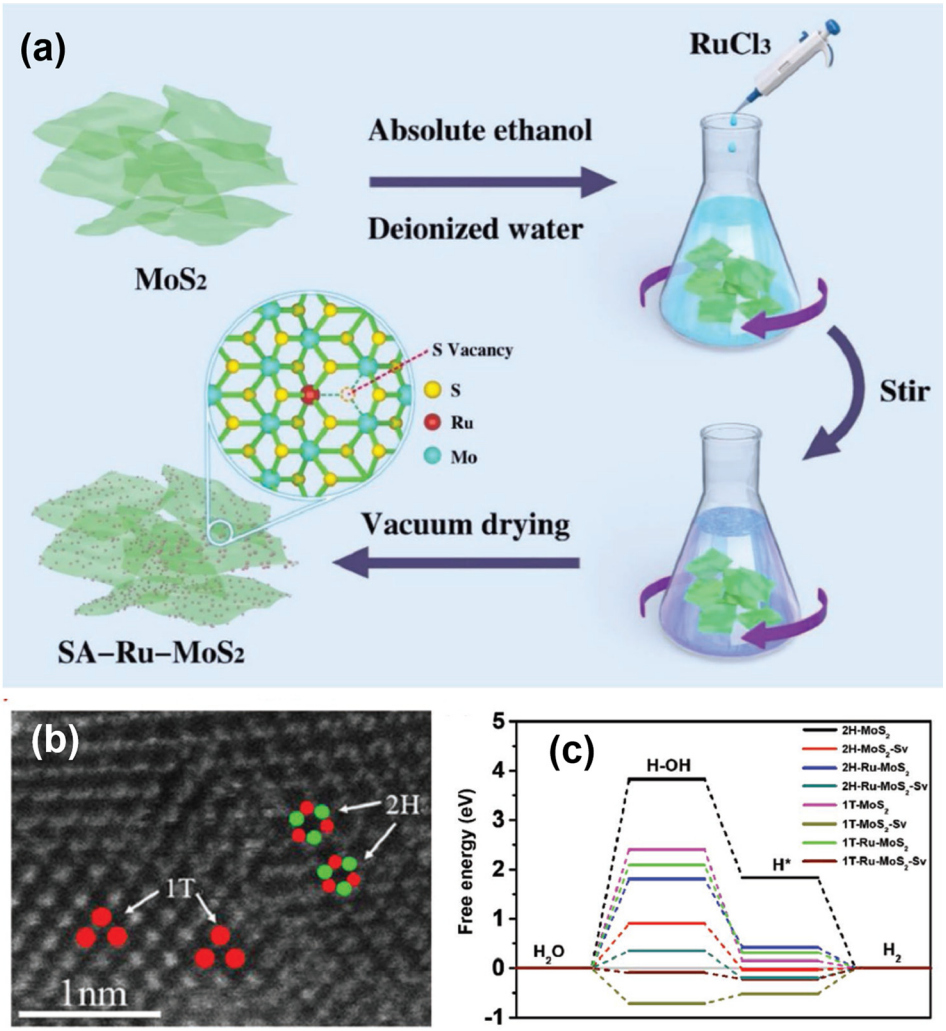

FIG. 14. (a) The schematic synthesis pathway of SA–Ru–MoS_2. (b) A dark-field scanning TEM image of the SA–Ru–MoS_2 sample. (c) Free energy diagrams toward the alkaline HER in different MoS_2 active sites. Reproduced with permission from Zhang *et al.*, Small Methods **3**(12), 1900653 (2019). Copyright 2019 Wiley-VCH.

between Ir, Ni, and Fe, the resulting $IrNi_{0.57}Fe_{0.82}$ sample allowed superior activity and high stability for both the HER and OER in 0.5 M $HClO_4$ aqueous solution. To yield a 10 mA cm^{-2} current density, this HER overpotential was only 24 mV. Wang *et al.* synthesized the ultrafine Au nanoparticles as acidic HER catalysts.[130] It was found that step-like structures were formed in these Au NPs during the consecutive electrochemical cycling process within the double layer region, which then triggered a dramatic enhancement in the HER activity. Specifically, the overpotential and Tafel slope was decreased by 128 mV and 23 mV dec^{-1}, as well as, the TOF value had a nearly twenty-time increase. Li *et al.* studied the effect of the Pd nanocube (NC) size on the HER activity.[134] Six samples with various particle sizes, ranging from 4.1 nm to 13.7 nm, were produced based on a solvothermal route with different halide species concentration (Br^- and Cl^-) and synthetic temperatures. The Pd NCs with 9.7 nm width showed a nearly 100% purity and afforded the optimal activity toward HER in acidic electrolytes.

Beyond the particle size, unique morphology may exhibit several novel physical and/or chemical properties and subsequently optimize the catalytic behavior.[134,135] In this aforementioned case reported by Li *et al.*, with the 9.7 nm-width Pd NCs as the seeds, different amounts of metal source, Na_2PdCl_4, were further introduced to prepare Pd nanoparticles with different shapes, i.e., truncated cubes, cuboctahedrons, truncated octahedrons, and octahedrons.[134] With the shapes varying from cube to octahedron, the proportions of Pd (100) to (111) crystal planes gradually decreased and so did the HER activity in acidic solutions. DFT calculations revealed that the Pd (100) facet had a higher electron density relative to the Pd (111) facet, thus offering more electrons during the HER process. Moreover, a stable intermediate state was more easily formed on the Pd (100) surface than on the Pd (111) surface. Guided by this fundamental proof, the same group subsequently fabricated the PdCu@Pd nanocubes with a Pt-like activity for hydrogen production under acidic conditions.[48] Similarly, Kuo and his co-workers recently reported the synthesis of well-defined silver nanocubes (AgNCs) with (100) plane and nano-octahedra (AgNOs) with (111) plane and studied their facet-dependent catalytic activities under acidic conditions.[135] It was observed that AgNOs (111) had better intrinsic activity for the electrocatalytic HER than that of AgNCs (100)

TABLE I. Performance of various representative non-Pt NMN HER electrocatalysts with different element compositions.

Catalyst	Electrolyte	Loading (mg cm^{-2})	Overpotential η_{10} (mV)	Tafel slope (mV dec^{-1})	Stability	References
Ir_6Ag_9 NTs	0.5 M H_2SO_4	13.3 μg_{Ir} cm^{-2}	20	27.5	−5 mA cm^{-2} @ 5 h	34
$Pd_{66}Ag_{17}Al_{17}$	1 M KOH	…	16.8	56	10 000 CV	35
	0.5 M H_2SO_4	…	∼35	26	30 000 CV	
Pd_3Ru	1 M KOH	0.015	42	…	…	39
Pd/Cu-Pt NRs	0.5 M H_2SO_4	0.040	22.8	25	5000 CV or −24 mV @ 15 h	41
PtRu	0.5 M H_2SO_4	13.9 μg_{Ru} cm^{-2}	8	25	10 000 CV or −15/40/30 mV @ 10 h	44
	1 M PBS		25	36		
	1 M KOH		19	28		
PtRu@RFCS-6h	0.5 M H_2SO_4	0.354	19.7	27.2	5000 CV or −10 mA cm^{-2} @ 48 h	43
RuAu-0.2	1 M KOH	0.056	24	37	1000 CV or −10 mA cm^{-2} @ 10 h	46
IrNi NCs	0.1 M $HClO_4$	12.5 μg_{Ir} cm^{-2}	19 (η_{20})	…	−5 mA cm^{-2} @ 2 h	50
IrNi NFs	0.1 M $HClO_4$	7.8 μg_{Ir} cm^{-2}	25	29.7	1000 CV or −10 mA cm^{-2} @ 6 h	51
AgNi-5	1 M KOH	1.32	24	61	−150 mV @ 5d	54
Au-Cu/CNFs-1:2	0.5 M H_2SO_4	…	83	70	−0.136 V @ 24 h	60
np-$Cu_{53}Ru_{47}$	1 M KOH	0.306	15	30	−15 mV @ 27 h	61
	1 M PBS		41	35	−40 mV @ 27 h	
IrW ND	0.1 M $HClO_4$	10.2 μg_{Ir} cm^{-2}	12	…	1000 CV	62
	0.1 M KOH		29	…		
IrNiTa MG nanofilm	0.5 M H_2SO_4	8.14 μg_{Ir} cm^{-2}	99	35	1000 CV or −10 mA cm^{-2} @ 10 h	65
Co-RuIr	0.1 M $HClO_4$	0.051	14	31.1	−10 mA cm^{-2} @ 25 h	67
$Ru_{38}Pd_{34}Ni_{28}$ NSs	1 M KOH		20	65	10 000 CV	68
$RuIrO_x$	0.5 M H_2SO_4	0.833	12	21	3000 CV	69
	1 M KOH		13	23		
w-Rh_2P NS	0.1 M $HClO_4$	0.0123	15.8	29.9	1000 CV	84
	0.1 M PBS		21.9	78.4		
	0.1 M KOH		18.3	61.5		
L-RuP	0.5 M H_2SO_4	0.185	19	37	−10 mA cm^{-2} @ 200 h	87
	1 M PBS		95	54		
	1 M KOH		18	34		
PdP_2@CB	0.5 M H_2SO_4	0.285	27.5	29.5	5000 CV or −27.5/84.6/35.4 mV @ 10 h	92
	1 M PBS		84.6	72.3		
	1 M KOH		35.4	42.1		
IrP_2@NC	0.5 M H_2SO_4	0.7	8	28	1000 CV	91
	1 M KOH		28	50		
RuS_2-500	1 M KOH	0.278	78	∼40	1000 CV	100
Hollow hexagonal Rh_2S_3	0.5 M H_2SO_4	0.153	122	44	10 000 CV	95
Li-$IrSe_2$	0.5 M H_2SO_4	0.25	55	…	−64/173/105 mV @ 10 h	99
	1 M PBS		120	…		
	1 M KOH		72	…		
Li-PPS	0.5 M H_2SO_4	0.282	52	29	10 000 CV or −20 mA cm^{-2} @ 12 h	103
Pd_2B NS	0.5 M H_2SO_4	…	15.3	22.5	1000 CV or initial −10 mA cm^{-2} @ 12 h	104
RuSi	0.5 M H_2SO_4	0.562	19	28.9	…	106
Rh_2C	1 M KOH	…	13 (η_5)	74.5	1000 CV or −5 mA cm^{-2} @ 10 h	73
HUST-100	0.5 M H_2SO_4	…	234	82	2000 CV	109
Rh-NiFe-LDH	1 M KOH	10.2 μg_{Rh} cm^{-2}	57	81.3	1000 CV	18
NiVIr LDH	1 M KOH	1.7	41 mV	55.3	2000 CV or −10 mA cm^{-2} @ 10 h	115
NiVRu LDH	1 M KOH	1.2	12	40	2000 CV or −50/200 mA cm^{-2} @ 200h	118

TABLE I. (*Continued.*)

Catalyst	Electrolyte	Loading (mg cm^{-2})	Overpotential η_{10} (mV)	Tafel slope (mV dec^{-1})	Stability	References
Ru–NiFe–P	1 M KOH	…	44	80	1000 CV	119
SA–Ru–MoS_2	1 M KOH	0.285	76	21	…	122
Pd-MoS_2	0.5 M H_2SO_4	0.222	78	62	5000 CV or −10 mA cm^{-2} @ 100 h	123

without laser irradiation, which could be due to the fact that AgNOs (111) had a lower hydrogen adsorption energy than AgNCs (100), thus leading to the easier hydrogen desorption on the AgNO (111) surface.

In 1D/2D nanostructures with anisotropic electron transport, nanowires, nanotubes, nanorods, and nanosheets have been widely reported to enhance the HER performance.[74,136–144] Huang's group proposed a facile and universal approach to prepare diverse wavy noble metal nanowires (NWs).[136] The synthesis was based on a wet-chemical route by uniformly mixing lead (II) formate [$Pb(HCOO)_2$], polyvinylpyrrolidone (PVP), and ethylene glycol ($C_2H_6O_2$), with different metal raw materials ($K_2RuCl_5{\cdot}H_2O$, $IrCl_3{\cdot}xH_2O$, K_2PtCl_4, or $RhCl_3$), and then undergoing a heat treatment at 180 °C, for diverse noble metal products. As a consequence, hcp-structured Ru and fcc-structured Rh, Ir, and Pt with the wavy nanowire shape were attained, respectively, as shown in Figs. 15(a)–15(f). Such wavy nanowire structures endowed these NMNs with ultrathin nature and massive defects that are instructive for electrocatalysis. All as-prepared noble metal NWs exhibited the outstanding HER performance comparable to the state-of-art Pt/C in both acidic and alkaline electrolytes, where the Ir wave NWs were the optimal ones with the overpotential of 15 and 38 mV at a 10 mA cm^{-2} current density in 0.5 M H_2SO_4 and 1 M KOH, respectively. Besides, these noble metal NWs as well as the RuO_2 NWs also showed attractive OER activity under both acidic and alkaline conditions, especially RuO_2 NWs. Coupling Ir NWs and RuO_2 NWs, an efficient water-splitting performance in different solutions was obtained, which was much superior to the results of the commercial Ir/C-Pt/C electrolyzer [Fig. 15(g)]. Subsequently, Huang's group further optimized the solid nanowires structure of Ir–Ag bimetal at the nanoscale by selective acid etching treatment into hollow Ir–Ag nanotubes.[34] According to experimental analysis, the optimized hollow nanostructure offered a higher surface area, favoring the formation of more active surface sites. Meanwhile, the surface was enriched in oxidized Ir atoms, which was highly active for both OER and HER catalysis. The synergistic control in morphological and electronic structures enabled the hollow Ir–Ag nanotubes with excellent bifunctional performance for both the HER and OER in the acidic environment. As another 1D nanostructure, IrO_2 or RuO_2 nanorods were also successfully constructed as highly efficient HER electrocatalysts.[74,141]

Regarding 2D nanosheets, ultrathin thickness is of paramount importance for electrocatalytic behavior, owing to likely more exposed active sites.[11,68,142–145] Kong *et al.* designed 2D Ru nanosheets via a facile solvothermal strategy and employed them as HER electrocatalysts.[144] The as-developed Ru nanosheets possessed ultrathin dimensions with only 5–7 atomic layers, good crystallinity, and a higher hydrogen adsorption (−0.289 eV) than the corresponding powder counterpart (−0.392 eV). Accordingly, they afforded excellent activity in 0.5 M H_2SO_4 aqueous solution, obviously better than the powder one. Zhao and his co-workers reported a high-temperature cyanogel-reduction approach to synthesize atomically thin RhCo nanosheet aggregates (RhCo-ANAs) with Rh *fcc* phase.[11] These nanosheets were about only 1.3 nm thin and chemically stable. They could serve as a robust electrocatalyst toward both the OER and HER in all pH ranges. In particular, under the neutral conditions where the electrocatalysis was relatively difficult to occur, RhCo nanosheet aggregates catalyzed the HER and OER with the η_{10} of only 31 and 310 mV, respectively, far lower than that of the benchmark samples, i.e., Pt/C and RuO_2 (55 and 480 mV, respectively). In 0.5 M H_2SO_4 and 1 M KOH solutions, the RhCo nanosheet aggregates also displayed better HER and OER activities than the benchmark Pt/C and RuO_2 samples, respectively [HER: RhCo: $\eta_{10} = 12.4/32.4$ mV (0.5 M H_2SO_4/1 M KOH); Pt/C: $\eta_{10} = 17.4/56.4$ mV (0.5 M H_2SO_4/1 M KOH)] [OER: RhCo: $\eta_{10} = \sim 250$ mV (0.5 M H_2SO_4/1 M KOH); RuO_2: $\eta_{10} = \sim 350$ mV (0.5 M H_2SO_4/1 M KOH)]. Besides, a remarkable stability was obtained for this catalyst. To further optimize the ultrathin nanosheet structure for enhancing the catalytic ability, constructing holes in them is an effective pathway that could largely increase the density of active sites, improve the mass transport efficiency, and promote electron transfer. However, it is still a challenging job for researchers and there are very few studies about the development of ultrathin noble metal NSs with porous structures. Li's group demonstrated the synthesis of a novel ordered porous nanosheet, i.e., an ultrathin Pd nanomesh (NM) through a top–down approach.[19] As depicted in Fig. 16(a), the initially obtained ultrathin Pd NSs were dispersed in a mixed solution of N,N-dimethylformamide (DMF) and distilled water with a volume ratio of 1:1 and then kept in ambient environment for 4 weeks, during which the moderate oxidative etching and removal of palladium atoms appeared, eventually generating the Pd NMs successfully. Noticeably, a slow or fast oxidative etching process by varying the operation conditions could lead to an unsuccessful transformation, with the formation of preserved Pd NSs and Pd wavy nanowires, respectively. The TEM images in Figs. 16(b) and 16(c) illustrated that in the ultrathin Pd NMs, ordered trigonal holes were widely created among the densely arrayed quasi-nanoribbons, and the corresponding width in average for holes and quasi-nanoribbons were approximately 11.4 and 3.4 nm, respectively. Additionally, according to the atomic force microscopy (AFM) measurements [Fig. 16(d)], the thickness of the Pd NSs was about 3.3 nm. In 0.5 M H_2SO_4, the Pd NMs exhibited high HER activity with a low η_{10} of 59.3 mV, which was close to the data of Pt/C [Fig. 16(e)]. After loading ultrafine Pt nanoparticles on Pd NMs (Pd NM/Pt, Pt: 13 wt. %), a smaller η_{10} of 21.3 mV was required, even

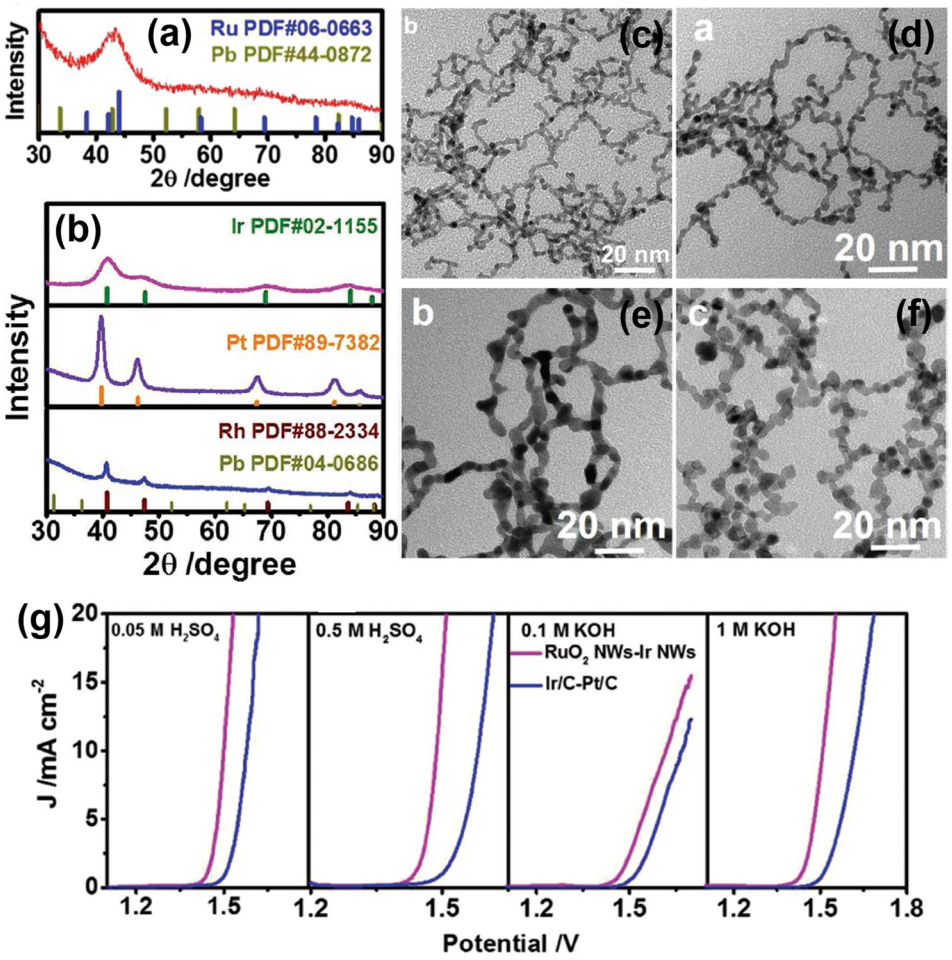

FIG. 15. X-ray diffraction (XRD) patterns of (a) Ru, (b) Ir, Pt, and Rh NWs. TEM images of (c) Ru, (d) Ir, (e) Pt, and (f) Rh NWs. (g) Overall water-splitting polarization curves of this RuO_2 NW–Ir NW couple and Ir/C-Pt/C in the pH-universal electrolytes. Reproduced with permission from Yang *et al.*, Adv. Funct. Mater. **28**(41), 1803722 (2018). Copyright 2018 Wiley-VCH.

surpassing Pt/C (27.7 mV). Furthermore, thanks to the unique nanostructure, the prominent activity of Pd NM/Pt was sustained after 2000 continuous cycles, while a 21% current drop under the overpotential of 50 mV was observed for the commercial Pt/C [Fig. 16(f)]. This finding opens a new avenue for designing unique porous framework in ultrathin 2D noble-metal NSs. Apart from the above three studies, there are also other studies on ultrathin 2D nanosheets as electrocatalysts for the HER, such as Rh NSs, Rh_2P NSs, RuPdM (M = Fe, Co, and Ni) NSs, RuCu NSs, and so forth.[68,84,143,145]

In Huang's group, different morphologies of metallic Rh, including tetrahedron (TH), concave tetrahedron (CT), and 2D nanosheet (NS), were well developed via simply tuning the OAm: 1-octadecene (ODE) volume ratio in the precursor solution (OAm: oleylamine and ODE: 1-octadecene), as observed from Figs. 17(a)–17(g).[15] Here, the different solvents with different reducing abilities governed the growth of diverse well-defined shapes. Experimental results suggested that the HER performance of metallic Rh nanomaterials was largely dependent on their morphologies. Rh NSs possessed a relatively larger electrochemical specific surface area and lower hydrogen binding energy, thus giving a better catalytic activity in the alkaline HER, even far outperforming Pt/C [Fig. 17(h)]. In the last year, a parallel study about various forms of Ag nanocrystals containing nanocube, nanowire, and nanosphere was also conducted by Mo *et al.*[146] They noticed that the Ag nanocubes had the highest HER activity at the applied potential of −1.5 V among the three forms owing to the lowest H adsorption strength. Rh_2P, with three nanostructures of monodisperse nanoparticle, monodisperse nanocube, and wrinkled nanosheet, was reported by three different groups, respectively, all of which demonstrated the phenomenal catalytic activity for HER in pH-universal electrolytes, obviously better than Pt/C. Figure 17(i) listed the comparison of their HER activity.[80,84,85]

Different from the above studies, several researchers also attempted to synthesize large-area and high-quality 3D porous nanoarchitectures.[147,148] Begum *et al.* presented the usage of a facile chemical method by the aid of the Zn precursor and cetyltrimethylammonium bromide (CTAB) surfactant to produce a 3D palladium nanonetwork (PdNN), in which the thickness of this network could be tunable via simply controlling the CTAB amount.[147] The as-obtained optimized PdNN had good 3D porous nanoarchitecture that was interwoven by plenty of 1D rod-like structures with a mean diameter of 4.9 nm. Such a unique 3D nanonetwork accelerated the electron transfer for the HER process and a large electrochemical

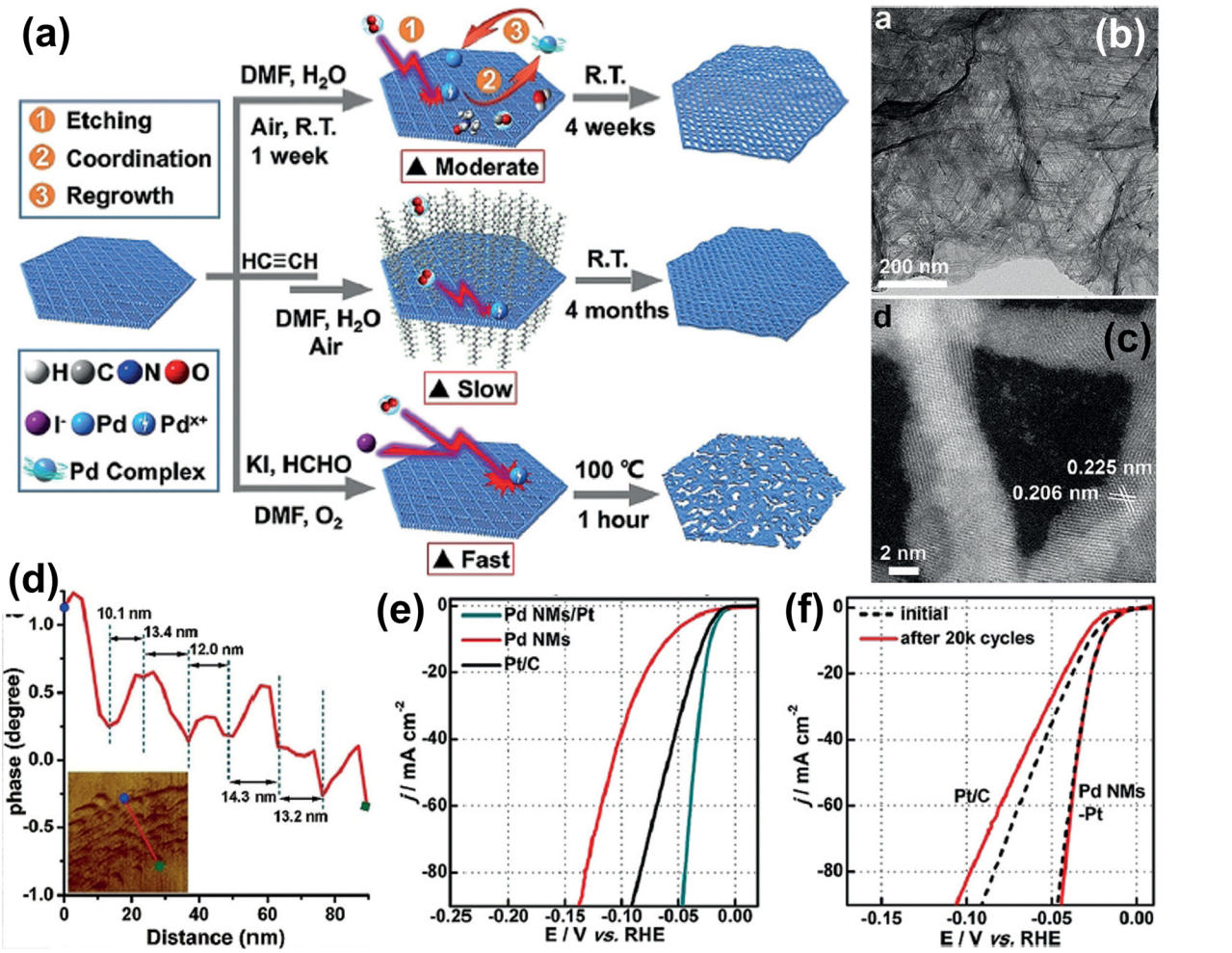

FIG. 16. (a) Illustration of the formation route of the ultrathin Pd NMs. (b) TEM and (c) HAADF-STEM images of Pd NMs. (d) The AFM result of Pd NMs. (e) HER polarization curves of Pd NMs/Pt, Pd NMs, and Pt/C in the acidic electrolyte. (f) The stability testing of Pd NMs/Pt and Pt/C. Reproduced with permission from Ge *et al.*, Angew. Chem., Int. Ed. **130**(13), 3493–3496 (2018). Copyright 2018 Wiley-VCH.

area provided highly HER active sites. Accordingly, its HER catalytic behavior under alkaline conditions was strengthened, in comparison with the particle counterparts. Also, based on an electrochemical surface treatment [Fig. 17(j)], an analogous nanomaterial, i.e., a spongy-like nanoporous Ag foam, was fabricated by Huang and Wu.[148] The treatment followed the repetitively electrochemical anodic formation of AgX (I, Br, or Cl)/cathodic reduction back to Ag (notably, the Ag product was named as Ag_X), where the growth rate of Ag played a crucial role in the final microstructure. Among three kinds of silver halides, the reducible ability of AgBr is neither strong nor weak, and hence causes a moderate Ag growth rate to finally form the high-density nanosized ligament in the Ag nanoporous network. As a HER electrocatalyst in 0.5 M H_2SO_4, the onset overpotential of Ag_{Br800} delivered an extraordinary diminution to 50 mV, which was around 200, 350, and 370 mV smaller than Ag_{Cl800}, Ag_{I800}, and the pristine Ag, respectively, as seen from Fig. 17(k).

A summary of the catalytic behavior toward the HER for various representative non-Pt NMN electrocatalysts with differed shapes in different media is shown in Table II.

C. Hybrid composite engineering

1. Bimetallic composites

As for the bimetallic nanostructures, apart from the conventional alloys, the novel core–shell-structured composites also have become the hotspot of the HER research field in the recent years.[149–153] Such nanostructures often exhibit improved catalytic properties for the HER because of a lattice strain generated in the boundary region of an ultrafine shell and internal core as well as a synergy during the course of electrocatalytic hydrogen production. In this topic about the noble metals, this core–shell structure with noble metal and noble metal or noble metal and transition metal are both exploited by different research teams.[149–155] Li's group, by using a combined solvothermal

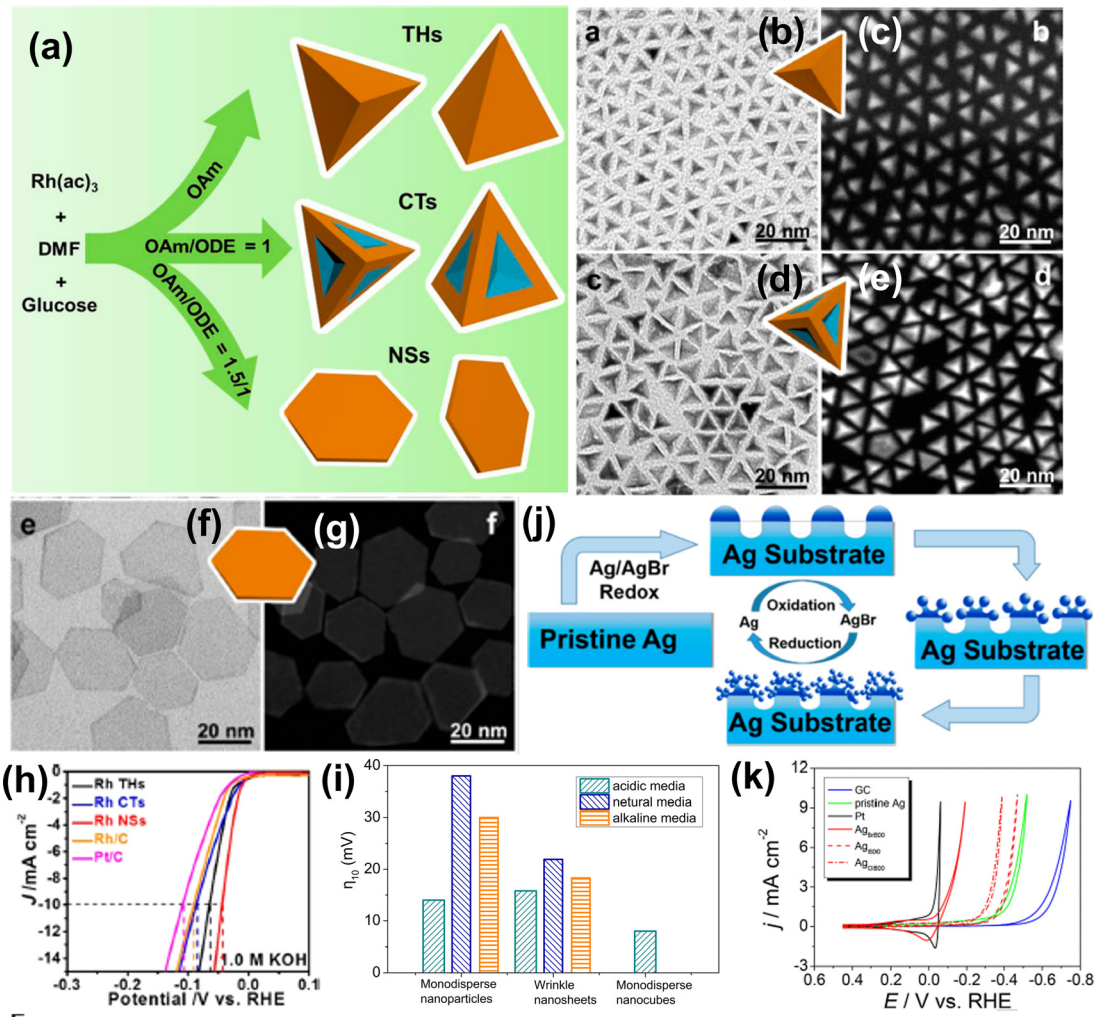

FIG. 17. (a) The synthetic procedure of the metallic Rh with different morphologies. (b), (d), and (f) TEM and (c), (e), and (g) HAADF-STEM images of Rh THs (b) and (c), Rh CTs (d) and (e), and Rh NSs (f) and (g). (h) HER polarization curves of Rh THs, Rh CTs, Rh NSs, Rh/C, and Pt/C in 1 M KOH. Reproduced with permission from Zhang *et al.*, Chem. Mater. **29**(11), 5009–5015 (2017). Copyright 2017 American Chemical Society. (i) The comparison of HER activities of Rh_2P with different nanostructures. (j) The formation route of the spongy-like nanoporous Ag foam. (k) The HER activity of different Ag electrodes and Pt in 0.5 M H_2SO_4. Reproduced with permission from Huang *et al.*, ACS Sustainable Chem. Eng. **6**(7), 8285–8290 (2018). Copyright 2018 American Chemical Society.

process, proposed the successful preparation of Pd@Ru core–shell nanorods with mesoporous structures, in which Pd and Ru were indexed to the face centered cubic phase (fcc) and the hexagonal close-packed phase (hcp).[149] With the presence of the Ru/Pd interface, an improved electrocatalytic property for alkaline HER with a low overpotential of 30 mV at a current density of 10 mA cm^{-2} and much large mass activity of 722.9 A g^{-1} at the overpotential of 60 mV was observed in comparison with pure Pd and Ru. In the Qiao's group, the reported core–shell Ru@Pt nanostructure expressed much more excellent HER catalytic peculiarities than the conventional strain-free RuPt alloy.[151] The strain effect on the Pt structure induced by Ru core dominantly enhanced the HER intrinsic activity in the alkaline environment. Specifically, the Pt shells with a highly compressive strain effectively accommodated an interfacial lattice mismatch from the fcc-structured Ru core, which enabled better interaction towards both hydrogen and hydroxyl species during this reaction, in turn, accelerating the ensemble HER process. Based on a most recent work by Bian *et al.*, the core–shell Au–Rh star-shaped decahedra was synthesized via the seed-mediated growth with decahedral Au nanoparticles as seeds.[154] From the HRTEM observations, these as-prepared core–shell nanoparticles showed a diameter of about 10 nm and the (111) planes were the dominated exposed facets [Figs. 18(a) and 18(b)]. By adjusting the amounts of Rh precursors, the researcher tuned the thickness of Rh shell. To yield the 10 mA cm^{-2} current density in the 0.5 M H_2SO_4 electrolyte, the optimal core–shell $Au_{75}Rh_{25}$ decahedra needed an overpotential of 64.1 mV, lower than the value of the Rh/C catalyst by 39.4 mV [Fig. 18(c)] and its Tafel slope (33.8 mV dec^{-1}) was also comparable to the benchmark Pt/C (30.2 mV dec^{-1}) [Fig. 18(d)]. As

TABLE II. Performance of various representative non-Pt NMN electrocatalysts with differed shapes.

Catalyst	Electrolyte	Loading (mg cm^{-2})	Overpotential η_{10} (mV)	Tafel slope (mV dec^{-1})	Stability	References
Ru@NG-2	1 M H_2SO_4	0.857	74	48	5000 CV or −100 mV @ 10 h	129
	1 M KOH		47	82		
$IrNi_{0.57}Fe_{0.82}$ NPs	0.5 M $HClO_4$	92 μg_{Ir} cm^{-2}	24	34.6	1000 CV or −10 mA cm^{-2} @ 5.5 h	64
Au NPs	0.5 M H_2SO_4	…	128	23	…	130
Pd NCs	0.5 M H_2SO_4	0.14	37 (onset)	62	…	134
Pd Octahedrons			>150 (onset)	98	…	
AgNCs	0.5 M H_2SO_4		>300	…		135
AgNOs			>400	…		
Ir NWs	0.05 M H_2SO_4	40.7 μg_{Ir} cm^{-2}	17	26	…	136
	0.5 M H_2SO_4		15	34	…	
	0.1 M KOH		73	46	…	
	1 M KOH		38	30	…	
Ir_6Ag_9 NTs	0.5 M H_2SO_4	13.3 μg_{Ir} cm^{-2}	20	27.5	−5 mA cm^{-2} @ 5 h	34
Ru nanosheet	0.5 M H_2SO_4	0.102	20	46	…	144
Ru powder			30	76	…	
RhCo-ANAs	0.5 M H_2SO_4	2	12.4	30.7	…	11
	1 M PBS		31	33.6	−50 mV @ 5 h	
	1 M KOH		32.4	31.9	…	
Pd NMs	0.5 M H_2SO_4	0.02	59.3	57	…	19
Rh THs	0.1 M KOH	15.3 μg_{Rh} cm^{-2}	64	79.5	−5 mA cm^{-2} @ 5 h	15
	1 M KOH		63	113.5		
Rh CTs	0.1 M KOH		66	117.7		
	1 M KOH		84	114.2		
Rh NSs	0.1 M KOH		37	74.7		
	1 M KOH		43	107.2		
Monodisperse Rh_2P NPs	0.5 M H_2SO_4	0.0306	14	31.7	1000 CV	85
	1 M PBS		38	46		
	1 M KOH		30	50		
w-Rh_2P NS	0.1 M $HClO_4$	0.0123	15.8	29.9	1000 CV	84
	0.1 M PBS		21.9	78.4		
	0.1 M KOH		18.3	61.5		
Monodisperse Rh_2P NCs	0.5 M H_2SO_4	3.7 μg_{Rh} cm^{-2}	~8	…	−1.72 mA mg_{metal}^{-1} @ 2000 s	80
3D PdNN	1 M KOH	16.9 μg_{Pd} cm^{-2}	110	121	1000 CV or −110 mA cm^{-2} @ 4.2 h	147
PdNPs		22.6 μg_{Pd} cm^{-2}	170	133		
Nanoporous Ag foam Ag_{Br800}	0.5 M H_2SO_4	…	50 (onset)	119	5000 CV or −0.12/0.15/0.18 V @ 60 h	148

the authors corroborated using computational calculations [Figs. 18(e) and 18(f)], the ensemble effect played the dominating role in promoting the hydrogen-production reaction rate by exposing some Au atoms on the Rh surface instead of the complete coverage by Rh shells. For the core–shell nanostructures composed of noble metal and TMs, core–shell Ag–Ni nanowires manifested superior HER activity under the alkaline conditions.[137] The pronounced electron interplay from the inter Ag gave rise to a remarkable increase in the catalytic performance when the optimized Ag/Ni atomic ratio was 1:1. Besides, the 1D nanostructure and conductive Ag nanowires further favored the HER by the exposure of more surface active sites and rapid charge transport. Starting with core–shell Pd/Fe_3O_4 nanoparticles, Xu's group adopted the electrochemical cycling to control coverage of $FeO_x(OH)_{2-2x}$ on the Pd surface [Figs. 19(a) and 19(b)], which provided additional water-dissociation sites for increasing the proton supply.[153] Markedly, at 40% coverage, the HER activity was improved by

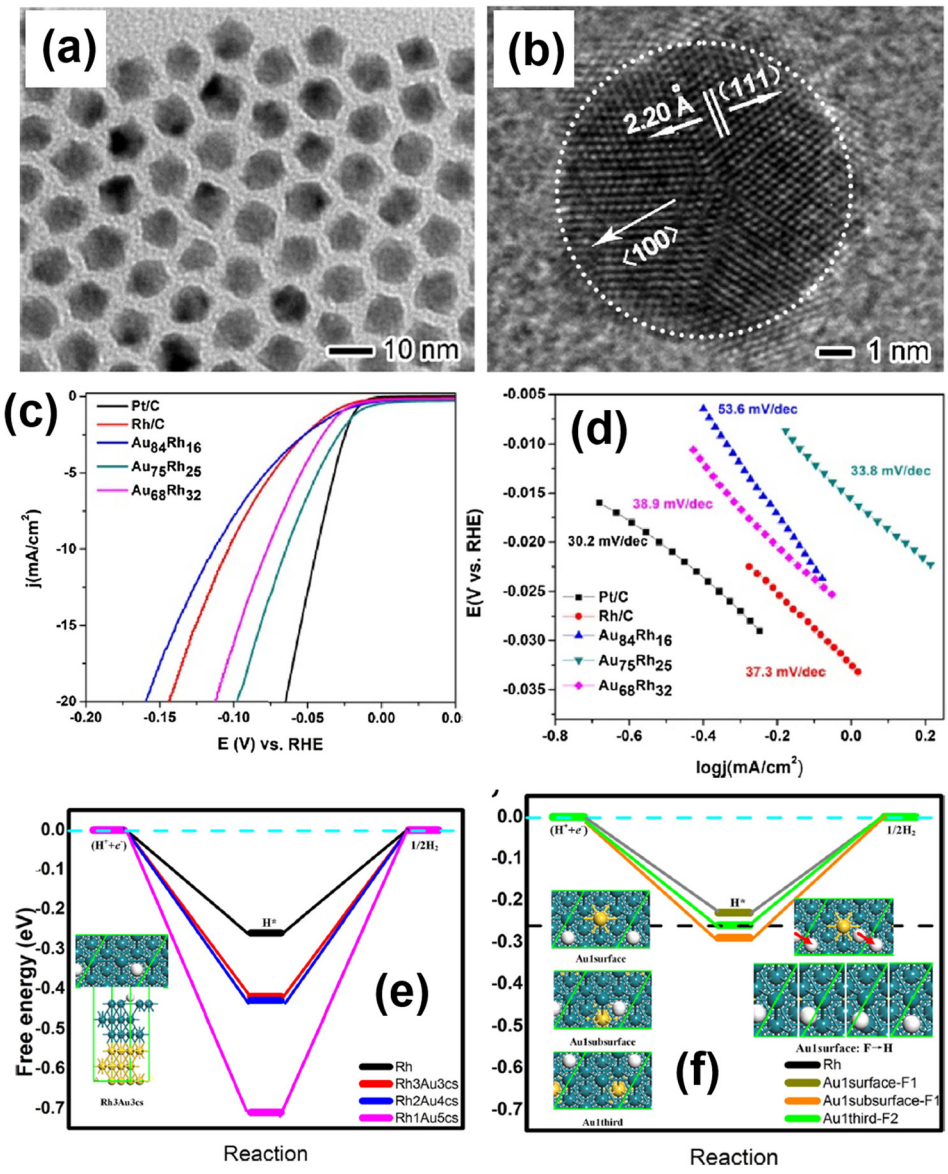

FIG. 18. (a) TEM and (b) HRTEM images of the core–shell Au–Rh star-shaped decahedra. (c) HER polarization curves and (d) the corresponding Tafel plots of $Au_{68}Rh_{32}$, $Au_{75}Rh_{25}$, $Au_{84}Rh_{16}$, Rh/C, and Pt/C in acidic media. The free energy diagrams of (e) the core–shell structure and (f) alloyed structure. Reproduced with permission from Bian *et al.*, Appl. Catal. B **263**, 118255 (2020). Copyright 2020 Elsevier.

19 folds of the results of pure Pd NPs [Fig. 19(c)], because such coverage could balance the water-dissociation rate and hydrogen-recombination rate to reach the highest efficiency. Besides these above studies, Ir–Ag core–shell nanotubes, Au@Pd core–shell nanoparticles, Au–Pt core–shell nanoparticles, core–shell Pt@Pd nanoflowers, Co@Pd core–shell nanoparticles, and Ni@Pd core–shell nanospheres are also proposed for the electrocatalytic HER.[34,155–159]

Slightly different from the simple core (monometal)–shell (monometal) structure, some groups utilized the bimetallic alloy as the core or shell for further amelioration of the activity.[60,160–163] Typically, Lv *et al.* first adopted the low-temperature solvothermal reduction to fabricate the alloyed NiAu nanoparticles as the pre-catalyst, and then electrochemical cycling between 0.6 and 1.0 V was conducted to transform the NiAu alloy to a core–shell NiAu/Au nanostructure.[160] This designed core–shell material exhibited much improved HER catalysis with a Pt-like activity and highly strong robustness. Theoretical results showed that these low-coordination Au sites around the shell were the main origin of the high activity. Such strategy could also be extended to other Au-based alloys, such as CoAu and FeAu. According to the study of Li *et al.*, a selective etching-deposition route was proposed to realize the implantation of trace Pd atoms into the near-surface lattice of Ag nanocubes, so as to form a heteroatom-rich Pd–Ag shell on the surface of Ag (Ag@PdAg).[162] Such atomic dilution substantially promoted electronic desorption of adsorbed H species. Consequently, the catalytic activity for HER was considerably increased by ∼14 times of that of Pd catalysts, along with a high endurance. Furthermore, a unique core–shell Pd@PtCu dodecahedron

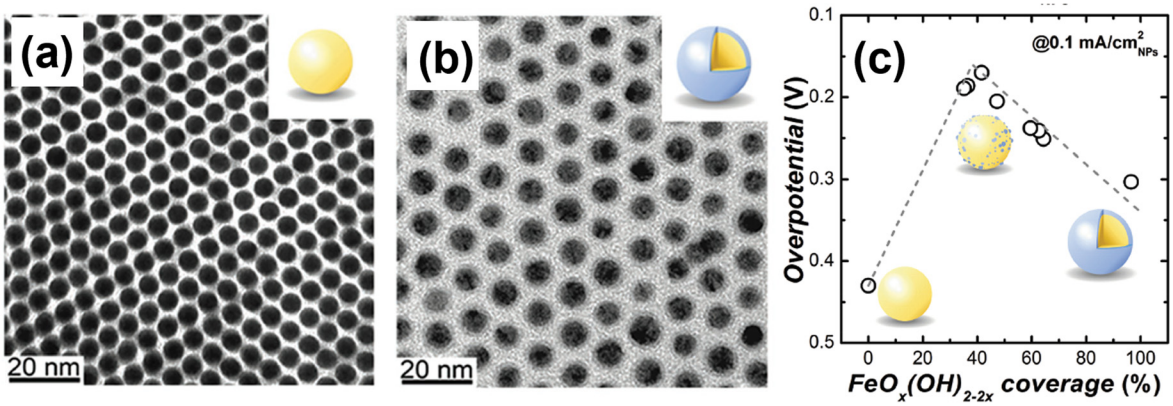

FIG. 19. TEM images of (a) Pd nanoparticles and (b) core–shell Pd/Fe_3O_4 nanoparticles. (c) The HER activity as a function of the $FeO_x(OH)_{2-2x}$ coverage. Reproduced with permission from Liao *et al.*, Adv. Energy Mater. **7**(21), 1701129 (2017). Copyright 2017 Wiley-VCH.

nanostructure was also reported by Mu's group, which demonstrated the extraordinary HER catalytic properties in acidic media.[163]

In addition, a handful of simple bimetallic heterostructure composites (M/M) without the core–shell structure were also synthesized for catalyzing HER.[164–166] For example, a Pd–Pt heterostructure, composed of Pt nanoparticles grown on Pd (100) nanosheets, could induce more free electrons transfer from Pd (100) to Pt, and thus recorded a Pt-outperformed electrocatalytic activity in base.[164] Besides, Joshi *et al.* physically mixed the Ru and W powder as an efficient electrocatalyst and discovered that a remarkable synergistical interaction was created in this mixture.[165] Typically, the d-band of Ru was decreased and its electron work function was increased, which were well supported by the calculation and experimental data. As such, the hydrogen-binding energy of the surface Ru was tuned to approach that of Pt(111), which in turn, led to the improvement of catalytic behavior. In a 0.5 M H_2SO_4 electrolyte medium, the overpotential at the current density of 10 mA cm^{-2} was 85 mV, much less than those of individual Ru and W (∼165 and 465 mV, respectively).

2. Hybridizing with stable metal compounds

According to extensive research, assembling NMNs with some stable metal compounds (such as transition metal oxides, hydroxide, chalcogenides, phosphides, nitrides, carbides, etc.) to form the heterostructured hybrids has been demonstrated to effectively boost the HER electrocatalytic property, owing to the chemical and electrical synergy between NMNs and other compounds.[79,167–183] Also, the good cost-competitiveness is balanced from a lowered amount of noble metals. Among a plethora of metal compounds, the 2D layered metal dichalcogenides, typically MoS_2, as the host material for hybridizing with noble metals are well documented.[184–194] Previously in 2015, a seminal study highlighted that Au metal localized surface plasmon resonance could activate the HER activity of MoS_2, with a about threefold improvement in the current density.[184] In this case, a hybrid of Au nanorods assembled onto exfoliated MoS_2 nanosheets (Au–MoS_2) was constructed, in which Au metal was identified as a light absorber to excite electron–hole pair while MoS_2 nanosheets acted as the electron acceptor and active centers to promote hydrogen production. Accordingly, the charge density of MoS_2 nanosheets was substantially increased, which in turn, modulated the energy level of this material more suitable for HER. Afterwards, following the metal-seeding principle, Li and his co-workers witnessed a unique design of vertically aligned and winged MoS_2 nanolayer surrounding the Au nanoarchitectures (w-Au@MoS_2), which resulted in the generation of plentiful edge-terminated active sites for driving hydrogen production, and simultaneously offered a low-resistance electron transport pathway within the w-Au@MoS_2 nanostructures through the mediation of the Au core.[186] Therefore, an enhanced and high-efficiency hydrogen evolution process in an acidic electrolyte was realized. Furthermore, in the last year, Zheng's group integrated ultrasmall Ir species with 2H-MoS_2, namely, Ir/MoS_2 heterostructures, through a simple two-step solvothermal method, and found an interesting phase transformation from 2H to 1T of MoS_2.[190] During the synthesis, $(NH_4)_6Mo_7O_{24}{\cdot}4H_2O$, and thiourea were first uniformly dissolved in water with the aid of stirring, and was heated at 220 °C for 18 h in a stainless steel autoclave. Subsequently, the as-obtained MoS_2 nanosheets were dispersed into ethylene glycol under ultrasonic treatment with adding a certain amount of H_2IrCl_6, and then the system was heated at 160 °C for 3 h. Thus, the Ir/MoS_2 heterostructures were produced. The coupling of the computational and experimental data stated that such phase transition was caused by the strong interaction between the MoS_2 support and Ir metal. From the HAADF-STEM images in Figs. 20(a)–20(e), it was shown that the as-formed 1T phase was present in these regions of MoS_2 surrounded by Ir nanoparticles. When applied as the electrocatalysts for HER and OER in alkaline solution, it only took the Ir/MoS_2 heterostructure a low overpotential of 44 and 330 mV, respectively, to reach a 10 mA cm^{-2} current density, and a Tafel slope of 32 and 44 mV dec^{-1}, respectively, superior to these data of the benchmark Pt/C and IrO_2 [Figs. 20(f)–20(i)]. Besides, a two-electrode water electrolyzer with the Ir/MoS_2 heterostructure as electrocatalysts offered a high performance, with a cell potential of only 1.57 V at the current density of 10 mA cm^{-2} [Fig. 20(j)]. The outstanding catalytic behavior of this material could be correlated to several aspects, i.e., enhanced electrical conductivity from 1T phase, better hydrophilicity and more active centers derived from numerous heterojunction interfaces, along with the synergy-promoted reaction kinetics.

Similarly, around the same time, a composite catalyst consisting of a bimetallic nanostructure (single-side-nucleated Au nanoislands with Pd nanosheets) co-assembled on the 2H-MoS_2 surface was

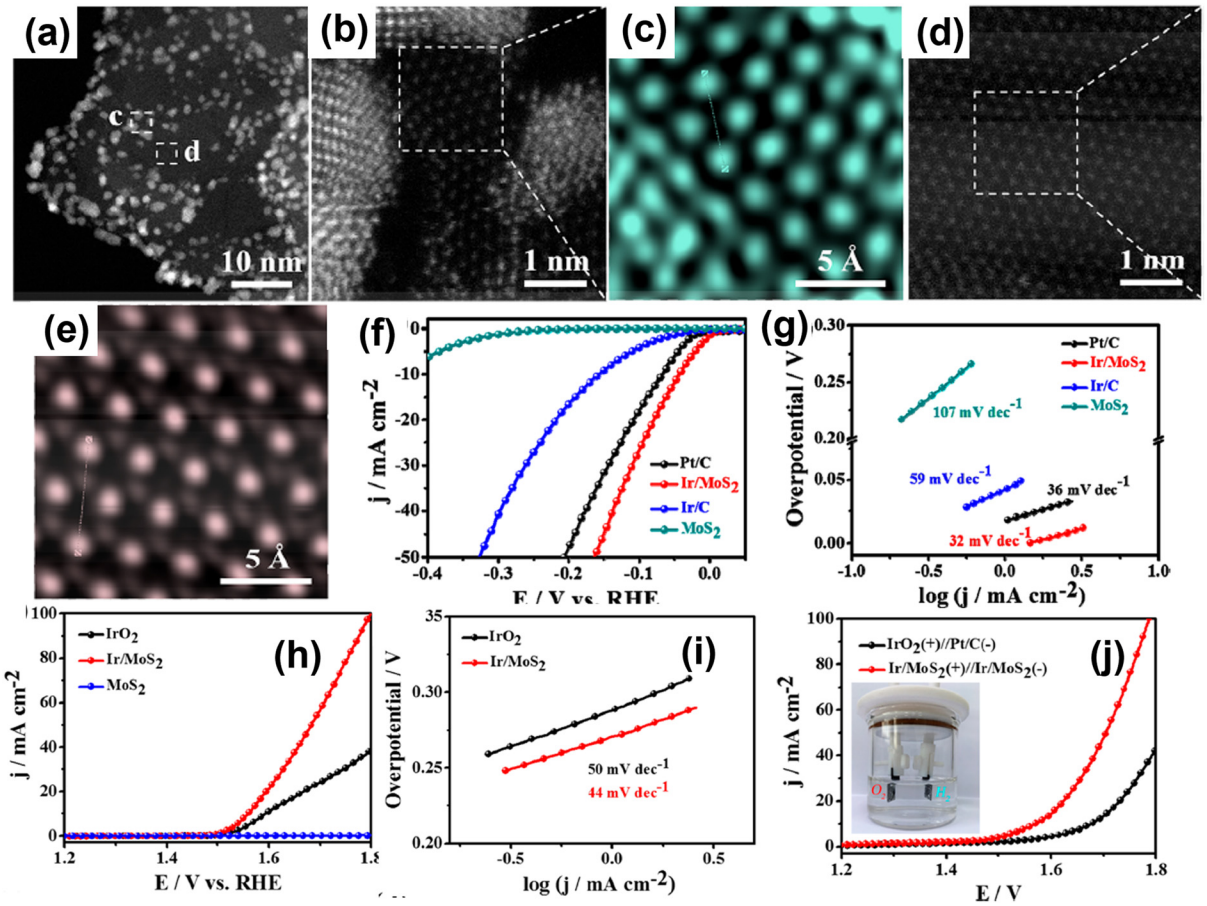

FIG. 20. (a) HAADF-STEM image and (b) and (d) the corresponding magnified one of the (c) and (d) areas in (a). (c) and (e) Filtered enlarged images of the marked parts in (b) and (d). (f) LSV curves and (g) corresponding Tafel plots of the Ir/MoS_2 heterostructure, MoS_2, commercial Ir/C, and Pt/C for the HER in 1 M KOH. (h) OER polarization curves and (i) the corresponding Tafel plots of the Ir/MoS_2 heterostructure, MoS_2, commercial IrO_2 in 1 M KOH. (j) The overall water-splitting activity of Ir/MoS_2–Ir/MoS_2 and commercial IrO_2–Pt/C in 1 M KOH. Reproduced with permission from Wei *et al.*, ACS Energy Lett. **4**(1), 368–374 (2018). Copyright 2018 American Chemical Society.

developed to also create the stable 1T-phase-dominated MoS_2 at the contacted area and manifested a dramatic improvement of catalytic activity for the HER under acidic conditions.[187] DFT results pointed out that lattice-mismatch-induced compressive strain evoked such a phase transition. As to the Rh-MoS_2 nanocomposite with a small amount of Rh (ca. 5.2%), driven by the H spillover from Rh to MoS_2, the hybrid material paralleled the satisfactory HER catalytic activity of the commercial Pt/C in acid.[192] In Yang's group, the exploited nanocomposite of single Ru atoms adhered to MoS_2 nanosheets on a carbon cloth substrate also had an attractive HER activity with the η_{10} values of 41, 61, and 114 mV in different electrolytes (1M KOH, 0.5 M H_2SO_4, and 1 M PBS, respectively.).[195] Such a nanostructure was revealed to contain a great deal of atomic Ru active sites, increased electrical conductivity and 3D porous architecture for rapid mass transfer, as well as a synergistic electron interplay, thus propelling its activity remarkably.

Regarding other metal compounds, various typical examples are also listed below. The strongly coupled Mo_2N–Au nanostructure displayed an electrocatalytic performance for the HER approaching to that of commercial Pt/C.[196] Pd nanoparticles sized ca. 3 nm firmly supported on flowerlike $NiCo_2S_4$ hollow sub-microspheres also presented low overpotentials of 83 and 87 mV to yield a 10 mA cm^{-2} current density toward the HER in 1 M KOH and 0.5 M H_2SO_4, while those for either Pd or $NiCo_2S_4$ were much larger.[197] Recently, Song and his co-workers fabricated Ag nanodots decorated the porous Cu_2O nanobelts network on the Cu foam (Ag@Cu_2O/CF) by the simple *in situ* growth in a mixed solution at room temperature [Fig. 21(a)].[198] Such Ag@Cu_2O/CF maneuvered a substantially boosted HER catalytic behavior, specifically with a η_{10} of 108 mV, a Tafel slope of 58 mV dec^{-1}, as well as excellent durability for over 20 h in alkaline media [Figs. 21(b)–21(d)]. This enhancement of performance was originated from the 3D porous nanoarchitecture that provided an abundance of Ag active centers, enabling an effective utilization of Ag metal and offering rapid charge/mass transportation pathway in catalyzing the HER, and more significantly the strong synergistic interaction between different parts, which tuned the H adsorption–desorption rate to reach a more suitable value [Fig. 21(e)]. Likewise, Ag nanoparticles were coupled with tungsten oxide (WO_3) to create a heteroarchitecture (denoted as Ag–WO_3).[199] The resultant intimate interplay between Ag and WO_3 also recorded an excellent

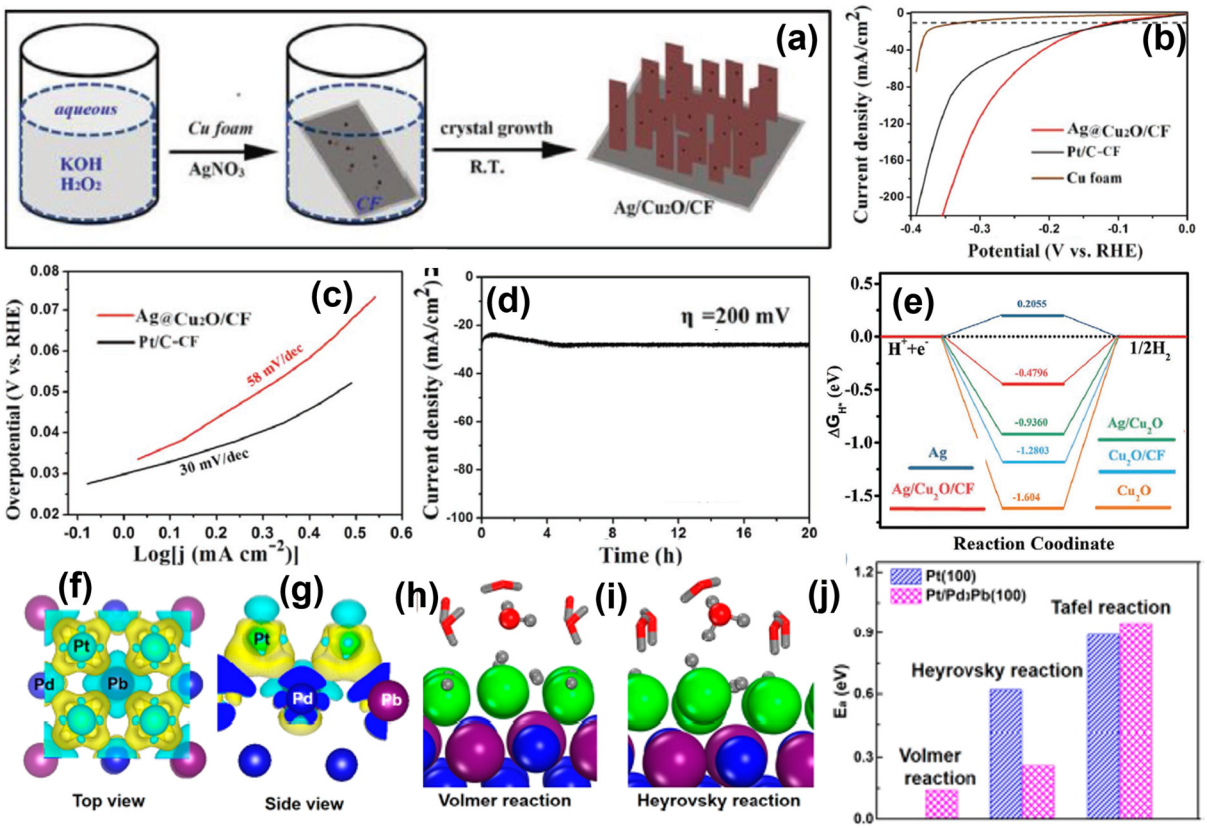

FIG. 21. (a) The synthesis route of the Ag@Cu_2O/CF hybrid. (b) HER polarization curves and (c) Tafel plots of different electrocatalysts in the alkaline solution. (d) Long-term durability test of this Ag@Cu_2O/CF composite. (e) The H-adsorption free energy of different materials. Reproduced with permission from Song *et al.*, Small **15**(29), 1804268 (2019). Copyright 2019 Wiley-VCH. (f) and (g) Charge density distribution model of the Pt/Pd_3Pb hybrid. Transition states for the (h) Volmer and (i) Heyrovsky steps on the surface of Pt/Pd_3Pb. (j) The calculated reaction barriers for different steps. Reproduced with permission from Yao *et al.*, J. Am. Chem. Soc. **141**(51), 19964–19968 (2019). Copyright 2019 American Chemical Society.

catalytic activity for the HER in acidic electrolytes. In another recent study, Yao *et al.* controllably deposited Pt submonolayer on Pd_3Pb nanoplates, namely, AL–Pt/Pd_3Pb. Such a heterojunction structure greatly optimized the electronic structure and atomic utilization efficiency of the active Pt atomic layer, thereby markedly improving the HER performance in acid.[200] Compared to commercial Pt/C, the overpotential at 10 mA cm^{-2} for AL–Pt/Pd_3Pb was lowered by ~16 mV (30 mV for Pt/C vs 13.8 mV for AL-Pt/Pd_3Pb) and its corresponding mass activity at the overpotential of 50 mV was increased by four times (1486 A/g_{Pt} for Pt/C vs 7834 A/g_{Pd+Pt} for AL–Pt/Pd_3Pb). DFT calculation results disclosed that a strong electrostatic interaction was created due to the electron transfer from Pd_3Pb to Pt, which could make the transition state stabilized and decrease the reaction barrier, so as to afford the enhanced activity [Figs. 21(f)–21(j)].

A hydroxide–metal–hydroxide composite system consisting of $Co(OH)_2$, Au, and $Ni(OH)_2$ has also been produced by Sultana and his co-workers to form multiheterogeneous $Co(OH)_2$–Au–$Ni(OH)_2$ nanosheets.[201] During the synthesis, highly distributed Au with a very low concentration was first attained through the galvanic replacement of $Co(OH)_2$, and then the as-formed Au directed the electrodeposition of $Ni(OH)_2$, enabling it homogeneous distribution on the surface. Notably, via adjusting the Au amount from 0.1 to 0.2 at. %, this composite material showed optimal activity toward the HER and OER. Moreover, it was found that in both cases Au was no longer confined to the middle of the material, but was redistributed throughout the composite sample on basis of electrochemical activation operation, which activated the overall catalysis process.

3. Integrating with conductive substrates

To further optimize the catalytic behavior of noble-metal materials under the HER conditions, integrating NM-based materials with some relatively conductive substrates is another impactful strategy.[20,127–129,202–216] Here, this robust conjugation between active noble-metal phases and conductive supports not only addresses the limitations of electric conductivity, but also shrinks the particle size and increases the dispersity of the metal particles along with reducing their dosage. Moreover, the strong synergistic effects can also take place between the two constituents, which will modulate the electronic structure, accelerate the charge transfer of them, and amend the hydrogen adsorption/desorption behavior, thereby promoting the hydrogen production.

a. Carbon-related supports. As for carbon supports, some representative merits, such as the superior conductivity, well-developed

pore architecture, controllable molecular structure, strong resistance to chemical attack, etc., make them hold a great promise as the matrixes. Up to now, plentiful composites of various nanocarbon supports with noble metal-based nanomaterials have been established, such as Pd NPs@N-carbon nanotubes (CNTs), Ru@ self-crosslinking (SC)-carbon quantum dots (CQDs), Au@NC, etc.[37,60,217–231]

Graphenes (G)/reduced graphene oxides (rGO) and carbon nanotubes (CNTs) are versatile candidates to support the noble metal-based particles for the HER.[37,221–227] For instance, Au–Ag nanocrystals with the multiply twinned structure directly grown on rGO hybrids (Au–Ag NC/rGO) were created by a facile microwave irradiation process.[37] The as-prepared Au–Ag NC/rGO displayed outstanding HER electrocatalytic activity and stability, characterized by small overpotentials and Tafel slopes, which was comparable to the commercial Pt/C. The high HER performance was related to abundant twin defects and the intimate electronic coupling between Au–Ag alloys and rGO. Recently, the hybrid Ir_VG (Ir on vertical graphene) developed by Roy *et al.* manifested remarkable catalytic peculiarities toward all-round water-splitting reactions (HER and OER in both the acid and base).[221] The resultant sample was produced through the novel e-beam evaporation technique with the minimal Ir mass loading, i.e., 50 μg cm^{-2}. Under acid and alkaline conditions, the Ir_VG showed the low η_{10} overpotentials (47 and 17 mV for HER, respectively; 300 and 320 mV for OER, respectively) and favorable Tafel slopes (43 and 29 mV dec^{-1} for the HER, respectively; 59 and 53 mV dec^{-1} for the OER, respectively), as well as excellent robustness. Similar to the aforementioned analysis, the highly active Ir species, the excellently conductive and superaerophobic VG, and the strong binding between them synergistically favored the overall catalytic process. For CNT substrates, Pd nanoparticle (Pd NP) hybridized N-doped CNTs were prepared by the electroless deposition of the K_2PdCl_4 solution.[222] At the overpotential of 100 mV, a current density of 32 mA cm^{-2} was reached for the Pd NP@N–CNT hybrid. Besides, polyallylamine-functionalized Rh nanosheet nanoassemblies supported on CNTs (PAH@Rh-NSNS/CNTs) were proposed by Bai and his co-workers.[225] Benefiting from the ultrathin morphology of 2D Rh nanosheets and 3D CNT networks, the PAH@Rh-NSNS/CNT nanohybrid functioned well as a HER electrocatalyst in acidic media. The observed overpotential at 10 mA cm^{-2} was just 5 mV, which was much better than that of commercial platinum nanocrystals.

Additionally, several other well-known carbon nanomaterials, such as XC-72 Vulcan carbon, Ketjenblack, graphite, carbon quantum dots (CQDs), and so forth, were often engaged as ideal conducting substrates to hybridize noble-metal nanomaterials.[49,50,127,128,229,232] Hu's group developed a facile solid-state approach [Fig. 22(a)], in which the mixed precursors [NaOH, $NaBH_4$, MCl_3 (M = Rh, Ru, and Ir), and carbon supports] were directly grinded in an agate mortar at room temperature, to anchor a series of noble metal nanoparticles (Rh, Ru, and Ir) on various carbon supports, such as XC-72 Vulcan carbon, Ketjenblack, Super P, etc., and eventually form the M NP/C (M = Rh, Ru, Ir) nanohybrids.[127] All resulting samples featured these noble metal NPs with an ultrasmall size, a good uniformity, and a high dispersion on the carbon matrixes [Fig. 22(b)]. The authors pointed out that such morphological properties were free from the types and surface areas of carbon, but was largely related to the standard reduction potentials of different metals. The lowest redox potential for Ru/Ru^{3+} corresponded to the smallest size, followed by Rh metal, and then Ir metal with the largest size [Figs. 22(c)–22(e)]. What's more, in absence of carbon supports, irregular and interconnected large particles were observed. By virtue of the high intrinsic activity of noble metals and above features, all as-prepared materials, i.e., Rh NP/C, Ir NP/C, and Ru NP/C, showed impressive HER activities and durability in 1 M KOH, among which, Rh NP/C was the most excellent one with only a 7 mV overpotential at 10 mA cm^{-2} [Fig. 22(f)], ranking among the top series of these noble metal electrocatalysts used for alkaline HER. Soon afterwards, the same group reported an analogous crafting of ultrafine-sized platinum-group metals (Ir, Rh, and Ru) well-dispersed on the as-formed porous carbon (PC) via efficient electroless deposition. This deposition process was triggered by surface oxygen-based-functional group-functionalized PC with strong reducibility.[128] As expected, these obtained nanohybrids also granted a remarkable catalytic performance toward hydrogen production in both alkaline and acid media. Freestanding zero-valent Pd (Pd^0)/graphdiyne (GDY) composites on carbon cloth was also constructed by solvothermal treatment of carbon cloth (CC) with pyridine and following electrochemical deposition in $PdCl_2$ solution, which contained the vertical arrays of interlaced GDY nanosheets on the surface of the smooth interweaved carbon fibers and the firmly attached Pd^0 atoms on GDY with a very low loading of about 0.2 wt. %.[223] Such chemical composition and unique micro-structures enabled the Pd^0/GDY sample to be an unusual cathodic electrocatalyst for HER with needing the overpotential of 55 mV to reach 10 mA cm^{-2}, a high mass activity of 61.5 A mg^{-1}_{metal}, and a long-term durability for at least 72 h. Combining appropriate amount of Ru dots with self-crosslinking CQDs (Ru@SC-CQDs) [Figs. 22(g) and 22(h)], Zhang's group demonstrated the decent catalytic ability for HER at all pH levels. The overpotentials of Ru@SC-CQDs were 29, 59, and 66 mV in 1 M KOH, 0.5 M H_2SO_4, and 1 M PBS, respectively.[229] Guided by experimental evidences and DFT calculations, a synergistic positive attribute of Ru dots and SC-CQDs should be answerable for the remarkable HER catalytic behavior [Fig. 22(i)]. Likewise, the admirable catalytic materials by introducing CQDs supports into RuM (M = Ni, Mn, and Cu) alloys over the whole pH range were also put forward by Zhang's group.[49]

In addition to above these as-formed carbon matrixes, various *in situ* formed functional carbon derived from the pyrolysis of organic precursors during the growth of metal nanoparticles can play a better role in uniformly and tightly anchoring metal nanoparticles or efficiently restricting their growth.[12,16,55–59,219] To this regard, Zhou and his co-workers designed small Au nanoparticles in a 20 nm size adhered on N-doped carbon architecture (Au@NC) by first bioreduction of Au^{3+} with microorganism (*Pycnoporus sanguineus* cells) to form this Au/microorganism composite and then calcining it in an Ar atmosphere for achieving the resulting Au@NC.[217] This Au@NC hybrid exhibited a good catalytic performance for HER under acidic conditions, with an onset potential of 54.1 mV and a Tafel slope of 76.8 mV dec^{-1}. Recently, as reported by Baek's group, the empty d orbitals in Ir sites could be well modulated through a strong interaction with the p orbitals of C/N atoms, which would further balance hydrogen adsorption/desorption behaviors around Ir sites, and thereby accelerated the related HER process [Figs. 23(a) and 23(b)].[203] Motivated by the theoretical calculations, Ir nanodots firmly supported on hollow nitrogenated carbon nanospheres with a low-Ir amount (about 7.16 wt. %) (denoted as IrHNC) were prepared via the confined pyrolysis of this polystyrene (PS) microsphere@Ir^{3+}–polydopamine

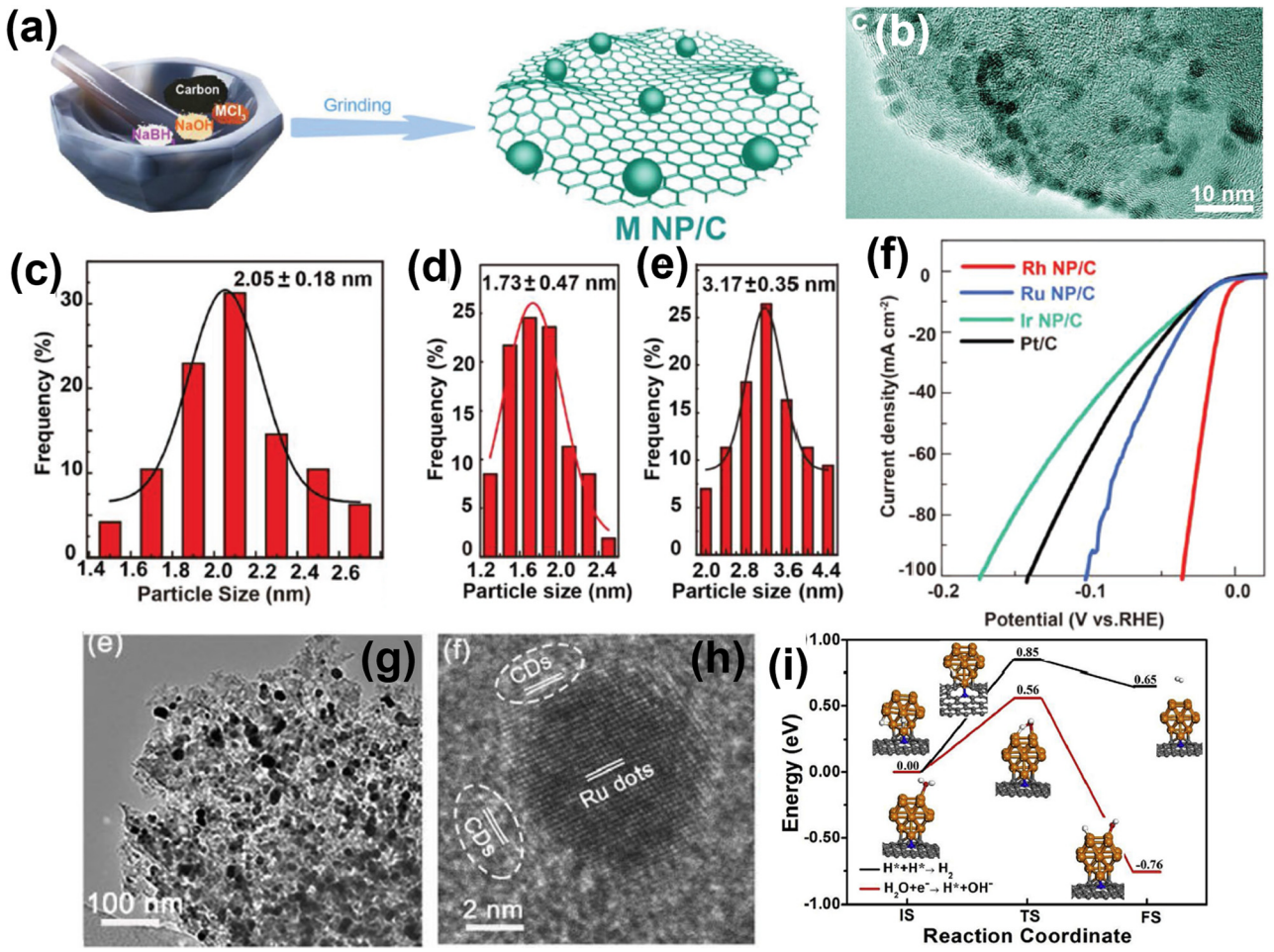

FIG. 22. (a) A schematic diagram depicting the formation process of the M NP/C (M = Rh, Ru, and Ir) nanohybrids. (b) A high-magnification TEM image of Rh NP/C. (c)–(e) The size distribution diagram of different metal nanoparticles, i.e., (c) Rh NP, (d) Ru NP, and (e) Ir NP. (f) The HER activity of M NP/C and Pt/C in alkaline media. Reproduced with permission from Wang *et al.*, Adv. Energy Mater. **8**(31), 1801698 (2018). Copyright 2018 Wiley-VCH. (g) TEM and (h) HRTEM images of the as-prepared Ru@SC-CQDs. (i) The proposed reaction steps for HER on Ru_{13} anchored on N doped SC-carbon dots (CDs) (water dissociation and hydrogen formation). Reproduced with permission from Liu *et al.*, Nano Energy **65**, 104023 (2019). Copyright 2019 Elsevier.

(PDA) composite [Fig. 23(c)]. As expected, the as-obtained IrHNC delivered an incredible HER activity in acidic electrolytes, which included the smallest reported a η_{10} of 4.5 mV, and the largest mass activity of 1.12 A mg_{Ir}^{-1} at the overpotential of 10 mV, and the TOF value of 4.21 H_2 s^{-1} at the 25 mV overpotential by far, strikingly surpassing pure Ir nanoparticles and the benchmark Pt/C [Figs. 23(d)–23(f)]. Analogously, in the same group, a prominent all-round HER catalysis previously has been presented by the ultrasmall-sized Ru nanoparticles uniformly coated with a two-dimensional holey nitrogenated carbon structure (Ru@C_2N), which was constructed via a combined polycondensation-reduction-pyrolysis route.[233] Later, importantly, it was discovered that RuN_xC_y moieties might stand out as the most active centers for HER in such a Ru–N–C system, as verified by Bai *et al.*[227] and Lu *et al.*[234] Another prominent study involving this metal-*in situ* carbon composite was reported by Li and his coworkers, who integrated Ru/Ni nanoparticles with 1D N-doped carbon nanofibers (RuNi–NCNFs) through an accessible electrospinning technique with subsequent carbonization treatment.[228] The synergistic effect stemming from Ru and Ni, conductive NCNF supports, and high active surface area granted RuNi–NCNFs a fascinating HER electrocatalytic activity in both the base and acid, yielding the small η_{10} values of 35 and 23 mV, respectively. Besides, a good OER activity for this material was also achieved in alkaline media. By utilizing the advantages of MOFs, a raw material with evenly and periodically distributed atoms and a distinguished self-sacrificial template, all sorts of functional carbon-metal-related nanostructured composites were fabricated.[55–59] Su and his co-workers, for the first time, synthesized the RuCo nanoalloys with a low concentration embedded in an N-doped graphene-like carbon layer (RuCo@NC) derived from a Ru cation-impregnated Co-based MOF, which manifested a splendid HER performance. In this system, such good catalytic properties were mainly ascribed to that the N-doped carbon shell with a well modified

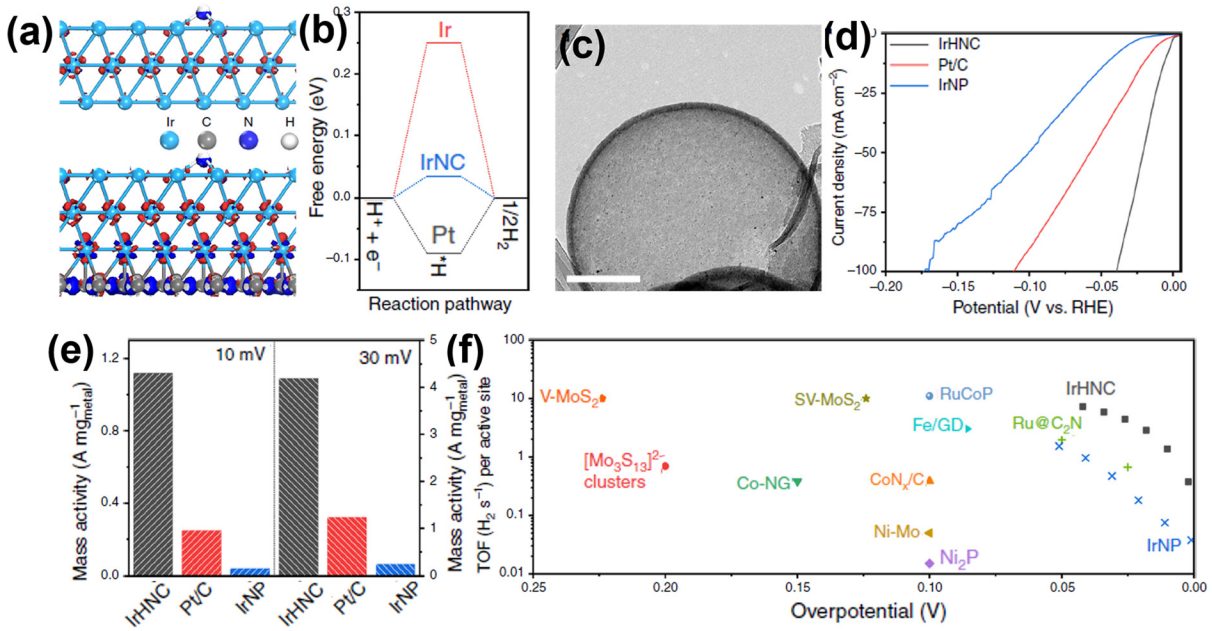

FIG. 23. (a) The electron-density isosurfaces for Ir (top) and IrHNC (down) with H adsorption. (b) The free energy of H adsorption for the Ir, IrHNC, and Pt. (c) The TEM image of IrHNC. (d) HER polarization curves of the as-obtained IrHNC, Ir nanoparticles, and benchmark Pt/C in an acidic solution. (e) The mass activities of these samples at 10 and 30 mV overpotentials. (f) The TOF comparison of the as-prepared IrHNC and other reported catalytic materials under acidic conditions. Reproduced with permission from Li *et al.*, Nat. Commun. **10**, 4060 (2019). Copyright 2019 Nature Publishing Group.

electronic structure from metal cores helped to favor the formation of carbon–hydrogen, thereupon optimizing ΔG_{H^*} of the HER, as elaborated in Sec. IV A 1.[58] Following this work, parallel catalytic mechanisms were extensively proposed in several other alloys@N-doped carbon systems for HER, like CoPd@NC, IrCo@NC, RuNi@NC, etc.[55–57,59] In another published work, a Ru-decorated hierarchical porous carbon nanohybrid (named as Ru–HPC) was prepared via a bimetallic MOF (CuRu–MOF)-based strategy.[235] The Ru–HPC showed ultrafine Ru nanoparticles, high exposure, hierarchical porous carbon structure, high conductivity and low Ru content, thus resulting in an extraordinary catalytic activity for HER.

It is worth mentioning that doping foreign non-metallic elements (such as N, B, F, P, etc.) into the carbon backbone can further ameliorate the catalytic properties in HER.[53,180,222–224,226–228,236] In particular, the N dopant is widely welcomed, as exemplified by numerous previous works, like above mentioned.[55–59,222–224,226–228] Heteroatom dopants can give rise to the asymmetric charge distribution of the adjacent C atoms via breaking their electroneutrality, which accordingly enhances the bonding filling between the bonding orbital of H∗ and the hybridized orbital of active C, eventually to diminish $|\Delta G_{H*}|$ for an improved HER activity.[55] For the above-discussed alloys@N-doped carbon systems, N atoms substantially served as a link for electron transfer from the alloy core to active C atoms neighboring on N dopants.[55–59] The electrons first transferred from the metal core to the N atoms of the carbon layer, and then these N atoms further tailored the electronic arrangements of adjacent C atoms, rendering these C atoms as electrocatalytically efficient active sites for the favorable formation of C–H. In a recent study, the authors analyzed the effects of graphene functionalization and doping by synthesizing four graphene materials, i.e., GO, rGO, electrochemically exfoliated graphene (G), N-doped graphene (NG) as supports to load small Pd nanoparticles.[224] It was found that among them, NG as a skeleton can produce the Pd nanoparticles in an ultrafine size (∼3 nm) and with high dispersion, and this Pd/NG composite presented the lowest HER overpotential in acid. N dopants, especially the graphitic N, were disclosed to play a critical role in immobilizing and stabilizing these as-formed Pd nanoparticles by the electronic interaction between Pd and N. Besides, B-doped functional carbon or F-doped graphene was also utilized as a skeleton for the growth of RhFe alloy or Rh nanoparticles, respectively.[53,226] Both B and F atoms could adjust the electronic structure of carbon scaffold to obtain a proper hydrogen-adsorption ability, which brought the striking enhancement in the HER activity. Most recently, through pyrolyzing the mixed precursors of H_3BO_3, $Ru(phen)_2Cl_2$, and graphene, Ru nanoclusters combined with B, N-codoped graphene (Ru NCs/BNG) were created.[236] Remarkably, when B was introduced into graphene structure, the agglomeration of metal particles was inhibited and induced the formation of Ru NCs nanodots with an ultra-small size (0.5–1 nm) [Figs. 24(a) and 24(b)]. Moreover, the vacant 2p orbitals in the B atom could be delocalized to Ru nanodots, which promoted the coordination effect of the electron-deficient Ru with the lone-pair electrons of O atoms from water molecules, thereby driving the cleavage of this H–OH bond and expediting the alkaline hydrogen-evolution dynamics [Figs. 24(d) and 24(e)]. As a consequence, a brilliant HER catalytic performance was realized in the Ru NCs/BNG catalyst, featured by a small overpotential of 14 mV at 10 mA cm^{-2} and stable long-time operation, which was better than that of 20% Pt [Fig. 24(c)].

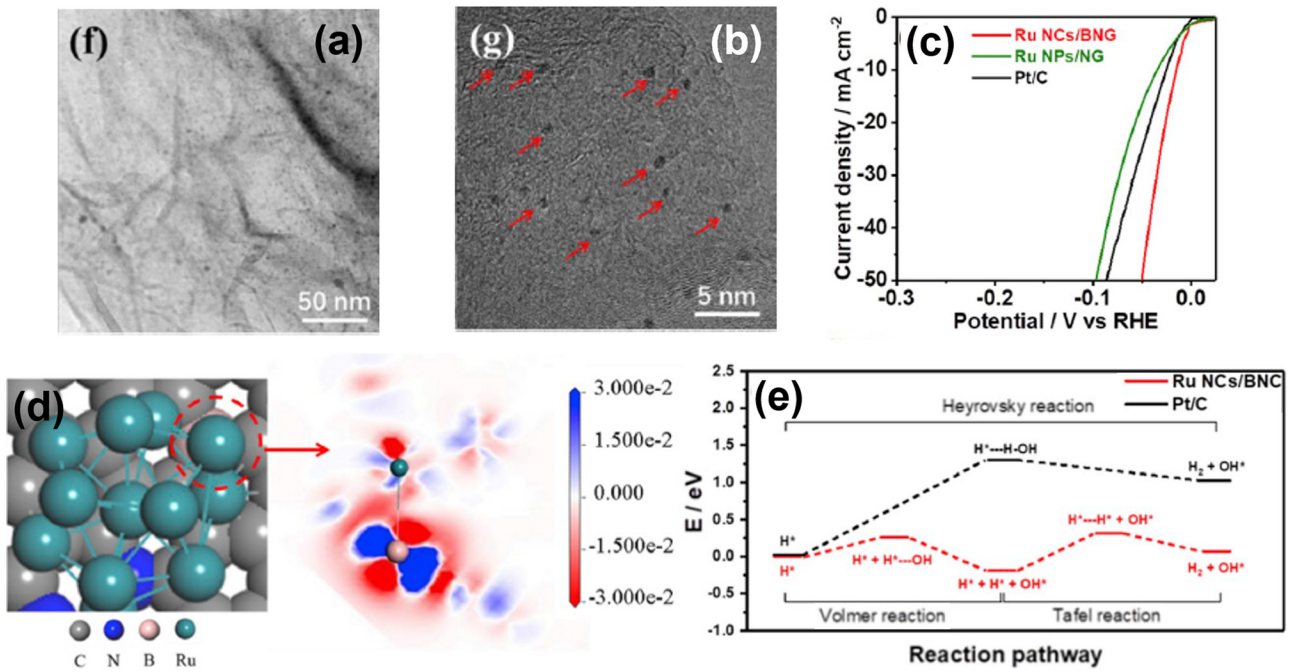

FIG. 24. (a) TEM and (b) HRTEM images of Ru NCs/BNG. (c) The HER activity of different catalytic materials in 1 M KOH. (d) The used calculation structure model and electronic density distribution. (e) Free energy of the HER pathway for different catalytic electrodes. Reproduced with permission from Ye *et al.*, Nano Energy **68**, 104301 (2020). Copyright 2020 Elsevier.

Semiconducting carbon nitrides (C_3N_4) are also selected as the supporting architecture to anchor noble metal nanoparticles, and become a new class of composite catalysts.[230,231,237–239] C_3N_4, as a supporting material for electrocatalysis, possesses multifold merits. With the existence of N heteroatoms and repetitive tri-s-triazine units in the C_3N_4 framework, metal nanoparticles can be readily coordinated and stabilized, which rendered the promoted electrical connection and electron transfer.[239] Barman's group communicated the synthesis of porous Au aerogel decorated on graphitic carbon nitride (Au-aerogel–CN_x) by adopting sodium borohydride as the reducing agent and undergoing ultrasonication.[237] On account of a unique synergistic interaction between the two components of porous Au aerogel and CN_x, such Au-aerogel–CN_x recorded a superior HER electrocatalytic activity with an onset overpotential of 30 mV and a Tafel slope of 53 mV dec^{-1} in 0.5 M H_2SO_4. In like manner, Pd nanoparticles hybridized on graphitic carbon nitrides (Pd–CN_x) with porous morphology have been proved as an efficient and stable pH-universal electrocatalyst for HER.[230] The porous structure in this Pd–CN_x catalyst ensured rapid mass transportation to the active centers and expedited the easy release of evolved gas. For another, the intimate coupling of Pd nanoparticles and CN_x scaffold offered sufficient mechanical adhesion and strong electronic contact as well as brought about a fast electron flow during the cathodic polarization. Also, integration of Ru with graphitic carbon nitrides (C_3N_4–Ru) was verified as an outstanding acidic HER electrocatalyst.[238] The high activity of C_3N_4–Ru was most likely originated from the generation of Ru–N moieties, where a synergy of Ru metal centers and the C_3N_4 supports accelerated the adsorption of hydrogen during the HER process.

b. Si nanowires. In the past few years, researchers found that Si nanowires (Si NWs) as supporting carriers could effectively suppress the coarsening and aggregation of metal particles grown on their surfaces, improve the utilization of these nanoparticles, and increase the active centres.[211–214,240–242] Additionally, albeit Si belongs to a semiconductor, the special surface defect in Si NWs endows them sufficient electric characteristics. More significantly, in the previously present theoretical and experimental results, Si NWs showed a low hydrogen desorption energy and thus hydrogen release on the hydrogen-terminated Si NWs was a rapid process, consequently offered an improvement of the HER electrocatalytic activity in the Si NWs-supported precious metals.[211–214,240–242] All above characteristics suggested that Si NWs were the promising support materials for electrocatalysis. So far, Shao's team gave the greatest focus on the research of this noble metal-Si NMs composite. Numerous composites, e.g., Rh/Si NWs, Rh–Ag–Si NWs, Pd/Si NWs, Ir/Si NWs, etc., have been built up as efficient HER electrocatalysts.[211–214,242] In 2016, through a *in situ* reduction pathway, a Rh/Si NWs composite was designed. Hydrogen adsorption tended to occur on the Rh site with a large adsorption energy while Si with a low adsorption energy was used to promote hydrogen evolution, thus ensuring a satisfactory HER activity in acidic media.[212] Meanwhile, Rh-adsorbed hydrogen could regenerate the Si poisoned by the hydroxyl, which stabilized the catalytic activity of the Rh/Si NWs material for a long time. Thereafter, this ternary Rh–Ag–Si system was also investigated as a highly active acidic catalyst for HER over this Pt–Ag–Si composite.[211] Specifically, the optimal Rh–Ag–Si yielded a η_{10} of 120 mV, a Tafel slope of 51 mV dec^{-1}, and a mass activity of 11.5 mA mg_{Rh}^{-1} in 0.5 M H_2SO_4, which were largely

superior to those of Pt–Ag–Si (a η_{10} of 190 mV, a Tafel slope of 54 mV dec^{-1}, and a mass activity of 2.3 mA mg_{Pt}^{-1}). The DFT results illuminated the activity difference origins, i.e., the atomic H migration-activation energies from Rh (111) to Si are smaller than the results from Pt (111) to Si through the Ag surface. Recently, they further tried to manipulate the Ir metal to achieve an incredible Pt-outperformed activity by hybridizing with Si NWs to form this Ir/Si NWs hybrid electrocatalyst.[214] Notably, according to the Sabatier principle, Ir has a more near-zero/ΔGH/ value (0.03 eV) compared to Pt (−0.09 eV), and thus theoretically it should possess better HER activity. Nevertheless, due to a larger enthalpy of atomization for Ir, it shows a stronger tendency to poor dispersion and severe aggregation. Here, as the authors showed, the coupling of Ir with Si NWs downsized the metal nanoparticles to ∼2.2 nm and drove the H_2-production process by the three pathways, i.e., H adsorption on Ir, H diffusion to Si, and H_2 desorption from Si. All these results permitted to attain the promotion on both activity and stability and exceed the commercial Pt/C in every aspect.

c. Metallic electrodes. Additionally, in some research teams, noble metals spontaneously deposited on diversified metallic electrodes [e.g., porous Ni, Au (111) or Au (100), Pt (poly), and Pd (poly) electrodes] also have been utilized for the study of HER.[215,216,243–253] Amon them, the single-crystal Au substrate modified with noble metals is a representative example. For the Pd-deposited single-crystal Au electrode, by employing different deposition ways and adjusting diverse Pd coverage, the electronic interplay between Pd overlayer and Au substrate could be modulated to obtain higher HER activity.[243–246] In 2011, Quaino *et al.* combined theory and experiments to focus on the ensemble influence on different Pd nanostructures decorated on Au (111), containing monolayer, clusters, monomers, and rows.[247] Remarkably, the activity of Pd/Au (111) was considerably proliferated when decreasing the Pd coverage and Pd with the nanostructure of small clusters in monoatomic height dimension, in which the density of states showed the strongest shift towards the Fermi level, even more than that in monolayer. Later, they continued to study the impact of successive Pd layers on Au (111) for HER and reported less negative adsorption free energy and lower barrier of Pd with two layers, thus showing a larger activity toward HER.[248] In a study published in the last year, the authors, by means of the electrochemical scanning tunneling microscopy (n-ECSTM) technology, found that the most active sites in sub-monolayer Pd/Au (111) were located close to the boundary between Pd atoms and Au.[216] Besides, the significant enhancement of the HER catalytic behavior in the Au (111) electrode with Rh overlayer (Rh/Au (111)) was first predicted by theoretical results in 2011, and then was further confirmed experimentally.[249,250] These reports have corroborated that this Rh/Au (111) electrode was highly active for the HER. The high activity was deemed to be associated with a strong electronic synergism between the two metals, which accelerated the different reaction pathways in hydrogen-evolution mechanism and so boosted the overall reaction rate. Subsequently, based on the XPS experimental results, this electronic effect was indeed attested.[251] Recently, Strbac *et al.* fully covered the Au (111) surface with Ir by the simple and fast spontaneous deposition. This composite electrode offered pronounced HER catalysis with respect to bare Au (111), but still was inferior to the bare Ir(poly).[246] According to the Strbac's team, HER catalysis was also investigated on the model Pd/Pt(poly) electrode, which yielded the improved catalytic activity under alkaline conditions in comparison with the bare Pt(poly).[252] Meanwhile, the study was extended to the similar Rh/Pt(poly) system, in which more excellent HER catalytic performance than that of Pd/Pt(poly) was achieved and explained by the larger susceptibility of the Rh deposit to the electronic interaction with this Pt(poly) support. Furthermore, their recent work displayed the bimetallic Ir/Pt(poly) electrode as an effective cathode for hydrogen production in base.[253] In this catalyst, the heterogeneity of surface active centers and the electron interplay between the Ir and Pt in a close contact synergistically promoted the adsorption of the H-related intermediates, thus which could effectively catalyze the HER.

Table III displays the comparison of the HER catalytic performance of various representative non-Pt noble metal-based hybrids in the different media.

D. Other modulation strategies

Apart from various design strategies mentioned above, several other approaches can also alter the catalytic activity of the non-Pt NMNs. The materials with identical chemical composition but different crystalline structures or exposed active facets displayed different atomic coordinations and electronic distributions and thus had a great effect on the HER catalytic activity.[12,254–259] Ru metal with a face-centered cubic (fcc) structure has been demonstrated to deliver higher HER activity than that with a hexagonal close packed (hcp) structure and yet the *fcc*-structured Ru crystal tended to be obtained through a relatively complex or peculiar synthetic route, which has been well summarized in our previous study and thereby will not be discussed in detail here.[12] Unlike this, other noble metals like Rh, Pd, Ag, Ir, and Au normally existed with the stable fcc phase, rather than the hcp phase.[136,259] Interestingly, the nanostructure sometimes can manipulate the phase structure. For example, hierarchical Ru nanotubes were reported to display a stable fcc structure, while ultrathin Au nanosheets possessed an anomalous hcp phase.[259] The amorphous phase possesses isotropic properties and disordered structures, which can enable a wide exposure of abundant active sites.[260,261] Consequently, the amorphous materials are highly likely to possess an outstanding electrocatalytic performance. In a recent report, Li *et al.* declared that a nanohybrid, consisting of amorphous ruthenium-sulfide nanoparticles and sulfur-doped graphene oxide (RuS_x/S-GO), acted as a Pt-like electrocatalyst for hydrogen production, requiring low overpotentials of 31, 46, and 58 mV to reach a 10 mA cm^{-2} benchmark current density under the acidic, neutral, and alkaline conditions, respectively, as well as robust durability.[94] A combination of experimental characterization and theoretical simulation evidenced that the isolated Ru single atoms in the RuS_x amorphous structure were the active sites for the HER process. Moreover, it was manifested that the tight coupling between small RuS_x nanoparticles and the S-GO support played a critical role in stabilizing the catalytic material. Likewise, amorphous $RuTe_2$ porous nanorods were also attained by Huang's group and demonstrated a significant improvement of HER catalytic behavior relative to its crystalline counterparts under both acidic and alkaline conditions.[97]

Regarding exposed facet control, it is generally realized by adjusting the particle morphologies.[135,257,258] For instance, Pd nanoparticles (NPs) with different shapes, such as spheres and octahedra, as well as simple nanocubes, are solely enclosed by the (111) and (100) facets.[257] This aspect has been well discussed in Sec. IV B. In addition, the novel

TABLE III. Performance of various representative non-Pt noble metal-based hybrids.

Catalyst	Electrolyte	Loading (mg cm^{-2})	Overpotential η_{10} (mV)	Tafel slope (mV dec^{-1})	Stability	References
Porous Pd@Ru NRs	1 M KOH	0.051	30	30	3000 CV or −31 mV @ 12 h	149
$Au_{75}Rh_{25}$ decahedra	0.5 M H_2SO_4	1.96 μg_{Rh} cm^{-2}	64.1	33.8	500 CV or −10 mA cm^{-2}@2.8 h	154
Ag–Ni NWs	0.1 M KOH	0.12	197	84	−10 mA cm^{-2} @ 3 h	137
$Pd/FeO_x(OH)_{2-2x}$	0.1 M KOH	0.0254	∼0 (onset)	131–162	…	153
NiAu/Au NPs	0.5 M H_2SO_4	0.068	7 (onset)	36	10 000 CV	160
Ag@PdAg nanocubes	0.5 M H_2SO_4	0.408	13.8 (η_0)	70	5000 CV	162
Pd@PtCu dodecahedron	0.5 M H_2SO_4	15 μg_{Pt} cm^{-2}	19	26.2	10 000 CV	163
	0.1 M KOH		60	…		
Pd–Pt heterostructure	1 M KOH	12 μg_{Pt} cm^{-2}	71	31	−70 mV @ 2.22 h	164
W+Ru	0.5 M H_2SO_4	5.6 μg_{Ru} cm^{-2} 114 μg_W cm^{-2}	85	46	−10 mA cm^{-2} @ 24 h	165
w-Au@MoS_2	0.5 M H_2SO_4	…	120	52.9	10 h CV	186
Ir/MoS_2	1 M KOH	0.285	44	32	9000 CV or −44 mV @ 18 h	190
1T MoS_2-Au/Pd	0.5 M H_2SO_4	0.214	50 (η_0)	63	1000 CV	187
Ru-MoS_2/CC	0.5 M H_2SO_4	46 μg_{Ru} cm^{-2}	61	…	−10 mA cm^{-2} @ 20 h	195
	1 M PBS		114	…	−10 mA cm^{-2} @ 10 h	
	1 M KOH		41	114	−10 mA cm^{-2} @ 10 h	
$NiCo_2S_4$/Pd	0.5 M H_2SO_4	0.306	87	70	−10 mA cm^{-2} @ 10 h	197
	1 M KOH		83	123		
Ag@Cu_2O/CF	1 M KOH	…	108	58	−200 mV @ 20 h	198
Ag-WO_3 (0.8)	0.5 M H_2SO_4	0.708	207	52.4	2000 CV	199
AL-Pt/Pd_3Pb	0.5 M H_2SO_4	40.8 μg_{Pt+Pd} cm^{-2}	13.8	18	10 000 CV or −14 mV @ 25 h	200
$Co(OH)_2$–Au–$Ni(OH)_2$	1 M NaOH	…	200	92	−5 mA cm^{-2} @ 24 h	201
Au–Ag NCs/rGO	0.5 M H_2SO_4	…	10 (η_0)	39	10 000 CV	37
Ir_VG	0.5 M H_2SO_4	50 μg_{Ir} cm^{-2}	47	43	1000 CV	221
	1 M KOH		17	29		
Pd NPs@N-CNTs	0.5 M H_2SO_4	0.285	32 (η_{100})	33	−0.25 V @2.78 h	222
PAH@Rh-NSNSs/CNT	0.5 M H_2SO_4	52 μg_{Rh} cm^{-2}	5	30	1000 CV	225
Rh NP/C	1 M KOH	0.589	7	19	1000 CV	127
Ru NP/C			69 (η_{50})	33		
Ir NP/C			109 (η_{50})	42		
Rh NP/PC	1 M KOH	0.6	33			128
	0.5 M H_2SO_4		21	34	1000 CV	
Ru NP/PC	1 M KOH		30			
	0.5 M H_2SO_4		63	63		
Ir NP/PC	1 M KOH		110			
	0.5 M H_2SO_4		30	35		
Pd^0/GDY	0.5 M H_2SO_4	0.447	55	47	1000 CV	223
Ru@SC-CQDs	0.5 M H_2SO_4	0.42	59	57	5000 CV or initial	229
	1 M PBS		66	158	−10 mA cm^{-2} @ 100 h	
	1 M KOH		29	57		
Au@NC	0.5 M H_2SO_4	0.357	54.1 (η_1)	76.8	1000 CV or −300 mV @ 20 h	217
IrHNC	0.5 M H_2SO_4	18 μg_{Ir} cm^{-2}	4.5	…	…	203
RuNi–NCNFs	0.5 M H_2SO_4	0.612	23	29	5500 CV or −62 mV @ 12 h	228
	1 M KOH		35	30	6000 CV or −40 mV @ 12 h	
RuCo@NC	1 M KOH	0.275	28	31	10 000 CV	58
Pd/NG	0.5 M H_2SO_4	0.212	199	∼80	…	224

TABLE III. (*Continued.*)

Catalyst	Electrolyte	Loading (mg cm^{-2})	Overpotential η_{10} (mV)	Tafel slope (mV dec^{-1})	Stability	References
Ru NCs/BNG	1 M KOH	0.707	14	28.9	2000 CV or −10 mA cm^{-2} @ 17 h	236
Au-aerogel–CN_x	0.5 M H_2SO_4	0.13 mg_{Au} cm^{-2}	30 (η_0)	53	10 000 CV or −0.15 V @ 10 h	237
Pd–CN_x	0.5 M H_2SO_4	43 μg_{Pd} cm^{-2}	55	35	10 000 CV or −60 mV @ 100 h	230
	0.5 M KOH		180 (η_5)	150	…	
C_3N_4–Ru	0.5 M H_2SO_4	0.153	140	57	1000 CV	238
Rh/Si NWs	0.5 M H_2SO_4	0.193	44 (onset)	24	−0.1/0.3 V @ 138.9 h	212
Rh–Ag–Si	0.5 M H_2SO_4	0.140	120	51	−0.25 V @ 12 h	211
Ir/Si NWs	0.5 M H_2SO_4	0.339	22	20	−10 mA cm^{-2} @ 13.9 h	214

worm-like Ir-oriented nanocrystalline assemblies (Ir ONAs) with more exposed low-index crystalline planes were also fabricated and featured superior HER activity in alkaline electrolytes compared to the nanoparticle counterparts (Ir NPs).[262] Such results could be partly ascribed to the fact that the quasi-1D nanostructure provided more low-index facet atoms with lower hydrogen binding energy.

V. NEW TRENDS IN THE ELECTROCATALYTIC HER

In this section, we briefly discuss the development of new trends in electrocatalytic hydrogen production, including pH universality and bifunctionality. Relative to other non-noble metal catalysts, the design of non-Pt NMNs is highly suitable for such trends.

A. pH universality

Of note, different electrolytic devices necessitate varied operating conditions.[6] Proton exchange membrane (PEM)-related electrolyzers need active and robust electrocatalysts that can operate in acidic media, while some water–alkali and chloro–alkali electrolysis cells typically require alkaline-stable HER catalysts. In some microbial electrolysis units, the operating environment is the neutral electrolyte. Thus, exploiting pH-universal HER catalytic materials could enormously broaden the application prospects. More significantly, given that most of the best electrocatalysts for the OER function well only in alkaline or neutral solution, the pH-compatible anodic electrocatalysts in the overall water splitting are relatively infrequent. Competent HER catalysts operating at all pH values offer the great chance to cooperate with OER catalytic materials for achieving the overall water splitting. As such, it is highly desirable but challenging to find versatile and efficient HER electrocatalysts that function well in a large window of solution pHs. Noble metals, due to their decent activity for electrocatalysis and being able to withstand extremely harsh conditions, like a strong acid or base, hold a great promise for pH-universal HER applications. Notwithstanding, not all the noble metal-based materials can adapt to a wide pH range. However, compared to active transition metals, noble metal-based materials have much more possibilities for the pH-universal HER with superior performance. So far, a plethora of non-Pt NMNs, such as IrW ND, $RuIrO_x$, PdP_2@CB, Li-$IrSe_2$, Ru-MoS_2/CC, Ru@SC-CQDs, etc., were shown to have splendid catalytic activity and durability for the HER over a wide range of pH values.[62,69,92,99,195,229] A summary of them is given in Table IV, some of which have been minutely introduced in the fourth section. Recently, Mahmood *et al.* presented ultrafine Ir nanoparticles uniformly embedded in a 3D cage-like organic network (Ir@CON) for the pH-universal HER.[219] The Ir@CON sample delivered prominent catalytic properties, with reaching 10 mA cm^{-2} by the overpotentials of 13.6 and 13.5 mV and achieving the TOF values of 0.66 and 0.2 H_2 s^{-1} at 25 mV in acidic and alkaline solutions, respectively. Construction of a 3D CON structure not only offered a large surface area, but also enabled a conductive platform that uniformly and stably anchored Ir nanoparticles to maximize active sites. Pleasingly, N, S-coordinated Ru single atoms supported on titanium carbide ($Ti_3C_2T_x$) MXene matrixes (Ru_{SA}–N–S–$Ti_3C_2T_x$) were further designed, which could apply to the HER with super behavior in a broad pH range.[263] The coordination of Ru single atoms and N/S sites on $Ti_3C_2T_x$ induced matrices optimized the electronic structure, thus affording more suitable Gibbs hydrogen adsorption energy.

B. Bifunctional water electrolysis

For the sake of cost-effective overall water splitting, the other aim is to construct active bifunctional electrocatalysts that could effectively catalyze the OER and HER at the same time. Based on numerous pioneering studies, non-Pt NMNs not only possess the pronounced HER catalytic performance in the pH range of 0–14, but also are considered as the most promising pH-universal OER catalysts, typically Ru or Ir-based materials, due to the moderate binding energy of the O-related reaction intermediates and great acid–base durability.[33] It is worth mentioning that pure Ru or Ir-based oxides or metals, especially Ru metal, are relatively unstable due to the dissolution from the excessive oxidation during the OER process, but various design tactics, such as forming alloys, optimizing morphology, constructing hybrids, tuning crystalline structures or facets, etc., greatly propel their OER stability.[12] Our previous review has given an important focus on this stability issue.[12] Here, overall, this "bifunctionality" concept can be accomplished by developing these novel non-Pt NMNs. For instance, an Ir/controllable IrO_x stabilized by Cucurbit[6]uril (CB[6]) worked as a distinguished bifunctional electrocatalyst for acidic water splitting (CB[6]-Ir2).[264] The overall water-splitting voltage was only 1.56 V at the 10 mA cm^{-2} current density and the activity at 5 mA cm^{-2} could be continuously maintained for at least 20 h, which strikingly went beyond the benchmark for Pt/C–Ir/C. In accordance to spectroscopic measurements and DFT calculations, the strong coordination bonding between surface Ir and CB[6] controllably created the surface-active

TABLE IV. Performance of various representative pH-universal non-Pt NMN electrocatalysts.

Catalyst	Electrolyte	Loading (mg cm^{-2})	Overpotential η_{10} (mV)	Tafel slope (mV dec^{-1})	Stability	References
$Pd_{66}Ag_{17}Al_{17}$	1 M KOH	…	16.8	56	10 000 CV	35
	0.5 M H_2SO_4	…	∼35	26	30 000 CV	
PtRu	0.5 M H_2SO_4	13.9 μg_{Ru} cm^{-2}	8	25	10 000 CV or −15/40/30 mV @10 h	44
	1 M PBS		25	36		
	1 M KOH		19	28		
np-$Cu_{53}Ru_{47}$	1 M KOH	0.306	15	30	−15 mV @ 27 h −40 mV @ 27 h	61
	1 M PBS		41	35		
IrW ND	0.1 M $HClO_4$	10.2 μg_{Ir} cm^{-2}	12	…	1000 CV	62
	0.1 M KOH		29	…		
$RuIrO_x$	0.5 M H_2SO_4	0.833	12	21	3000 CV	69
	1 M KOH		13	23		
w-Rh_2P NS	0.1 M $HClO_4$	0.0123	15.8	29.9	1000 CV	84
	0.1 M PBS		21.9	78.4		
	0.1 M KOH		18.3	61.5		
L-RuP	0.5 M H_2SO_4	0.185	19	37	−10 mA cm^{-2} @ 200 h	87
	1 M PBS		95	54		
	1 M KOH		18	34		
PdP_2@CB	0.5 M H_2SO_4	0.285	27.5	29.5	5000 CV or −27.5/84.6/35.4 mV @ 10 h	92
	1 M PBS		84.6	72.3		
	1 M KOH		35.4	42.1		
IrP_2@NC	0.5 M H_2SO_4	0.7	8	28	1000 CV	91
	1 M KOH		28	50		
RuS_x/S-GO	0.5 M H_2SO_4	1	31	40	Initial −50 mA cm^{-2} @ 12 h	94
	1 M PBS		46	39		
	1 M KOH		58	56		
Li-$IrSe_2$	0.5 M H_2SO_4	0.25	55	…	−64/173/105 mV @ 10 h	99
	1 M PBS		120	…		
	1 M KOH		72	…		
RuB_2	0.5 M H_2SO_4	0.281	18	38.9	−10 mA cm^{-2} @ 50 h	72
	1 M KOH		28	28.7		
Ru@NG-2	1 M H_2SO_4	0.857	74	48	5000 CV or −100 mV @ 10 h	129
	1 M KOH		47	82		
Ir NWs	0.05 M H_2SO_4	40.7 μg_{Ir} cm^{-2}	17	26	…	136
	0.5 M H_2SO_4		15	34	…	
	0.1 M KOH		73	46	…	
	1 M KOH		38	30	…	
RhCo–ANAs	0.5 M H_2SO_4	2	12.4	30.7	…	11
	1 M PBS		31	33.6	−50 mV @ 5 h	
	1 M KOH		32.4	31.9	…	
Monodisperse Rh_2P NPs	0.5 M H_2SO_4	0.0306	14	31.7	1000 CV	85
	1 M PBS		38	46		
	1 M KOH		30	50		
Pd@PtCu dodecahedron	0.5 M H_2SO_4	15 μg_{Pt} cm^{-2}	19	26.2	10 000 CV	163
	0.1 M KOH		60	…		
Ru-MoS_2/CC	0.5 M H_2SO_4	46 μg_{Ru} cm^{-2}	61	…	−10 mA cm^{-2} @ 20 h	195
	1 M PBS		114	…	−10 mA cm^{-2} @ 10 h	
	1 M KOH		41	114	−10 mA cm^{-2} @ 10 h	

TABLE IV. (*Continued.*)

Catalyst	Electrolyte	Loading (mg cm^{-2})	Overpotential η_{10} (mV)	Tafel slope (mV dec^{-1})	Stability	References
$NiCo_2S_4$/Pd	0.5 M H_2SO_4	0.306	87	70	−10 mA cm^{-2} @ 10 h	197
	1 M KOH		83	123		
Ir_VG	0.5 M H_2SO_4	50 μg_{Ir} cm^{-2}	47	43	1000 CV	221
	1 M KOH		17	29		
Rh NP/PC	1 M KOH	0.6	33	…	1000 CV	128
	0.5 M H_2SO_4		21	34		
Ru NP/PC	1 M KOH		30	…		
	0.5 M H_2SO_4		63	63		
Ir NP/PC	1 M KOH		110	…		
	0.5 M H_2SO_4		30	35		
Ru@SC-CQDs	0.5 M H_2SO_4	0.42	59	57	5000 CV or Initial −10 mA cm^{-2} @ 100 h	229
	1 M PBS		66	158		
	1 M KOH		29	57		
RuNi-NCNFs	0.5 M H_2SO_4	0.612	23	29	5500 CV or −62 mV @ 12 h	228
	1 M KOH		35	30	6000 CV or −40 mV @ 12 h	
Pd-CN_x	0.5 M H_2SO_4	43 μg_{Pd} cm^{-2}	55	35	10 000 CV or −60 mV @ 100 h	230
	0.5 M KOH		180 (η_5)	150	…	
Ir@CON	0.5 M H_2SO_4	0.5	13.6	27	10 000 CV	219
	1 M KOH		13.5	29		
Ru_{SA}-N-S-$Ti_3C_2T_x$	0.5 M H_2SO_4	1	76	90	3000 CV	263
	0.5 M Na_2SO_4		275	…	1000 CV	
	0.5 M NaOH		99	…	4000 CV	

IrO_x species and promoted their stabilization, which contributed to the superb activity and stability as observed. Lai *et al.* explored a novel composite of various single-atom sites (M_1= Fe_1, Ni_1, Ru_1, Pd_1, Pt_1, and Ir_1) anchored on the ZIF-67-derived Co/NC substrate (namely M_1@Co/NC), which featured two different active domains, that is M_1@Co and M_1@NC, being responsible for the OER and HER in basic solution, respectively.[265] To be noted, the Ir_1@Co/NC was the best one for the overall water splitting, showing a 1.603 V cell potential at 10 mA cm^{-2}. Reported by Huang's group, channel-rich RuCu nanosheets (NSs) that crystallized Ru integrated with amorphous Cu were also proven as active and robust electrocatalysts for the OER and HER at a wide range of pH values.[145] By controlling the synthesis temperature, the RuCu nanosheets as the optimal OER and HER catalysts were achieved at 350 and 250 °C, respectively. The assembly of two electrodes with the optimized RuCu material as the cathode and anode offered an attractive electrocatalytic system with cell voltages of only 1.50, 1.49, 1.55, and 1.49 V in 0.05 M H_2SO_4, 0.5 M H_2SO_4, 0.1 M KOH, and 1 M KOH solutions, respectively, and high stability over 30 h, which were the highest performance results among those reported electrocatalysts used for water electrolysis and much better than the results of Pt/C–Ir/C. Additionally, in the fourth part, the bifunctional water electrolysis was well reflected by some representative cases, like IrNi NCs, IrW ND, $RuIrO_x$, Li-$IrSe_2$, NiVIr LDH, Ir_VG, etc.[50,62,69,99,115,221] Table V lists the overall water-splitting performance of various non-Pt NMN catalysts under different operation conditions. Of note, most of them are also obviously superior to those of other representative bifunctional electrocatalysts for overall water splitting, as summarized in Table VI.

VI. CONCLUSIONS AND OUTLOOK

Over the past few years, considerable breakthroughs have been continuously attained for the construction of non-Pt noble metal-based nanomaterials toward more prominent hydrogen-evolution behavior. In this comprehensive review, we summarize the recent progresses of them, particularly over the past five years. These non-Pt noble metals, with suitable hydrogen-adsorption energy and robust corrosion resistance, afforded splendid catalytic performance over a wide pH range. Through the rational compositional and structural tailoring: (i) creating alloys (noble metal–noble metal or noble metal–-transition metal), (ii) constructing novel metal compounds, such as oxides, phosphides, chalcogenides, carbides, etc., (iii) decreasing the particle size to a few nanometers or designing unique nanostructures, i.e., 1D, 2D, and 3D shapes, (iv) coupling with carbon-free active materials or supporting with conductive substrates, and (v) adjusting crystalline structures or exposed facets, the number of active sites, the electron conductivity, and the reaction kinetics could be remarkably ameliorated, correspondingly leading to the considerable improvement in electrocatalytic performances, in accompaniment with reducing the dosage of noble metals. Some representative non-Pt NMN electrocatalysts are listed in Tables I–III. Moreover, the development of non-Pt NMNs highly follows the desired trends in the electrocatalytic HER (Tables IV and V), that is, they could work well in pH-

TABLE V. Summary of various non-Pt NMN catalysts toward overall water splitting in different media.

Catalyst	Electrolyte		η_{10} (mV)	Cell voltage (V) at 10 mA cm^{-2}	Stability	Loading (mg cm^{-2})	References
Ir_6Ag_9 NTs	0.5 M H_2SO_4	OER	285	1.55	1000 CV or 5 mA cm^{-2} @ 32 h	13.3 μg_{Ir} cm^{-2}	34
		HER	20				
IrNi NCs	0.5 M H_2SO_4	OER	>300	1.58	1.6 V @ 10 h	12.5 μg_{Ir} cm^{-2}	50
		HER	>20				
IrNi NFs	0.5 M H_2SO_4	OER	330	1.6	1000 CV	30 μg_{Ir} cm^{-2}	51
		HER	40				
IrW ND	0.5 M H_2SO_4		…	1.48	10 mA cm^{-2} @ 8 h	30 μg_{Ir} cm^{-2}	62
	1M PBS		…	1.55 (onset)	…		
	1 M KOH		…	1.50 (onset)	…		
Co-RuIr	0.1 M $HClO_4$	OER	235	1.52	10 mA cm^{-2} @ 25 h	…	67
		HER	14				
$RuIrO_x$	0.5 M H_2SO_4	OER	233	1.45	Initial 10 mA cm^{-2} @ 20 h	1	69
		HER	12				
	PBS (pH = 3/7/9)	…		1.52/1.51/1.53			
	1 M KOH	OER	250	1.47			
		HER	13				
PdP_2@CB	1 M PBS	OER	277	1.59	Initial 10/50 mA cm^{-2} @ 10 h	0.285	92
		HER	84.6				
	1 M KOH	OER	270	1.72 (at 50 mA cm^{-2})			
		HER	35.4				
RuS_2-500	1 M KOH	OER	282	1.527	10 mA cm^{-2} @ 20 h	1.5	100
		HER	78				
Li-$IrSe_2$	0.5 M H_2SO_4	OER	220	1.44	1.47 V @ 24 h 1.57 V @ 24 h 1.52 V @ 24 h	3	99
		HER	55				
	1 M PBS	OER	315	1.50			
		HER	120				
	1 M KOH	OER	270	1.48			
		HER	72				
NiFeRu–LDH	1 M KOH	OER	225	1.52	10 mA cm^{-2} @ 10 h	1.2	117
		HER	29				
Rh–NiFe–LDH	1 M KOH	OER	206	1.46	1.5 V @ 2.78 h	1.2	18
		HER	57				
NiVIr LDH	1 M KOH	OER	203	1.49	10 mA cm^{-2} @ >15 h	1.7	115
		HER	41				
Ru–NiFe–P	1 M KOH	OER	242 (η_{100})	1.47	~1.47 V @ 20 h	…	119
		HER	44				
RhCo–ANAs	0.5 M H_2SO_4	OER	>220	1.51	…	2	11
		HER	12.4				
	1 M PBS	OER	310	1.54	1.54 V @ 20 h		
		HER	31				
	1 M KOH	OER	>220	1.47	…		
		HER	32.4				
Ir/MoS_2	1 M KOH	OER	330	1.57	…	…	190
		HER	44				
$Co(OH)_2$–Au–$Ni(OH)_2$	1 M NaOH	OER	340	1.75	10 mA cm^{-2} @ 0.5 h	…	201
		HER	200				
Ir_VG	0.5 M H_2SO_4	OER	300	1.58	…	50 μg_{Ir} cm^{-2}	221

TABLE V. (*Continued.*)

Catalyst	Electrolyte		η_{10} (mV)	Cell voltage (V) at 10 mA cm^{-2}	Stability	Loading (mg cm^{-2})	References
		HER	47				
	1 M KOH	OER	320	1.57	…		
		HER	17				
RuNi–NCNFs	1 M KOH	OER	290	1.564	1.57 V @ 0.5 h	2.5	228
		HER	35				
CB[6]-Ir2	0.5 M H_2SO_4	OER	270	1.56	5 mA cm^{-2} @ 20 h	…	264
		HER	50–60				
Ir_1@Co/NC	1 M KOH	OER	260	1.603	1.61 V @ 5 h	0.2	265
		HER	60				
RuCu NSs	0.05 M H_2SO_4	OER	240	1.50		…	145
		HER	27				
	0.5 M H_2SO_4	OER	236	1.49	10 mA cm^{-2} @ 15 h		
		HER	19				
	0.1 M KOH	OER	276	1.55			
		HER	40				
	1 M KOH	OER	234	1.49	10 mA cm^{-2} @ 30 h		
		HER	20				

universal electrolytes and simultaneously catalyze the OER and HER under the same conditions, which are crucial for large-scale applications.

Despite these enormous promising advances, there always exists a lot of insufficient understanding, accompanied by the booming development. For this attractive field, there is still a long way to go. Many significant points are profiled below, some of which are not only suited to non-Pt NMN catalysts, but also beneficial to the development of other electrocatalysts.

First, currently, in order to acquire various effective non-Pt NMN HER electrocatalysts with a low concentration of noble metal, multifarious synthetic tactics have been widely adopted. However, it should be noted that most of these synthesis routes are much complicated with high energy-consumption, which leads to the high production cost of catalysts as well as sometimes offers poor quality and yield of the final products. All of these are very hard to meet the requirement for commercialization. Therefore, it is of great significance to develop gentle and simple methods for large-scale synthesis of the admirable catalysts with less precious metal.

Second, albeit predecessors have designed a great deal of non-Pt NMNs with different nanostructures, constructing non-Pt NMNs with several novel morphologies still faces a huge challenge. Limited porous morphologies, especially for nanosheets, hindered the excavation and exploitation of more superior and robust HER electrocatalysts. As is generally agreed, structuring hierarchical porous catalysts can provide rich accessible pores, a large inventory of defects, and large surface areas, which is in favor of the active site exposure, charge transfer, and mass diffusion. Hydrogen evolution is a surface-dependent and gas-involving process, in which the amounts of active sites and the ability of electron/mass transfer for a catalytic material highly affect the resulting catalytic performance. Accordingly, it is highly desirable to explore porous-structured non-Pt NMN electrocatalysts via reasonable and effective pathways, such as templating or self-corrosion methods.

Third, to precisely probe the catalytic activity and exhaustively understand the electronic structure–property relationship in these outstanding catalytic materials, some *in situ* spectroscopic techniques, like *in situ* Raman, XRD, XAS, etc., are highly desirable in widespread use. Besides, DFT calculation is regarded as a powerful tool to simulate the HER electrocatalytic process occurring on the surface of the catalytic material at the molecular scale. Specifically, it can predict the energy barrier of water dissociation and adsorption/desorption energies of hydrogen intermediates, so as to distinguish the active sites and reveal the possible rate-determining step. Of note, the construction of reasonable calculation models plays a fatal role in accurate simulation, which should be closer to the real reaction system.

Fourth, according to the above summary, it is found that all non-Pt noble metals, including Ru, Rh, Pd, Ag, Ir, and Au, show immense potential in hydrogen generation at all pH ranges, typically Ru, Rh, Pd, and Ir. Nevertheless, until now, in view of superb OER behavior, especially in acidic media, almost all bifunctional non-Pt NMN electrocatalysts are only limited to Ir/Ru-involving materials. For the larger cost reduction and convenience in the assembly of electrolyzers, in the next step, more attention should be devoted to developing more new and qualified bifunctional catalysts for both the OER and HER with high activities under pH-universal conditions. Exploiting more novel regulation tactics to concurrently activate the OER and HER in Rh, Pd, Ag, and Au or integrating the OER-active material with the HER-active component provides reasonable approaches to realize the bifunctionality of a catalyst.

Fifth, there is a lack of standardized measurements on the performance comparison between different catalysts from different reports. For example, in different research groups, the preparation methods of the working electrode, the used catalyst loadings, methods for

TABLE VI. Summary of various other representative bifunctional electrocatalysts toward overall water splitting in different media.

Catalyst	Electrolyte		η_{10} (mV)	Cell voltage (V) at 10 mA cm^{-2}	Stability	Loading (mg cm^{-2})	References
$SrNb_{0.1}Co_{0.7}Fe_{0.2}O_3$-$\delta$ nanorods (SNCF-NRs)	1 M KOH	OER	370	1.68	10 mA cm^{-2} @ 30 h	3	266
		HER	232				
CoP@a-CoOx plate/C	1 M KOH	OER	232	1.66	10 mA cm^{-2} @ 30 h	5	261
		HER	132				
N-WC	0.5 M H_2SO_4	OER	~220	<1.7 (at 30 mA cm^{-2})	…	5	267
		HER	113				
NC-CNT/CoP	0.5 M H_2SO_4	OER	350	1.66	1.7 V @ 20 h	1.5	268
		HER	62				
	1M PBS	OER	420	1.69	1.75 V @ 20 h		
		HER	45				
	1 M KOH	OER	240	1.63	1.75 V @ 20 h		
		HER	120				
single-walled carbon nanotubes (SWCNTs)/$MoSe_2$-2:Mo_2C	0.5 M H_2SO_4	OER	197	…	…	…	269
		HER	49				
	1 M KOH	OER	241				
		HER	89				
NiCo-nitrides/$NiCo_2O_4$/GF	0.5 M H_2SO_4	OER	460	1.57	1.4 V @ 40 h	…	270
		HER	432				
	1 M PBS	OER	673	…			
		HER	418				
	1 M KOH	OER	183	…			
		HER	71				
Co/CoP-5	0.5 M H_2SO_4	OER	…	1.89 (at 1 mA cm^{-2})	20 mA cm^{-2} @ 12 h	5	271
		HER	178				
	1 M PBS	OER	…	1.51	10 mA cm^{-2} @ 12 h		
		HER	138				
	1 M KOH	OER	340	1.45	1 mA cm^{-2} @ 12 h		
		HER	253				
Mo-Co_9S_8@C	0.5 M H_2SO_4	OER	370	1.68	1.65 V @ 24 h … 1.65 V @ 24 h	1	272
		HER	98				
	0.5 M Na_2SO_4	OER	290 (η_0)	…			
		HER	140				
	1 M KOH	OER	200	1.56			
		HER	113				
$MoSe_2$ NS/MoO_2 nanobelt (NB)/CNT-M	0.5 M H_2SO_4	OER	162 (η_{20})	1.63	2 V @ 10 h	…	273
		HER	97				
S-$NiFe_2O_4$/nickel foam (NF)	1 M PBS	OER	494	1.95	1.95 V @ 24 h	…	274
		HER	197				
CoO/Co_4N	1 M PBS	OER	398	1.79	10 mA cm^{-2} @ 50 h	3.8	275
		HER	145				
$NiCo_2Te_4$/perylene-3,4,9,10-tetracarboxylic dianhydride (PTCDA)	1 M PBS	OER	120	1.55	1.61 V @ 30 h	…	276
		HER	60				
p-FGDY/CC	0.5 M H_2SO_4	OER	570	1.80	…	…	277
		HER	92				
	1 M PBS	OER	623	…	…		
		HER	…				
	1 M KOH	OER	460	1.75	1.76 V @ 7 h		

TABLE VI. (*Continued.*)

Catalyst	Electrolyte		η_{10} (mV)	Cell voltage (V) at 10 mA cm^{-2}	Stability	Loading (mg cm^{-2})	References
		HER	82				
CoMoNiS-NF-31	0.5 M H_2SO_4	OER	228	1.45	1.53 V @ 20 h	1.86	278
		HER	103				
	1 M PBS	OER	405	1. 80	1.80 V @ 20 h		
		HER	117				
	1 M KOH	OER	166	1.54	1.70 V @ 20 h		
		HER	113				
Cu-CoP nanosheet arrays (NAs)/CP	1 M PBS	OER	411	1.72	10 mA cm^{-2} @ 60 h		279
		HER	81				

measuring stability, and methods to calculate the specific activity or TOF highly differ, which makes the performance evaluation of various materials more difficult and less meaningful. Thus, in future studies, it is extremely imperative to encourage researchers to test the HER properties under standard conditions and provide a unified evaluation standard.

Lastly, to further meet pragmatic configurations of the electrolyzers, the integration of binder-free 3D electrodes to electrolytic cells should be the focus of future research. The design of 3D free-standing electrodes helps us to promote faster charge transfer in the absence of low-conductivity binders and largely suppress the electrode detachment, as well as afford more active sites. Besides, the study of the large current density in the electrocatalysts also should attract much attention in the future.

ACKNOWLEDGMENTS

M. Ni thanks the funding support (Project Nos. PolyU 152214/17E and PolyU 152064/18E) from the Research Grant Council, University Grants Committee, Hong Kong SAR.

DATA AVAILABILITY

Data sharing is not applicable to this article as no new data were created or analyzed in this study.

REFERENCES

[1]Y. Zhao, W. Gao, S. Li, G. R. Williams, A. H. Mahadi, and D. Ma, "Solar-versus thermal-driven catalysis for energy conversion," Joule **3**(4), 920–937 (2019).
[2]S. Chu and A. Majumdar, "Opportunities and challenges for a sustainable energy future," Nature **488**(7411), 294–303 (2012).
[3]REN21, see http://www.ren21.net/about-ren21/about-us/ for "Renewables 2018 Global Status Report, 2018."
[4]C. G. Morales-Guio, S. D. Tilley, H. Vrubel, M. Grätzel, and X. Hu, "Hydrogen evolution from a copper (I) oxide photocathode coated with an amorphous molybdenum sulphide catalyst," Nat. Commun. **5**, 3059 (2014).
[5]R. Banos, F. Manzano-Agugliaro, F. G. Montoya, C. Gil, A. Alcayde, and J. Gomez, "Optimization methods applied to renewable and sustainable energy: A review," Renewable Sustainable Energy Rev. **15**(4), 1753–1766 (2011).
[6]J. Wang, F. Xu, H. Jin, Y. Chen, and Y. Wang, "Non-noble metal-based carbon composites in hydrogen evolution reaction: Fundamentals to applications," Adv. Mater. **29**(14), 1605838 (2017).
[7]S. Yuan, S.-Y. Pang, and J. Hao, "2D transition metal dichalcogenides, carbides, nitrides, and their applications in supercapacitors and electrocatalytic hydrogen evolution reaction," Appl. Phys. Rev. **7**, 021304 (2020).
[8]S. Anantharaj, S. R. Ede, K. Karthick, S. S. Sankar, K. Sangeetha, P. E. Karthik, and S. Kundu, "Precision and correctness in the evaluation of electrocatalytic water splitting: Revisiting activity parameters with a critical assessment," Energy Environ. Sci. **11**(4), 744–771 (2018).
[9]J. Yu, R. Ran, Y. Zhong, W. Zhou, M. Ni, and Z. Shao, "Advances in porous perovskites: Synthesis and electrocatalytic performance in fuel cells and metal-air batteries," Energy Environ. Mater. **3**(2), 121–145 (2020).
[10]J. Zhu, L. Hu, P. Zhao, L. Y. S. Lee, and K.-Y. Wong, "Recent advances in electrocatalytic hydrogen evolution using nanoparticles," Chem. Rev. **120**(2), 851–918 (2020).
[11]Y. Zhao, J. Bai, X.-R. Wu, P. Chen, P.-J. Jin, H.-C. Yao, and Y. Chen, "Atomically ultrathin RhCo alloy nanosheet aggregates for efficient water electrolysis in broad pH range," J. Mater. Chem. A **7**(27), 16437–16446 (2019).
[12]J. Yu, Q. He, G. Yang, W. Zhou, Z. Shao, and M. Ni, "Recent advances and prospective in ruthenium-based materials for electrochemical water splitting," ACS Catal. **9**(11), 9973–10011 (2019).
[13]C. Li and J.-B. Baek, "Recent advances in noble metal (Pt, Ru, and Ir)-based electrocatalysts for efficient hydrogen evolution reaction," ACS Omega **5**(1), 31–40 (2020).
[14]Z. W. Seh, J. Kibsgaard, C. F. Dickens, I. Chorkendorff, J. K. Nørskov, and T. F. Jaramillo, "Combining theory and experiment in electrocatalysis: Insights into materials design," Science **355**(6321), eaad4998 (2017).
[15]N. Zhang, Q. Shao, Y. Pi, J. Guo, and X. Huang, "Solvent-mediated shape tuning of well-defined rhodium nanocrystals for efficient electrochemical water splitting," Chem. Mater. **29**(11), 5009–5015 (2017).
[16]P. Jiang, H. Huang, J. Diao, S. Gong, S. Chen, J. Lu, C. Wang, Z. Sun, G. Xia, and K. Yang, "Improving electrocatalytic activity of iridium for hydrogen evolution at high current densities above 1000 mA cm^{-2}," Appl. Catal. B **258**(5), 117965 (2019).
[17]J. Feng, F. Lv, W. Zhang, P. Li, K. Wang, C. Yang, B. Wang, Y. Yang, J. Zhou, and F. Lin, "Iridium-based multimetallic porous hollow nanocrystals for efficient overall-water-splitting catalysis," Adv. Mater. **29**(47), 1703798 (2017).
[18]B. Zhang, C. Zhu, Z. Wu, E. Stavitski, Y. H. Lui, T.-H. Kim, H. Liu, L. Huang, X. Luan, and L. Zhou, "Integrating Rh species with NiFe-layered double hydroxide for overall water splitting," Nano Lett. **20**(1), 136–144 (2020).
[19]J. Ge, P. Wei, G. Wu, Y. Liu, T. Yuan, Z. Li, Y. Qu, Y. Wu, H. Li, and Z. Zhuang, "Ultrathin palladium nanomesh for electrocatalysis," Angew. Chem., Int. Ed. **130**(13), 3493–3496 (2018).
[20]J. Wang, Z. Wei, S. Mao, H. Li, and Y. Wang, "Highly uniform Ru nanoparticles over N-doped carbon: pH and temperature-universal hydrogen release from water reduction," Energy Environ. Sci. **11**(4), 800–806 (2018).
[21]Y. Shi and B. Zhang, "Recent advances in transition metal phosphide nanomaterials: Synthesis and applications in hydrogen evolution reaction," Chem. Soc. Rev. **45**(6), 1529–1541 (2016).

[22]T. F. Jaramillo, K. P. Jørgensen, J. Bonde, J. H. Nielsen, S. Horch, and I. Chorkendorff, "Identification of active edge sites for electrochemical H_2 evolution from MoS_2 nanocatalysts," Science **317**(5834), 100–102 (2007).
[23]G. Zhang, K. V. Vasudevan, B. L. Scott, and S. K. Hanson, "Understanding the mechanisms of cobalt-catalyzed hydrogenation and dehydrogenation reactions," J. Am. Chem. Soc. **135**(23), 8668–8681 (2013).
[24]R. Parsons, "The rate of electrolytic hydrogen evolution and the heat of adsorption of hydrogen," Trans. Faraday Soc. **54**, 1053–1063 (1958).
[25]S. Trasatti, "Work function, electronegativity, and electrochemical behaviour of metals: III. Electrolytic hydrogen evolution in acid solutions," J. Electroanal. Chem. Interfacial Electrochem. **39**(1), 163–184 (1972).
[26]T. R. Cook, D. K. Dogutan, S. Y. Reece, Y. Surendranath, T. S. Teets, and D. G. Nocera, "Solar energy supply and storage for the legacy and nonlegacy worlds," Chem. Rev. **110**(11), 6474–6502 (2010).
[27]J. K. Nørskov, T. Bligaard, A. Logadottir, J. Kitchin, J. G. Chen, S. Pandelov, and U. Stimming, "Trends in the exchange current for hydrogen evolution," J. Electrochem. Soc. **152**(3), J23–J26 (2005).
[28]E. Skúlason, V. Tripkovic, M. E. Björketun, S. Gudmundsdottir, G. Karlberg, J. Rossmeisl, T. Bligaard, H. Jónsson, and J. K. Nørskov, "Modeling the electrochemical hydrogen oxidation and evolution reactions on the basis of density functional theory calculations," J. Phys. Chem. C **114**(42), 18182–18197 (2010).
[29]S. W. Chee, J. M. Arce-Ramos, W. Li, A. Genest, and U. Mirsaidov, "Structural changes in noble metal nanoparticles during CO oxidation and their impact on catalyst activity," Nat. Commun. **11**, 2133 (2020).
[30]B. Hasa, J. Vakros, and A. D. Katsaounis, "Effect of TiO_2 on Pt-Ru-based anodes for methanol electroreforming," Appl. Catal. B **237**(5), 811–816 (2018).
[31]Q.-Y. Hu, R.-H. Zhang, D. Chen, Y.-F. Guo, W. Zhan, L.-M. Luo, and X.-W. Zhou, "Facile aqueous phase synthesis of 3D-netlike Pd-Rh nanocatalysts for methanol oxidation," Int. J. Hydrogen Energy **44**(31), 16287–16296 (2019).
[32]H. Ziaei-Azad and N. Semagina, "Iridium addition enhances hydrodesulfurization selectivity in 4,6-dimethyldibenzothiophene conversion on palladium," Appl. Catal. B **191**(15), 138–146 (2016).
[33]Q. Shi, C. Zhu, D. Du, and Y. Lin, "Robust noble metal-based electrocatalysts for oxygen evolution reaction," Chem. Soc. Rev. **48**(12), 3181–3192 (2019).
[34]M. Zhu, Q. Shao, Y. Qian, and X. Huang, "Superior overall water splitting electrocatalysis in acidic conditions enabled by bimetallic Ir-Ag nanotubes," Nano Energy **56**, 330–337 (2019).
[35]R.-Q. Yao, Y.-T. Zhou, H. Shi, Q.-H. Zhang, L. Gu, Z. Wen, X.-Y. Lang, and Q. Jiang, "Nanoporous palladium-silver surface alloys as efficient and pH-universal catalysts for the hydrogen evolution reaction," ACS Energy Lett. **4**(6), 1379–1386 (2019).
[36]W. Choi, G. Hu, K. Kwak, M. Kim, D-e Jiang, J.-P. Choi, and D. Lee, "Effects of metal-doping on hydrogen evolution reaction catalyzed by MAu_{24} and M_2Au_{36} nanoclusters (M = Pt, Pd," ACS Appl. Mater. Interfaces **10**(51), 44645–44653 (2018).
[37]Y. Qin, X. Dai, X. Zhang, X. Huang, H. Sun, D. Gao, Y. Yu, P. Zhang, Y. Jiang, and H. Zhuo, "Microwave-assisted synthesis of multiply-twinned Au-Ag nanocrystals on reduced graphene oxide for high catalytic performance towards hydrogen evolution reaction," J. Mater. Chem. A **4**(10), 3865–3871 (2016).
[38]L. Chang, D. Cheng, L. Sementa, and A. Fortunelli, "Hydrogen evolution reaction (HER) on Au@Ag ultrananoclusters as electro-catalysts," Nanoscale **10**(37), 17730–17737 (2018).
[39]X. Qin, L. Zhang, G.-L. Xu, S. Zhu, Q. Wang, M. Gu, X. Zhang, C. Sun, P. B. Balbuena, and K. Amine, "The role of Ru in improving the activity of Pd toward hydrogen evolution and oxidation reactions in alkaline solutions," ACS Catal. **9**(10), 9614–9621 (2019).
[40]W. Shen, B. Wu, F. Liao, B. Jiang, and M. Shao, "Optimizing the hydrogen evolution reaction by shrinking Pt amount in Pt-Ag/SiNW nanocomposites," Int. J. Hydrogen Energy **42**(22), 15024–15030 (2017).
[41]T. Chao, X. Luo, W. Chen, B. Jiang, J. Ge, Y. Lin, G. Wu, X. Wang, Y. Hu, and Z. Zhuang, "Atomically dispersed copper-platinum dual sites alloyed with palladium nanorings catalyze the hydrogen evolution reaction," Angew. Chem., Int. Ed. **129**(50), 16263–16267 (2017).
[42]J. Lu, L. Zhang, S. Jing, L. Luo, and S. Yin, "Remarkably efficient PtRh alloyed with nanoscale WC for hydrogen evolution in alkaline solution," Int. J. Hydrogen Energy **42**(9), 5993–5999 (2017).
[43]K. Li, Y. Li, Y. Wang, J. Ge, C. Liu, and W. Xing, "Enhanced electrocatalytic performance for the hydrogen evolution reaction through surface enrichment of platinum nanoclusters alloying with ruthenium in situ embedded in carbon," Energy Environ. Sci. **11**(5), 1232–1239 (2018).
[44]L. Li, G. Zhang, B. Wang, T. Yang, and S. Yang, "Electrochemical formation of PtRu bimetallic nanoparticles for highly efficient and pH-universal hydrogen evolution reaction," J. Mater. Chem. A **8**(4), 2090–2098 (2020).
[45]L. Zhang, H. Liu, S. Liu, M. Norouzi Banis, Z. Song, J. Li, L. Yang, M. Markiewicz, Y. Zhao, and R. Li, "Pt/Pd single-atom alloys as highly active electrochemical catalysts and the origin of enhanced activity," ACS Catal. **9**(10), 9350–9358 (2019).
[46]C. H. Chen, D. Wu, Z. Li, R. Zhang, C. G. Kuai, X. R. Zhao, C. K. Dong, S. Z. Qiao, H. Liu, and X. W. Du, "Ruthenium-based single-atom alloy with high electrocatalytic activity for hydrogen evolution," Adv. Energy Mater. **9**(20), 1803913 (2019).
[47]J. Mao, C.-T. He, J. Pei, W. Chen, D. He, Y. He, Z. Zhuang, C. Chen, Q. Peng, and D. Wang, "Accelerating water dissociation kinetics by isolating cobalt atoms into ruthenium lattice," Nat. Commun. **9**, 4958 (2018).
[48]J. Li, F. Li, S.-X. Guo, J. Zhang, and J. Ma, "PdCu@Pd nanocube with Pt-like activity for hydrogen evolution reaction," ACS Appl. Mater. Interfaces **9**(9), 8151–8160 (2017).
[49]Y. Liu, X. Li, Q. Zhang, W. Li, Y. Xie, H. Liu, L. Shang, Z. Liu, Z. Chen, L. Gu, Z. Tang, T. Zhang, and S. Lu, "A general route to prepare low-ruthenium-content bimetallic electrocatalysts for pH-universal hydrogen evolution reaction by using carbon quantum dots," Angew. Chem., Int. Ed. **59**(4), 1718–1726 (2020).
[50]Y. Pi, Q. Shao, P. Wang, J. Guo, and X. Huang, "General formation of monodisperse IrM (M = Ni, Co, Fe) bimetallic nanoclusters as bifunctional electrocatalysts for acidic overall water splitting," Adv. Funct. Mater. **27**(27), 1700886 (2017).
[51]F. Lv, W. Zhang, W. Yang, J. Feng, K. Wang, J. Zhou, P. Zhou, and S. Guo, "Ir-based alloy nanoflowers with optimized hydrogen binding energy as bifunctional electrocatalysts for overall water splitting," Small Methods **4**(6), 1900129 (2020).
[52]I. Golvano-Escobal, S. Suriñach, M. D. Baró, S. Pané, J. Sort, and E. Pellicer, "Electrodeposition of sizeable and compositionally tunable rhodium-iron nanoparticles and their activity toward hydrogen evolution reaction," Electrochim. Acta **194**(10), 263–275 (2016).
[53]L. Zhang, J. Lu, S. Yin, L. Luo, S. Jing, A. Brouzgou, J. Chen, P. K. Shen, and P. Tsiakaras, "One-pot synthesized boron-doped RhFe alloy with enhanced catalytic performance for hydrogen evolution reaction," Appl. Catal. B **230**(15), 58–64 (2018).
[54]R. Majee, A. Kumar, T. Das, S. Chakraborty, and S. Bhattacharyya, "Tweaking nickel with minimal silver in a heterogeneous alloy of decahedral geometry to deliver platinum-like hydrogen evolution activity," Angew. Chem., Int. Ed. **59**(7), 2881–2889 (2020).
[55]P. Jiang, J. Chen, C. Wang, K. Yang, S. Gong, S. Liu, Z. Lin, M. Li, G. Xia, and Y. Yang, "Tuning the activity of carbon for electrocatalytic hydrogen evolution via an iridium-cobalt alloy core encapsulated in nitrogen-doped carbon cages," Adv. Mater. **30**(9), 1705324 (2018).
[56]S. Gong, C. Wang, P. Jiang, K. Yang, J. Lu, M. Huang, S. Chen, J. Wang, and Q. Chen, "O species-decorated graphene shell encapsulating iridium-nickel alloy as an efficient electrocatalyst towards hydrogen evolution reaction," J. Mater. Chem. A **7**(25), 15079–15088 (2019).
[57]J. Chen, G. Xia, P. Jiang, Y. Yang, R. Li, R. Shi, J. Su, and Q. Chen, "Active and durable hydrogen evolution reaction catalyst derived from Pd-doped metal-organic frameworks," ACS Appl. Mater. Interfaces **8**(21), 13378–13383 (2016).
[58]J. Su, Y. Yang, G. Xia, J. Chen, P. Jiang, and Q. Chen, "Ruthenium-cobalt nanoalloys encapsulated in nitrogen-doped graphene as active electrocatalysts for producing hydrogen in alkaline media," Nat. Commun. **8**, 14969 (2017).
[59]Y. Xu, S. Yin, C. Li, K. Deng, H. Xue, X. Li, H. Wang, and L. Wang, "Low-ruthenium-content NiRu nanoalloys encapsulated in nitrogen-doped carbon as highly efficient and pH-universal electrocatalysts for the hydrogen evolution reaction," J. Mater. Chem. A **6**(4), 1376–1381 (2018).
[60]J. Wang, H. Zhu, D. Yu, J. Chen, J. Chen, M. Zhang, L. Wang, and M. Du, "Engineering the composition and structure of bimetallic Au-Cu alloy

nanoparticles in carbon nanofibers: Self-supported electrode materials for electrocatalytic water splitting," ACS Appl. Mater. Interfaces **9**(23), 19756–19765 (2017).
[61]Q. Wu, M. Luo, J. Han, W. Peng, Y. Zhao, D. Chen, M. Peng, J. Liu, F. M. de Groot, and Y. Tan, "Identifying electrocatalytic sites of the nanoporous copper-ruthenium alloy for hydrogen evolution reaction in alkaline electrolyte," ACS Energy Lett. **5**(1), 192–199 (2020).
[62]F. Lv, J. Feng, K. Wang, Z. Dou, W. Zhang, J. Zhou, C. Yang, M. Luo, Y. Yang, and Y. Li, "Iridium-tungsten alloy nanodendrites as pH-universal water-splitting electrocatalysts," ACS Cent. Sci. **4**(9), 1244–1252 (2018).
[63]Z. Zhang, P. Li, Q. Wang, Q. Feng, Y. Tao, J. Xu, C. Jiang, X. Lu, J. Fan, and M. Gu, "Mo modulation effect on the hydrogen binding energy of hexagonal-close-packed Ru for hydrogen evolution," J. Mater. Chem. A 7(6), 2780–2786 (2019).
[64]L. Fu, G. Cheng, and W. Luo, "Colloidal synthesis of monodisperse trimetallic IrNiFe nanoparticles as highly active bifunctional electrocatalysts for acidic overall water splitting," J. Mater. Chem. A **5**(47), 24836–24841 (2017).
[65]Z. J. Wang, M. X. Li, J. H. Yu, X. B. Ge, Y. H. Liu, and W. H. Wang, "Low-iridium-content IrNiTa metallic glass films as intrinsically active catalysts for hydrogen evolution reaction," Adv. Mater. **32**(4), 1906384 (2020).
[66]H. Li, Q. Tang, B. He, and P. Yang, "Robust electrocatalysts from an alloyed Pt-Ru-M (M = Cr, Fe, Co, Ni, Mo)-decorated Ti mesh for hydrogen evolution by seawater splitting," J. Mater. Chem. A **4**(17), 6513–6520 (2016).
[67]J. Shan, T. Ling, K. Davey, Y. Zheng, and S. Z. Qiao, "Transition-metal-doped RuIr bifunctional nanocrystals for overall water splitting in acidic environments," Adv. Mater. **31**(17), 1900510 (2019).
[68]D. Zhang, H. Zhao, B. Huang, B. Li, H. Li, Y. Han, Z. Wang, X. Wu, Y. Pan, and Y. Sun, "Advanced ultrathin RuPdM (M = Ni, Co, Fe) nanosheets electrocatalyst boosts hydrogen evolution," ACS Cent. Sci. **5**(12), 1991–1997 (2019).
[69]Z. Zhuang, Y. Wang, C.-Q. Xu, S. Liu, C. Chen, Q. Peng, Z. Zhuang, H. Xiao, Y. Pan, and S. Lu, "Three-dimensional open nano-netcage electrocatalysts for efficient pH-universal overall water splitting," Nat. Commun. **10**, 4875 (2019).
[70]J. Yu, X. Wu, H. Zhang, M. Ni, W. Zhou, and Z. Shao, "Core effect on the performance of N/P codoped carbon encapsulating noble-metal phosphide nanostructures for hydrogen evolution reaction," ACS Appl. Energy Mater. **2**(4), 2645–2653 (2019).
[71]J. Yu, Y. Guo, S. Miao, M. Ni, W. Zhou, and Z. Shao, "Spherical ruthenium disulfide-sulfur-doped graphene composite as an efficient hydrogen evolution electrocatalyst," ACS Appl. Mater. Interfaces **10**(40), 34098–34107 (2018).
[72]Q. Li, X. Zou, X. Ai, H. Chen, L. Sun, and X. Zou, "Revealing activity trends of metal diborides toward pH-universal hydrogen evolution electrocatalysts with Pt-like activity," Adv. Energy Mater. **9**(5), 1803369 (2018).
[73]T. Wakisaka, K. Kusada, D. Wu, T. Yamamoto, T. Toriyama, S. Matsumura, H. Akiba, O. Yamamuro, K. Ikeda, and T. Otomo, "Rational synthesis for a noble metal carbide," J. Am. Chem. Soc. **142**(3), 1247–1253 (2020).
[74]J. Ahmed and Y. Mao, "Ultrafine iridium oxide nanorods synthesized by molten salt method toward electrocatalytic oxygen and hydrogen evolution reactions," Electrochim. Acta **212**(10), 686–693 (2016).
[75]Y.-B. Cho, A. Yu, C. Lee, M. H. Kim, and Y. Lee, "Fundamental study of facile and stable hydrogen evolution reaction at electrospun Ir and Ru mixed oxide nanofibers," ACS Appl. Mater. Interfaces **10**(1), 541–549 (2018).
[76]J. Yu, X. Wu, D. Guan, Z. Hu, S.-C. Weng, H. Sun, Y. Song, R. Ran, W. Zhou, and M. Ni, "Monoclinic $SrIrO_3$: An easily-synthesized conductive perovskite oxide with outstanding performance for overall water splitting in alkaline solution," Chem. Mater. **32**(11), 4509–4517 (2020).
[77]J. Wang, Y. Ji, R. Yin, Y. Li, Q. Shao, and X. Huang, "Transition metal-doped ultrathin RuO_2 networked nanowires for efficient overall water splitting across a broad pH range," J. Mater. Chem. A **7**(11), 6411–6416 (2019).
[78]Y. Zhu, H. A. Tahini, Z. Hu, J. Dai, Y. Chen, H. Sun, W. Zhou, M. Liu, S. C. Smith, and H. Wang, "Unusual synergistic effect in layered Ruddlesden-Popper oxide enables ultrafast hydrogen evolution," Nat. Commun. **10**, 149 (2019).
[79]M. K. Kundu, R. Mishra, T. Bhowmik, and S. Barman, "Rhodium metal-rhodium oxide (Rh-Rh_2O_3) nanostructures with Pt-like or better activity towards hydrogen evolution and oxidation reactions (HER, HOR) in acid and base: Correlating its HOR/HER activity with hydrogen binding energy and oxophilicity of the catalyst," J. Mater. Chem. A **6**(46), 23531–23541 (2018).
[80]H. Duan, D. Li, Y. Tang, Y. He, S. Ji, R. Wang, H. Lv, P. P. Lopes, A. P. Paulikas, and H. Li, "High-performance Rh_2P electrocatalyst for efficient water splitting," J. Am. Chem. Soc. **139**(15), 5494–5502 (2017).
[81]Z. Pu, I. S. Amiinu, Z. Kou, W. Li, and S. Mu, "RuP_2-based catalysts with platinum-like activity and higher durability for the hydrogen evolution reaction at all pH values," Angew. Chem., Int. Ed. **56**(38), 11559–11564 (2017).
[82]Q. Qin, H. Jang, L. Chen, G. Nam, X. Liu, and J. Cho, "Low loading of Rh_xP and RuP on N, P codoped carbon as two trifunctional electrocatalysts for the oxygen and hydrogen electrode reactions," Adv. Energy Mater. **8**(29), 1801478 (2018).
[83]Z. Pu, I. S. Amiinu, D. He, M. Wang, G. Li, and S. Mu, "Activating rhodium phosphide-based catalysts for the pH-universal hydrogen evolution reaction," Nanoscale **10**(26), 12407–12412 (2018).
[84]K. Wang, B. Huang, F. Lin, F. Lv, M. Luo, P. Zhou, Q. Liu, W. Zhang, C. Yang, and Y. Tang, "Wrinkled Rh_2P nanosheets as superior pH-universal electrocatalysts for hydrogen evolution catalysis," Adv. Energy Mater. **8**(27), 1801891 (2018).
[85]F. Yang, Y. Zhao, Y. Du, Y. Chen, G. Cheng, S. Chen, and W. Luo, "A monodisperse Rh_2P-based electrocatalyst for highly efficient and pH-universal hydrogen evolution reaction," Adv. Energy Mater. **8**(18), 1703489 (2018).
[86]J. Q. Chi, X. J. Zeng, X. Shang, B. Dong, Y. M. Chai, C. G. Liu, M. Marin, and Y. Yin, "Embedding RhP_x in N, P co-doped carbon nanoshells through synergetic phosphorization and pyrolysis for efficient hydrogen evolution," Adv. Funct. Mater. **29**(33), 1901790 (2019).
[87]J. Yu, Y. Guo, S. She, S. Miao, M. Ni, W. Zhou, M. Liu, and Z. Shao, "Bigger is surprisingly better: Agglomerates of larger RuP nanoparticles outperform benchmark Pt nanocatalysts for the hydrogen evolution reaction," Adv. Mater. **30**(39), 1800047 (2018).
[88]Q. Chang, J. Ma, Y. Zhu, Z. Li, D. Xu, X. Duan, W. Peng, Y. Li, G. Zhang, and F. Zhang, "Controllable synthesis of ruthenium phosphides (RuP and RuP_2) for pH-universal hydrogen evolution reaction," ACS Sustainable Chem. Eng. **6**(5), 6388–6394 (2018).
[89]R. Ge, S. Wang, J. Su, Y. Dong, Y. Lin, Q. Zhang, and L. Chen, "Phase-selective synthesis of self-supported RuP films for efficient hydrogen evolution electrocatalysis in alkaline media," Nanoscale **10**(29), 13930–13935 (2018).
[90]J. Q. Chi, W. K. Gao, J. H. Lin, B. Dong, K. L. Yan, J. F. Qin, B. Liu, Y. M. Chai, and C. G. Liu, "Hydrogen evolution activity of ruthenium phosphides encapsulated in nitrogen-and phosphorous-codoped hollow carbon nanospheres," ChemSusChem **11**(4), 743–752 (2018).
[91]Z. Pu, J. Zhao, I. S. Amiinu, W. Li, M. Wang, D. He, and S. Mu, "A universal synthesis strategy for P-rich noble metal diphosphide-based electrocatalysts for the hydrogen evolution reaction," Energy Environ. Sci. **12**(3), 952–957 (2019).
[92]F. Luo, Q. Zhang, X. Yu, S. Xiao, Y. Ling, H. Hu, L. Guo, Z. Yang, L. Huang, and W. Cai, "Palladium phosphide as a stable and efficient electrocatalyst for overall water splitting," Angew. Chem., Int. Ed. **57**(45), 14862–14867 (2018).
[93]K. Wang, Q. Chen, Y. Hu, W. Wei, S. Wang, Q. Shen, and P. Qu, "Crystalline $Ru_{0.33}Se$ nanoparticles-decorated TiO_2 nanotube arrays for enhanced hydrogen evolution reaction," Small **14**(37), 1802132 (2018).
[94]P. Li, X. Duan, S. Wang, L. Zheng, Y. Li, H. Duan, Y. Kuang, and X. Sun, "Amorphous ruthenium-sulfide with isolated catalytic sites for Pt-like electrocatalytic hydrogen production over whole pH range," Small **15**(46), 1904043 (2019).
[95]D. Yoon, B. Seo, J. Lee, K. S. Nam, B. Kim, S. Park, H. Baik, S. H. Joo, and K. Lee, "Facet-controlled hollow Rh_2S_3 hexagonal nanoprisms as highly active and structurally robust catalysts toward hydrogen evolution reaction," Energy Environ. Sci. **9**(3), 850–856 (2016).
[96]P. Hota, S. Bose, D. Dinda, P. Das, U. K. Ghorai, S. Bag, S. Mondal, and S. K. Saha, "Nickel-doped silver sulfide: An efficient air-stable electrocatalyst for hydrogen evolution from neutral water," ACS Omega **3**(12), 17070–17076 (2018).
[97]J. Wang, L. Han, B. Huang, Q. Shao, H. L. Xin, and X. Huang, "Amorphization activated ruthenium-tellurium nanorods for efficient water splitting," Nat. Commun. **10**, 5692 (2019).

[98]H. Huang, X. Fan, D. J. Singh, and W. Zheng, "Modulation of hydrogen evolution catalytic activity of basal plane in monolayer platinum and palladium dichalcogenides," ACS Omega **3**(8), 10058–10065 (2018).

[99]T. Zheng, C. Shang, Z. He, X. Wang, C. Cao, H. Li, R. Si, B. Pan, S. Zhou, and J. Zeng, "Intercalated iridium diselenide electrocatalysts for efficient pH-universal water splitting," Angew. Chem., Int. Ed. **131**(41), 14906–14911 (2019).

[100]Y. Zhu, H. A. Tahini, Y. Wang, Q. Lin, Y. Liang, C. M. Doherty, Y. Liu, X. Li, J. Lu, and S. C. Smith, "Pyrite-type ruthenium disulfide with tunable disorder and defects enables ultra-efficient overall water splitting," J. Mater. Chem. A **7**(23), 14222–14232 (2019).

[101]N. Singh, J. Hiller, H. Metiu, and E. McFarland, "Investigation of the electrocatalytic activity of rhodium sulfide for hydrogen evolution and hydrogen oxidation," Electrochim. Acta **145**(1), 224–230 (2014).

[102]V. Shokhen, Y. Kostikov, I. Borge-Durán, Y. Gershinsky, I. Grinberg, G. D. Nessim, and D. Zitoun, "Scalable silver oxo-sulfide catalyst for electrochemical water splitting," ACS Appl. Energy Mater. **2**(1), 788–796 (2019).

[103]X. Zhang, Z. Luo, P. Yu, Y. Cai, Y. Du, D. Wu, S. Gao, C. Tan, Z. Li, and M. Ren, "Lithiation-induced amorphization of $Pd_3P_2S_8$ for highly efficient hydrogen evolution," Nat. Catal. **1**(6), 460–468 (2018).

[104]L. Chen, L.-R. Zhang, L.-Y. Yao, Y.-H. Fang, L. He, G.-F. Wei, and Z.-P. Liu, "Metal boride better than Pt: HCP Pd_2B as a superactive hydrogen evolution reaction catalyst," Energy Environ. Sci. **12**(10), 3099–3105 (2019).

[105]G. Wang, J. Liu, Y. Sui, M. Wang, L. Qiao, F. Du, and B. Zou, "Palladium structure engineering induced by electrochemical H intercalation boosts hydrogen evolution catalysis," J. Mater. Chem. A **7**(24), 14876–14881 (2019).

[106]H. Chen, X. Ai, W. Liu, Z. Xie, W. Feng, W. Chen, and X. Zou, "Promoting subordinate, efficient ruthenium sites with interstitial silicon for Pt-like electrocatalytic activity," Angew. Chem., Int. Ed. **58**(33), 11409–11413 (2019).

[107]J. Fan, X. Cui, S. Yu, L. Gu, Q. Zhang, F. Meng, Z. Peng, L. Ma, J.-Y. Ma, and K. Qi, "Interstitial hydrogen atom modulation to boost hydrogen evolution in Pd-based alloy nanoparticles," ACS Nano **13**(11), 12987–12995 (2019).

[108]S.-C. Lim, C.-Y. Chan, K.-T. Chen, and H.-Y. Tuan, "The shape-controlled synthesis of gallium-palladium ($GaPd_2$) nanomaterials as high-performance electrocatalysts for the hydrogen evolution reaction," Nanoscale **11**(17), 8518–8527 (2019).

[109]S. Li, L. Zhang, Y. Lan, K. P. O'Halloran, H. Ma, and H. Pang, "Polyoxometalate-encapsulated twenty-nuclear silver-tetrazole nanocage frameworks as highly active electrocatalysts for the hydrogen evolution reaction," Chem. Commun. **54**(16), 1964–1967 (2018).

[110]D. Eguchi, M. Sakamoto, and T. Teranishi, "Ligand effect on the catalytic activity of porphyrin-protected gold clusters in the electrochemical hydrogen evolution reaction," Chem. Sci. **9**(1), 261–265 (2018).

[111]G. Hu, Z. Wu, and D-e Jiang, "Stronger-than-Pt hydrogen adsorption in a Au_{22} nanocluster for the hydrogen evolution reaction," J. Mater. Chem. A **6**(17), 7532–7537 (2018).

[112]N. Kuwamura, Y. Kurioka, and T. Konno, "A platinum(ii)-palladium(ii)-nickel(ii) heterotrimetallic coordination polymer showing a cooperative effect on catalytic hydrogen evolution," Chem. Commun. **53**(5), 846–849 (2017).

[113]X. Gao and W. Chen, "Highly stable and efficient $Pd_6(SR)_{12}$ cluster catalysts for the hydrogen and oxygen evolution reactions," Chem. Commun. **53**(70), 9733–9736 (2017).

[114]M. A. Sayeed and A. P. O'Mullane, "A multifunctional gold doped $Co(OH)_2$ electrocatalyst tailored for water oxidation, oxygen reduction, hydrogen evolution and glucose detection," J. Mater. Chem. A **5**(45), 23776–23784 (2017).

[115]S. Li, C. Xi, Y.-Z. Jin, D. Wu, J.-Q. Wang, T. Liu, H.-B. Wang, C.-K. Dong, H. Liu, and S. A. Kulinich, "Ir-O-V catalytic group in Ir-doped $NiV(OH)_2$ for overall water splitting," ACS Energy Lett. **4**(8), 1823–1829 (2019).

[116]Q.-Q. Chen, C.-C. Hou, C.-J. Wang, X. Yang, R. Shi, and Y. Chen, "Ir^{4+}-doped NiFe LDH to expedite hydrogen evolution kinetics as a Pt-like electrocatalyst for water splitting," Chem. Commun. **54**(49), 6400–6403 (2018).

[117]G. Chen, T. Wang, J. Zhang, P. Liu, H. Sun, X. Zhuang, M. Chen, and X. Feng, "Accelerated hydrogen evolution kinetics on NiFe-layered double hydroxide electrocatalysts by tailoring water dissociation active sites," Adv. Mater. **30**(10), 1706279 (2018).

[118]D. Wang, Q. Li, C. Han, Q. Lu, Z. Xing, and X. Yang, "Atomic and electronic modulation of self-supported nickel-vanadium layered double hydroxide to accelerate water splitting kinetics," Nat. Commun. **10**, 3899 (2019).

[119]M. Qu, Y. Jiang, M. Yang, S. Liu, Q. Guo, W. Shen, M. Li, and R. He, "Regulating electron density of NiFe-P nanosheets electrocatalysts by a trifle of Ru for high-efficient overall water splitting," Appl. Catal. B **263**, 118324 (2020).

[120]K.-L. Yan, X. Shang, L.-M. Zhang, B. Dong, Z.-Z. Liu, J.-Q. Chi, W.-K. Gao, Y.-M. Chai, and C.-G. Liu, "Boosting electrocatalytic activity of binary Ag-Fe-doped Co_2P nanospheres as bifunctional electrocatalysts for overall water splitting," Electrochim. Acta **249**(20), 16–25 (2017).

[121]X. Zhang, F. Zhou, S. Zhang, Y. Liang, and R. Wang, "Engineering MoS_2 basal planes for hydrogen evolution via synergistic ruthenium doping and nanocarbon hybridization," Adv. Sci. **6**(10), 1900090 (2019).

[122]J. Zhang, X. Xu, L. Yang, D. Cheng, and D. Cao, "Single-atom Ru doping induced phase transition of MoS_2 and S vacancy for hydrogen evolution reaction," Small Methods **3**(12), 1900653 (2019).

[123]Z. Luo, Y. Ouyang, H. Zhang, M. Xiao, J. Ge, Z. Jiang, J. Wang, D. Tang, X. Cao, and C. Liu, "Chemically activating MoS_2 via spontaneous atomic palladium interfacial doping towards efficient hydrogen evolution," Nat. Commun. **9**, 2120 (2018).

[124]K. Vasu, O. E. Meiron, A. N. Enyashin, R. Bar-Ziv, and M. Bar-Sadan, "Effect of Ru doping on the properties of $MoSe_2$ nanoflowers," J. Phys. Chem. C **123**(3), 1987–1994 (2019).

[125]C. Huang, X. Wang, D. Wang, W. Zhao, K. Bu, J. Xu, X. Huang, Q. Bi, J. Huang, and F. Huang, "Atomic pillar effect in Pd_xNbS_2 to boost basal plane activity for stable hydrogen evolution," Chem. Mater. **31**(13), 4726–4731 (2019).

[126]D. Wang, X. Wang, Y. Lu, C. Song, J. Pan, C. Li, M. Sui, W. Zhao, and F. Huang, "Atom-scale dispersed palladium in a conductive $Pd_{0.1}TaS_2$ lattice with a unique electronic structure for efficient hydrogen evolution," J. Mater. Chem. A **5**(43), 22618–22624 (2017).

[127]Q. Wang, M. Ming, S. Niu, Y. Zhang, G. Fan, and J. S. Hu, "Scalable solid-state synthesis of highly dispersed uncapped metal (Rh, Ru, Ir) nanoparticles for efficient hydrogen evolution," Adv. Energy Mater. **8**(31), 1801698 (2018).

[128]M. Ming, Y. Zhang, C. He, L. Zhao, S. Niu, G. Fan, and J. S. Hu, "Room-temperature sustainable synthesis of selected platinum group metal (PGM = Ir, Rh, and Ru) nanocatalysts well-dispersed on porous carbon for efficient hydrogen evolution and oxidation," Small **15**(49), 1903057 (2019).

[129]B. K. Barman, D. Das, and K. K. Nanda, "Facile synthesis of ultrafine Ru nanocrystal supported N-doped graphene as an exceptional hydrogen evolution electrocatalyst in both alkaline and acidic media," Sustainable Energy Fuels **1**(5), 1028–1033 (2017).

[130]Y. Wang, Y. Sun, H. Liao, S. Sun, S. Li, J. W. Ager, and Z. J. Xu, "Activation effect of electrochemical cycling on gold nanoparticles towards the hydrogen evolution reaction in sulfuric acid," Electrochim. Acta **209**(10), 440–447 (2016).

[131]K. A. Kuttiyiel, K. Sasaki, W.-F. Chen, D. Su, and R. R. Adzic, "Core-shell, hollow-structured iridium-nickel nitride nanoparticles for the hydrogen evolution reaction," J. Mater. Chem. A **2**(3), 591–594 (2014).

[132]T. D. Tran, M. T. Nguyen, H. V. Le, D. N. Nguyen, Q. D. Truong, and P. D. Tran, "Gold nanoparticles as an outstanding catalyst for the hydrogen evolution reaction," Chem. Commun. **54**(27), 3363–3366 (2018).

[133]J. Zheng, S. Zhou, S. Gu, B. Xu, and Y. Yan, "Size-dependent hydrogen oxidation and evolution activities on supported palladium nanoparticles in acid and base," J. Electrochem. Soc. **163**(6), F499 (2016).

[134]J. Li, P. Zhou, F. Li, J. Ma, Y. Liu, X. Zhang, H. Huo, J. Jin, and J. Ma, "Shape-controlled synthesis of Pd polyhedron supported on polyethyleneimine-reduced graphene oxide for enhancing the efficiency of hydrogen evolution reaction," J. Power Sources **302**(20), 343–351 (2016).

[135]T.-R. Kuo, Y.-C. Lee, H.-L. Chou, M. G. Swathi, C.-Y. Wei, C.-Y. Wen, Y.-H. Chang, X.-Y. Pan, and D.-Y. Wang, "Plasmon-enhanced hydrogen evolution on specific facet of silver nanocrystals," Chem. Mater. **31**(10), 3722–3728 (2019).

[136]J. Yang, Y. Ji, Q. Shao, N. Zhang, Y. Li, and X. Huang, "A universal strategy to metal wavy nanowires for efficient electrochemical water splitting at pH-universal conditions," Adv. Funct. Mater. **28**(41), 1803722 (2018).

[137]C. Zhang, S. Liu, Z. Mao, X. Liang, and B. Chen, "Ag-Ni core-shell nanowires with superior electrocatalytic activity for alkaline hydrogen evolution reaction," J. Mater. Chem. A **5**(32), 16646–16652 (2017).

[138]L. Fu, F. Yang, G. Cheng, and W. Luo, "Ultrathin Ir nanowires as high-performance electrocatalysts for efficient water splitting in acidic media," Nanoscale **10**(4), 1892–1897 (2018).
[139]L. Zhang, L. Liu, H. Wang, H. Shen, Q. Cheng, C. Yan, and S. Park, "Electrodeposition of rhodium nanowires arrays and their morphology-dependent hydrogen evolution activity," Nanomaterials **7**(5), 103 (2017).
[140]Q. Lu, A. L. Wang, H. Cheng, Y. Gong, Q. Yun, N. Yang, B. Li, B. Chen, Q. Zhang, and Y. Zong, "Synthesis of hierarchical 4H/fcc Ru nanotubes for highly efficient hydrogen evolution in alkaline media," Small **14**(30), 1801090 (2018).
[141]R. Nazir, U. Basak, and S. Pande, "Synthesis of one-dimensional RuO_2 nanorod for hydrogen and oxygen evolution reaction: An efficient and stable electrocatalyst," Colloids Surf. A **560**(5), 141–148 (2019).
[142]Y. Han, Y. Yan, Z. Wu, Y. Jiang, X. Li, Q. Xu, X. Yang, H. Zhang, and D. Yang, "Facile synthesis of Pd@Ru nanoplates with controlled thickness as efficient catalysts for hydrogen evolution reaction," CrystEngComm **20**(30), 4230–4236 (2018).
[143]Y. Zhao, S. Xing, X. Meng, J. Zeng, S. Yin, X. Li, and Y. Chen, "Ultrathin Rh nanosheets as a highly efficient bifunctional electrocatalyst for isopropanol-assisted overall water splitting," Nanoscale **11**(19), 9319–9326 (2019).
[144]X. Kong, K. Xu, C. Zhang, J. Dai, S. Norooz Oliaee, L. Li, X. Zeng, C. Wu, and Z. Peng, "Free-standing two-dimensional Ru nanosheets with high activity toward water splitting," ACS Catal. **6**(3), 1487–1492 (2016).
[145]Q. Yao, B. Huang, N. Zhang, M. Sun, Q. Shao, and X. Huang, "Channel-rich RuCu nanosheets for pH-universal overall water splitting electrocatalysis," Angew. Chem., Int. Ed. **58**(39), 13983–13988 (2019).
[146]J. Mo, B. I. Stefanov, T. H. Lau, T. Chen, S. Wu, Z. Wang, X.-Q. Gong, I. Wilkinson, G. n Schmid, and S. C. E. Tsang, "Superior performance of Ag over Pt for hydrogen evolution reaction in water electrolysis under high overpotentials," ACS Appl. Energy Mater. **2**(2), 1221–1228 (2019).
[147]H. Begum, M. S. Ahmed, and S. Jeon, "Highly efficient dual active palladium nanonetwork electrocatalyst for ethanol oxidation and hydrogen evolution," ACS Appl. Mater. Interfaces **9**(45), 39303–39311 (2017).
[148]J.-F. Huang and Y.-C. Wu, "Making Ag present Pt-like activity for hydrogen evolution reaction," ACS Sustainable Chem. Eng. **6**(7), 8285–8290 (2018).
[149]Y. Luo, X. Luo, G. Wu, Z. Li, G. Wang, B. Jiang, Y. Hu, T. Chao, H. Ju, and J. Zhu, "Mesoporous Pd@ Ru core-shell nanorods for hydrogen evolution reaction in alkaline solution," ACS Appl. Mater. Interfaces **10**(40), 34147–34152 (2018).
[150]C. Yang, H. Lei, W. Zhou, J. Zeng, Q. Zhang, Y. Hua, and C. Xu, "Engineering nanoporous Ag/Pd core/shell interfaces with ultrathin Pt doping for efficient hydrogen evolution reaction over a wide pH range," J. Mater. Chem. A **6**(29), 14281–14290 (2018).
[151]X. Wang, Y. Zhu, A. Vasileff, Y. Jiao, S. Chen, L. Song, B. Zheng, Y. Zheng, and S.-Z. Qiao, "Strain effect in bimetallic electrocatalysts in the hydrogen evolution reaction," ACS Energy Lett. **3**(5), 1198–1204 (2018).
[152]Y.-C. Shi, S.-S. Chen, J.-J. Feng, X.-X. Lin, W. Wang, and A.-J. Wang, "Dicationic ionic liquid mediated fabrication of Au@Pt nanoparticles supported on reduced graphene oxide with highly catalytic activity for oxygen reduction and hydrogen evolution," Appl. Surf. Sci. **441**(31), 438–447 (2018).
[153]H. Liao, C. Wei, J. Wang, A. Fisher, T. Sritharan, Z. Feng, and Z. J. Xu, "A multisite strategy for enhancing the hydrogen evolution reaction on a nano-Pd surface in alkaline media," Adv. Energy Mater. **7**(21), 1701129 (2017).
[154]T. Bian, B. Xiao, B. Sun, L. Huang, S. Su, Y. Jiang, J. Xiao, A. Yuan, H. Zhang, and D. Yang, "Local epitaxial growth of Au-Rh core-shell star-shaped decahedra: A case for studying electronic and ensemble effects in hydrogen evolution reaction," Appl. Catal. B **263**, 118255 (2020).
[155]Z. Zong, K. Xu, D. Li, Z. Tang, W. He, Z. Liu, X. Wang, and Y. Tian, "Peptide templated Au@ Pd core-shell structures as efficient bi-functional electrocatalysts for both oxygen reduction and hydrogen evolution reactions," J. Catal. **361**, 168–176 (2018).
[156]Y. Shi, T.-T. Zhai, Y. Zhou, W.-X. Xu, D.-R. Yang, F.-B. Wang, and X.-H. Xia, "Atomic level tailoring of the electrocatalytic activity of Au-Pt core-shell nanoparticles with controllable Pt layers toward hydrogen evolution reaction," J. Electroanal. Chem. **819**(15), 442–446 (2018).
[157]X.-X. Lin, A.-J. Wang, K.-M. Fang, J. Yuan, and J.-J. Feng, "One-pot seedless aqueous synthesis of reduced graphene oxide (rGO)-supported core-shell Pt@Pd nanoflowers as advanced catalysts for oxygen reduction and hydrogen evolution," ACS Sustainable Chem. Eng. **5**(10), 8675–8683 (2017).
[158]H. Yang, Z. Tang, K. Wang, W. Wu, Y. Chen, Z. Ding, Z. Liu, and S. Chen, "Co@Pd core-shell nanoparticles embedded in nitrogen-doped porous carbon as dual functional electrocatalysts for both oxygen reduction and hydrogen evolution reactions," J. Colloid Interface Sci. **528**(15), 18–26 (2018).
[159]J. Li, P. Zhou, F. Li, R. Ren, Y. Liu, J. Niu, J. Ma, X. Zhang, M. Tian, and J. Jin, "Ni@ Pd/PEI-rGO stack structures with controllable Pd shell thickness as advanced electrodes for efficient hydrogen evolution," J. Mater. Chem. A **3**(21), 11261–11268 (2015).
[160]H. Lv, Z. Xi, Z. Chen, S. Guo, Y. Yu, W. Zhu, Q. Li, X. Zhang, M. Pan, and G. Lu, "A new core/shell NiAu/Au nanoparticle catalyst with Pt-like activity for hydrogen evolution reaction," J. Am. Chem. Soc. **137**(18), 5859–5862 (2015).
[161]A. Papaderakis, N. Pliatsikas, P. Patsalas, D. Tsiplakides, S. Balomenou, A. Touni, and S. Sotiropoulos, "Hydrogen evolution at Ir-Ni bimetallic deposits prepared by galvanic replacement," J. Electroanal. Chem. **808**(1), 21–27 (2018).
[162]Y. Li, S. Chen, R. Long, H. Ju, Z. Wang, X. Yu, F. Gao, Z. Cai, C. Wang, and Q. Xu, "Near-surface dilution of trace Pd atoms to facilitate Pd-H bond cleavage for giant enhancement of electrocatalytic hydrogen evolution," Nano Energy **34**, 306–312 (2017).
[163]M. Bao, I. S. Amiinu, T. Peng, W. Li, S. Liu, Z. Wang, Z. Pu, D. He, Y. Xiong, and S. Mu, "Surface evolution of PtCu alloy shell over Pd nanocrystals leads to superior hydrogen evolution and oxygen reduction reactions," ACS Energy Lett. **3**(4), 940–945 (2018).
[164]J. Fan, K. Qi, L. Zhang, H. Zhang, S. Yu, and X. Cui, "Engineering Pt/Pd interfacial electronic structures for highly efficient hydrogen evolution and alcohol oxidation," ACS Appl. Mater. Interfaces **9**(21), 18008–18014 (2017).
[165]U. Joshi, S. Malkhandi, Y. Ren, T. L. Tan, S. Y. Chiam, and B. S. Yeo, "Ruthenium-tungsten composite catalyst for the efficient and contamination-resistant electrochemical evolution of hydrogen," ACS Appl. Mater. Interfaces **10**(7), 6354–6360 (2018).
[166]J. Ding, Q. Shao, Y. Feng, and X. Huang, "Ruthenium-nickel sandwiched nanoplates for efficient water splitting electrocatalysis," Nano Energy **47**, 1–7 (2018).
[167]Y. Zhang, J. Shi, G. Han, M. Li, Q. Ji, D. Ma, Y. Zhang, C. Li, X. Lang, and Y. Zhang, "Chemical vapor deposition of monolayer WS_2 nanosheets on Au foils toward direct application in hydrogen evolution," Nano Res. **8**(9), 2881–2890 (2015).
[168]S. Zhao, R. Jin, Y. Song, H. Zhang, S. D. House, J. C. Yang, and R. Jin, "Atomically precise gold nanoclusters accelerate hydrogen evolution over MoS_2 nanosheets: The dual interfacial effect," Small **13**(43), 1701519 (2017).
[169]K. Zhou, Q. Zhang, Z. Wang, C. Wang, C. Han, X. Ke, Z. Zheng, H. Wang, J. Liu, and H. Yan, "A Setaria-inflorescence-structured catalyst based on nickel-cobalt wrapped silver nanowire conductive networks for highly efficient hydrogen evolution," J. Mater. Chem. A **7**(46), 26566–26573 (2019).
[170]X. Ding, Y. Xia, Q. Li, S. Dong, X. Jiao, and D. Chen, "Interface engineering of $Co(OH)_2$/Ag/FeP hierarchical superstructure as efficient and robust electrocatalyst for overall water splitting," ACS Appl. Mater. Interfaces **11**(8), 7936–7945 (2019).
[171]J. Joo, H. Jin, A. Oh, B. Kim, J. Lee, H. Baik, S. H. Joo, and K. Lee, "An IrRu alloy nanocactus on $Cu_{2-x}S@IrS_y$ as a highly efficient bifunctional electrocatalyst toward overall water splitting in acidic electrolytes," J. Mater. Chem. A **6**(33), 16130–16138 (2018).
[172]Z. Deng, J. Wang, Y. Nie, and Z. Wei, "Tuning the interface of Ni@$Ni(OH)_2$/Pd/rGO catalyst to enhance hydrogen evolution activity and stability," J. Power Sources **352**(1), 26–33 (2017).
[173]C. Ray, S. Dutta, Y. Negishi, and T. Pal, "A new stable Pd-Mn_3O_4 nanocomposite as an efficient electrocatalyst for the hydrogen evolution reaction," Chem. Commun. **52**(36), 6095–6098 (2016).
[174]L. Zhang, Z.-J. Zhao, M. N. Banis, L. Li, Y. Zhao, Z. Song, Z. Wang, T.-K. Sham, R. Li, and M. Zheng, "Selective atomic layer deposition of RuO_x catalysts on shape-controlled Pd nanocrystals with significantly enhanced hydrogen evolution activity," J. Mater. Chem. A **6**(47), 24397–24406 (2018).
[175]S. Liu, Q. Liu, Y. Lv, B. Chen, Q. Zhou, L. Wang, Q. Zheng, C. Che, and C. Chen, "Ru decorated with NiCoP: An efficient and durable hydrogen

evolution reaction electrocatalyst in both acidic and alkaline conditions," Chem. Commun. **53**(98), 13153–13156 (2017).
[176]D. Yoon, J. Lee, B. Seo, B. Kim, H. Baik, S. H. Joo, and K. Lee, "Cactus-like hollow Cu_{2-x} S@Ru nanoplates as excellent and robust electrocatalysts for the alkaline hydrogen evolution reaction," Small **13**(29), 1700052 (2017).
[177]Q.-Q. Chen, X. Yang, C.-C. Hou, K. Li, and Y. Chen, "Inlay of ultrafine Ru nanoparticles into a self-supported $Ni(OH)_2$ nanoarray for hydrogen evolution with low overpotential and enhanced kinetics," J. Mater. Chem. A **7**(18), 11062–11068 (2019).
[178]J. Xu, T. Liu, J. Li, B. Li, Y. Liu, B. Zhang, D. Xiong, I. Amorim, W. Li, and L. Liu, "Boosting the hydrogen evolution performance of ruthenium clusters through synergistic coupling with cobalt phosphide," Energy Environ. Sci. **11**(7), 1819–1827 (2018).
[179]Y. Liu, S. Liu, Y. Wang, Q. Zhang, L. Gu, S. Zhao, D. Xu, Y. Li, J. Bao, and Z. Dai, "Ru modulation effects in the synthesis of unique rod-like Ni@Ni_2P-Ru heterostructures and their remarkable electrocatalytic hydrogen evolution performance," J. Am. Chem. Soc. **140**(8), 2731–2734 (2018).
[180]J. Yu, G. Li, H. Liu, L. Zhao, A. Wang, Z. Liu, H. Li, H. Liu, Y. Hu, and W. Zhou, "Ru-Ru_2P@NPC and NPC@RuO_2 synthesized via environment-friendly and solid-phase phosphating process by saccharomycetes as N/P sources and carbon template for overall water splitting in acid electrolyte," Adv. Funct. Mater. **29**(22), 1901154 (2019).
[181]Y. Liu, X. Lu, Z. Che, C. Zhang, M. Han, J. Bao, and Z. Dai, "Amorphous $Y(OH)_3$-promoted Ru/$Y(OH)_3$ nanohybrids with high durability for electrocatalytic hydrogen evolution in alkaline media," Chem. Commun. **54**(86), 12202–12205 (2018).
[182]L. Wang, Q. Zhou, Z. Pu, Q. Zhang, X. Mu, H. Jing, S. Liu, C. Chen, and S. Mu, "Surface reconstruction engineering of cobalt phosphides by Ru inducement to form hollow Ru-RuP_x-Co_xP pre-electrocatalysts with accelerated oxygen evolution reaction," Nano Energy **53**, 270–276 (2018).
[183]Z. Liu, Z. Li, J. Li, J. Xiong, S. Zhou, J. Liang, W. Cai, C. Wang, Z. Yang, and H. Cheng, "Engineering of Ru/Ru_2P interfaces superior to Pt active sites for catalysis of the alkaline hydrogen evolution reaction," J. Mater. Chem. A **7**(10), 5621–5625 (2019).
[184]Y. Shi, J. Wang, C. Wang, T.-T. Zhai, W.-J. Bao, J.-J. Xu, X.-H. Xia, and H.-Y. Chen, "Hot electron of Au nanorods activates the electrocatalysis of hydrogen evolution on MoS_2 nanosheets," J. Am. Chem. Soc. **137**(23), 7365–7370 (2015).
[185]J. Zhang, T. Wang, L. Liu, K. Du, W. Liu, Z. Zhu, and M. Li, "Molybdenum disulfide and Au ultrasmall nanohybrids as highly active electrocatalysts for hydrogen evolution reaction," J. Mater. Chem. A **5**(8), 4122–4128 (2017).
[186]Y. Li, M. B. Majewski, S. M. Islam, S. Hao, A. A. Murthy, J. G. DiStefano, E. D. Hanson, Y. Xu, C. Wolverton, and M. G. Kanatzidis, "Morphological engineering of winged Au@MoS_2 heterostructures for electrocatalytic hydrogen evolution," Nano Lett. **18**(11), 7104–7110 (2018).
[187]B. Shang, X. Cui, L. Jiao, K. Qi, Y. Wang, J. Fan, Y. Yue, H. Wang, Q. Bao, and X. Fan, "Lattice-mismatch-induced ultrastable 1T-phase MoS_2-Pd/Au for plasmon-enhanced hydrogen evolution," Nano Lett. **19**(5), 2758–2764 (2019).
[188]Z. Liu, X. Zhang, Y. Gong, Q. Lu, Z. Zhang, H. Cheng, Q. Ma, J. Chen, M. Zhao, and B. Chen, "Synthesis of MoX_2 (X = Se or S) monolayers with high-concentration 1T′ phase on 4H/fcc-Au nanorods for hydrogen evolution," Nano Res. **12**(6), 1301–1305 (2019).
[189]F. Scaglione, Y. Xue, F. Celegato, P. Rizzi, and L. Battezzati, "Amorphous molybdenum sulphide@nanoporous gold as catalyst for hydrogen evolution reaction in acidic environment," J. Mater. Sci. **53**(17), 12388–12398 (2018).
[190]S. Wei, X. Cui, Y. Xu, B. Shang, Q. Zhang, L. Gu, X. Fan, L. Zheng, C. Hou, and H. Huang, "Iridium-triggered phase transition of MoS_2 nanosheets boosts overall water splitting in alkaline media," ACS Energy Lett. **4**(1), 368–374 (2019).
[191]S. Liu, M. Li, C. Wang, P. Jiang, L. Hu, and Q. Chen, "Tuning the electronic structure of Se via constructing Rh-$MoSe_2$ nanocomposite to generate high-performance electrocatalysis for hydrogen evolution reaction," ACS Sustainable Chem. Eng. **6**(7), 9137–9144 (2018).
[192]Y. Cheng, S. Lu, F. Liao, L. Liu, Y. Li, and M. Shao, "Rh-MoS_2 nanocomposite catalysts with Pt-like activity for hydrogen evolution reaction," Adv. Funct. Mater. **27**(23), 1700359 (2017).
[193]M. D. Sharma, C. Mahala, and M. Basu, "Nanosheets of $MoSe_2$@ M (M = Pd and Rh) function as widespread pH tolerable hydrogen evolution catalyst," J. Colloid Interface Sci. **534**(15), 131–141 (2019).
[194]J. Liu, Y. Zheng, D. Zhu, A. Vasileff, T. Ling, and S.-Z. Qiao, "Identification of pH-dependent synergy on Ru/MoS_2 interface: A comparison of alkaline and acidic hydrogen evolution," Nanoscale **9**(43), 16616–16621 (2017).
[195]D. Wang, Q. Li, C. Han, Z. Xing, and X. Yang, "Single-atom ruthenium based catalyst for enhanced hydrogen evolution," Appl. Catal. B **249**(15), 91–97 (2019).
[196]A. Morozan, V. Goellner, A. Zitolo, E. Fonda, B. Donnadieu, D. Jones, and F. Jaouen, "Synergy between molybdenum nitride and gold leading to platinum-like activity for hydrogen evolution," Phys. Chem. Chem. Phys. **17**(6), 4047–4053 (2015).
[197]G. Sheng, J. Chen, Y. Li, H. Ye, Z. Hu, X.-Z. Fu, R. Sun, W. Huang, and C.-P. Wong, "Flowerlike $NiCo_2S_4$ hollow sub-microspheres with mesoporous nanoshells support Pd nanoparticles for enhanced hydrogen evolution reaction electrocatalysis in both acidic and alkaline conditions," ACS Appl. Mater. Interfaces **10**(26), 22248–22256 (2018).
[198]C. Song, Z. Zhao, X. Sun, Y. Zhou, Y. Wang, and D. Wang, "In situ growth of Ag nanodots decorated Cu_2O porous nanobelts networks on copper foam for efficient HER electrocatalysis," Small **15**(29), 1804268 (2019).
[199]J. Ma, Z. Ma, B. Liu, S. Wang, R. Ma, and C. Wang, "Composition of Ag-WO_3 core-shell nanostructures as efficient electrocatalysts for hydrogen evolution reaction," J. Solid State Chem. **271**, 246–252 (2019).
[200]Y. Yao, X.-K. Gu, D. He, Z. Li, W. Liu, Q. Xu, T. Yao, Y. Lin, H.-J. Wang, and C. Zhao, "Engineering the electronic structure of submonolayer Pt on intermetallic Pd_3Pb via charge transfer boosts the hydrogen evolution reaction," J. Am. Chem. Soc. **141**(51), 19964–19968 (2019).
[201]U. K. Sultana, J. D. Riches, and A. P. O'Mullane, "Gold doping in a layered Co-Ni hydroxide system via galvanic replacement for overall electrochemical water splitting," Adv. Funct. Mater. **28**(43), 1804361 (2018).
[202]B. Zhang, H. Zhu, M. Zou, X. Liu, H. Yang, M. Zhang, W. Wu, J. Yao, and M. Du, "Design and fabrication of size-controlled Pt-Au bimetallic alloy nanostructure in carbon nanofibers: A bifunctional material for biosensors and the hydrogen evolution reaction," J. Mater. Sci. **52**(13), 8207–8218 (2017).
[203]F. Li, G.-F. Han, H.-J. Noh, J.-P. Jeon, I. Ahmad, S. Chen, C. Yang, Y. Bu, Z. Fu, and Y. Lu, "Balancing hydrogen adsorption/desorption by orbital modulation for efficient hydrogen evolution catalysis," Nat. Commun. **10**, 4060 (2019).
[204]D. Bernsmeier, L. Chuenchom, B. Paul, S. Rümmler, B. Smarsly, and R. Kraehnert, "Highly active binder-free catalytic coatings for heterogeneous catalysis and electrocatalysis: Pd on mesoporous carbon and its application in butadiene hydrogenation and hydrogen evolution," ACS Catal. **6**(12), 8255–8263 (2016). (
[205]S. Bai, C. Wang, M. Deng, M. Gong, Y. Bai, J. Jiang, and Y. Xiong, "Surface polarization matters: Enhancing the hydrogen-evolution reaction by shrinking Pt shells in Pt-Pd-graphene stack structures," Angew. Chem., Int. Ed. **53**(45), 12120–12124 (2014).
[206]Q.-L. Zhu, F.-Z. Song, Q.-J. Wang, N. Tsumori, Y. Himeda, T. Autrey, and Q. Xu, "A solvent-switched in situ confinement approach for immobilizing highly-active ultrafine palladium nanoparticles: Boosting catalytic hydrogen evolution," J. Mater. Chem. A **6**(14), 5544–5549 (2018).
[207]R. Ding, Q. Chen, Q. Luo, L. Zhou, Y. Wang, Y. Zhang, and G. Fan, "Salt template-assisted in situ construction of Ru nanoclusters and porous carbon: Excellent catalysts toward hydrogen evolution, ammonia-borane hydrolysis, and 4-nitrophenol reduction," Green Chem. **22**(3), 835–842 (2020).
[208]J. Liu, G. Ding, J. Yu, X. Liu, X. Zhang, J. Guo, J. Zhang, W. Ren, and R. Che, "Visualizing spatial potential and charge distribution in Ru/N-doped carbon electrocatalysts for superior hydrogen evolution reaction," J. Mater. Chem. A **7**(30), 18072–18080 (2019).
[209]Q. Hu, G. Li, X. Huang, Z. Wang, H. Yang, Q. Zhang, J. Liu, and C. He, "Electronic structure engineering of single atomic Ru by Ru nanoparticles to enable enhanced activity for alkaline water reduction," J. Mater. Chem. A **7**(33), 19531–19538 (2019).
[210]Y. Li, J. Abbott, Y. Sun, J. Sun, Y. Du, X. Han, G. Wu, and P. Xu, "Ru nanoassembly catalysts for hydrogen evolution and oxidation reactions in electrolytes at various pH values," Appl. Catal. B **258**(5), 117952 (2019).

[211]B. Jiang, Y. Sun, F. Liao, W. Shen, H. Lin, H. Wang, and M. Shao, "Rh-Ag-Si ternary composites: Highly active hydrogen evolution electrocatalysts over Pt-Ag-Si," J. Mater. Chem. A **5**(4), 1623–1628 (2017).
[212]L. Zhu, H. Lin, Y. Li, F. Liao, Y. Lifshitz, M. Sheng, S.-T. Lee, and M. Shao, "A rhodium/silicon co-electrocatalyst design concept to surpass platinum hydrogen evolution activity at high overpotentials," Nat. Commun. **7**, 12272 (2016).
[213]B. Jiang, L. Yang, F. Liao, M. Sheng, H. Zhao, H. Lin, and M. Shao, "A stepwise-designed Rh-Au-Si nanocomposite that surpasses Pt/C hydrogen evolution activity at high overpotentials," Nano Res. **10**(5), 1749–1755 (2017).
[214]M. Sheng, B. Jiang, B. Wu, F. Liao, X. Fan, H. Lin, Y. Li, Y. Lifshitz, S.-T. Lee, and M. Shao, "Approaching the volcano top: Iridium/silicon nanocomposites as efficient electrocatalysts for the hydrogen evolution reaction," ACS Nano **13**(3), 2786–2794 (2019).
[215]V. Pérez-Herranz, R. Medina, P. Taymans, C. González-Buch, E. Ortega, G. Sánchez-Loredo, and G. J. Labrada-Delgado, "Modification of porous nickel electrodes with silver nanoparticles for hydrogen production," J. Electroanal. Chem. **808**(1), 420–426 (2018).
[216]Y. Liang, C. Csoklich, D. McLaughlin, O. Schneider, and A. S. Bandarenka, "Revealing active sites for hydrogen evolution at Pt and Pd atomic layers on Au surfaces," ACS Appl. Mater. Interfaces **11**(13), 12476–12480 (2019).
[217]W. Zhou, T. Xiong, C. Shi, J. Zhou, K. Zhou, N. Zhu, L. Li, Z. Tang, and S. Chen, "Bioreduction of precious metals by microorganism: Efficient Gold@N-doped carbon electrocatalysts for the hydrogen evolution reaction," Angew. Chem., Int. Ed. **55**(29), 8416–8420 (2016).
[218]J. Zhang, G. Wang, Z. Liao, P. Zhang, F. Wang, X. Zhuang, E. Zschech, and X. Feng, "Iridium nanoparticles anchored on 3D graphite foam as a bifunctional electrocatalyst for excellent overall water splitting in acidic solution," Nano Energy **40**, 27–33 (2017).
[219]J. Mahmood, M. A. R. Anjum, S. H. Shin, I. Ahmad, H. J. Noh, S. J. Kim, H. Y. Jeong, J. S. Lee, and J. B. Baek, "Encapsulating iridium nanoparticles inside a 3D cage-like organic network as an efficient and durable catalyst for the hydrogen evolution reaction," Adv. Mater. **30**(52), 1805606 (2018).
[220]H. Wang, M. Ming, M. Hu, C. Xu, Y. Wang, Y. Zhang, D. Gao, J. Bi, G. Fan, and J.-S. Hu, "Size and electronic modulation of iridium nanoparticles on nitrogen-functionalized carbon toward advanced electrocatalysts for alkaline water splitting," ACS Appl. Mater. Interfaces **10**(26), 22340–22347 (2018).
[221]S. B. Roy, K. Akbar, J. H. Jeon, S.-K. Jerng, L. Truong, K. Kim, Y. Yi, and S.-H. Chun, "Iridium on vertical graphene as an all-round catalyst for robust water splitting reactions," J. Mater. Chem. A **7**(36), 20590–20596 (2019).
[222]S. Zhou, X. Chen, P. Yu, F. Gao, and L. Mao, "Nitrogen-doped carbon nanotubes as an excellent substrate for electroless deposition of Pd nanoparticles with a high efficiency toward the hydrogen evolution reaction," Electrochem. Commun. **90**, 91–95 (2018).
[223]H. Yu, Y. Xue, B. Huang, L. Hui, C. Zhang, Y. Fang, Y. Liu, Y. Zhao, Y. Li, and H. Liu, "Ultrathin nanosheet of graphdiyne-supported palladium atom catalyst for efficient hydrogen production," iScience **11**(25), 31–41 (2019).
[224]K. Guo, L. J. Rowland, L. H. Isherwood, G. Glodan, and A. Baidak, "Photon-induced synthesis of ultrafine metal nanoparticles on graphene as electrocatalysts: Impact of functionalization and doping," J. Mater. Chem. A **8**(2), 714–723 (2020).
[225]J. Bai, S.-H. Xing, Y.-Y. Zhu, J.-X. Jiang, J.-H. Zeng, and Y. Chen, "Polyallylamine-Rh nanosheet nanoassemblies-carbon nanotubes organic-inorganic nanohybrids: A electrocatalyst superior to Pt for the hydrogen evolution reaction," J. Power Sources **385**(1), 32–38 (2018).
[226]W. Shen, L. Ge, Y. Sun, F. Liao, L. Xu, Q. Dang, Z. Kang, and M. Shao, "Rhodium nanoparticles/F-doped graphene composites as multifunctional electrocatalyst superior to Pt/C for hydrogen evolution and formic acid oxidation reaction," ACS Appl. Mater. Interfaces **10**(39), 33153–33161 (2018).
[227]L. Bai, Z. Duan, X. Wen, R. Si, Q. Zhang, and J. Guan, "Highly dispersed ruthenium-based multifunctional electrocatalyst," ACS Catal. **9**(11), 9897–9904 (2019).
[228]M. Li, H. Wang, W. Zhu, W. Li, C. Wang, and X. Lu, "RuNi nanoparticles embedded in N-doped carbon nanofibers as a robust bifunctional catalyst for efficient overall water splitting," Adv. Sci. **7**(2), 1901833 (2020).
[229]Y. Liu, Y. Yang, Z. Peng, Z. Liu, Z. Chen, L. Shang, S. Lu, and T. Zhang, "Self-crosslinking carbon dots loaded ruthenium dots as an efficient and super-stable hydrogen production electrocatalyst at all pH values," Nano Energy **65**, 104023 (2019).
[230]T. Bhowmik, M. K. Kundu, and S. Barman, "Palladium nanoparticle-graphitic carbon nitride porous synergistic catalyst for hydrogen evolution/oxidation reactions over a broad range of pH and correlation of its catalytic activity with measured hydrogen binding energy," ACS Catal. **6**(3), 1929–1941 (2016).
[231]T. Bhowmik, M. K. Kundu, and S. Barman, "Growth of one-dimensional RuO_2 nanowires on g-carbon nitride: An active and stable bifunctional electrocatalyst for hydrogen and oxygen evolution reactions at all pH values," ACS Appl. Mater. Interfaces **8**(42), 28678–28688 (2016).
[232]W. Li, Y. Liu, M. Wu, X. Feng, S. A. Redfern, Y. Shang, X. Yong, T. Feng, K. Wu, and Z. Liu, "Carbon-quantum-dots-loaded ruthenium nanoparticles as an efficient electrocatalyst for hydrogen production in alkaline media," Adv. Mater. **30**(31), 1800676 (2018).
[233]J. Mahmood, F. Li, S.-M. Jung, M. S. Okyay, I. Ahmad, S.-J. Kim, N. Park, H. Y. Jeong, and J.-B. Baek, "An efficient and pH-universal ruthenium-based catalyst for the hydrogen evolution reaction," Nat. Nanotechnol. **12**(5), 441–446 (2017).
[234]B. Lu, L. Guo, F. Wu, Y. Peng, J. E. Lu, T. J. Smart, N. Wang, Y. Z. Finfrock, D. Morris, and P. Zhang, "Ruthenium atomically dispersed in carbon outperforms platinum toward hydrogen evolution in alkaline media," Nat. Commun. **10**, 631 (2019).
[235]T. Qiu, Z. Liang, W. Guo, S. Gao, C. Qu, H. Tabassum, H. Zhang, B. Zhu, R. Zou, and Y. Shao-Horn, "Highly exposed ruthenium-based electrocatalysts from bimetallic metal-organic frameworks for overall water splitting," Nano Energy **58**, 1–10 (2019).
[236]S. Ye, F. Luo, T. Xu, P. Zhang, H. Shi, S. Qin, J. Wu, C. He, X. Ouyang, and Q. Zhang, "Boosting the alkaline hydrogen evolution of Ru nanoclusters anchored on B/N-doped graphene by accelerating water dissociation," Nano Energy **68**, 104301 (2020).
[237]M. K. Kundu, T. Bhowmik, and S. Barman, "Gold aerogel supported on graphitic carbon nitride: An efficient electrocatalyst for oxygen reduction reaction and hydrogen evolution reaction," J. Mater. Chem. A **3**(46), 23120–23135 (2015).
[238]Y. Peng, B. Lu, L. Chen, N. Wang, J. E. Lu, Y. Ping, and S. Chen, "Hydrogen evolution reaction catalyzed by ruthenium ion-complexed graphitic carbon nitride nanosheets," J. Mater. Chem. A **5**(34), 18261–18269 (2017).
[239]R. Nazir, P. Fageria, M. Basu, and S. Pande, "Decoration of carbon nitride surface with bimetallic nanoparticles (Ag/Pt, Ag/Pd, and Ag/Au) via galvanic exchange for hydrogen evolution reaction," J. Phys. Chem. C **121**(36), 19548–19558 (2017).
[240]L. Zhu, Q. Cai, F. Liao, M. Sheng, B. Wu, and M. Shao, "Ru-modified silicon nanowires as electrocatalysts for hydrogen evolution reaction," Electrochem. Commun. **52**, 29–33 (2015).
[241]F. Liao, B. Jiang, W. Shen, Y. Chen, Y. Li, Y. Shen, K. Yin, and M. Shao, "Ir-Au bimetallic nanoparticle modified silicon nanowires with ultralow content of Ir for hydrogen evolution reaction," ChemCatChem **11**(8), 2126–2130 (2019).
[242]K. Yin, Y. Cheng, B. Jiang, F. Liao, and M. Shao, "Palladium-silicon nanocomposites as a stable electrocatalyst for hydrogen evolution reaction," J. Colloid Interface Sci. **522**(15), 242–248 (2018).
[243]S. Pandelov and U. Stimming, "Reactivity of monolayers and nano-islands of palladium on Au (1 1 1) with respect to proton reduction," Electrochim. Acta **52**(18), 5548–5555 (2007).
[244]P. J. Schäfer and L. A. Kibler, "Incorporation of Pd into Au (111): Enhanced electrocatalytic activity for the hydrogen evolution reaction," Phys. Chem. Chem. Phys. **12**(46), 15225–15230 (2010).
[245]M. Smiljanić, I. Srejić, B. Grgur, Z. Rakočević, and S. Štrbac, "Catalysis of hydrogen evolution on Au (111) modified by spontaneously deposited Pd nanoislands," Electrocatalysis **3**, 369–375 (2012).
[246]S. Strbac, I. Srejic, and Z. Rakocevic, "Electrocatalysis of hydrogen evolution reaction on Au (111) by spontaneously deposited iridium in acid solution," J. Electrochem. Soc. **165**(15), J3335–J3341 (2018).
[247]P. Quaino, E. Santos, H. Wolfschmidt, M. Montero, and U. Stimming, "Theory meets experiment: Electrocatalysis of hydrogen oxidation/evolution at Pd-Au nanostructures," Catal. Today **177**(1), 55–63 (2011).

[248]P. Quaino and E. Santos, "Hydrogen evolution reaction on palladium multilayers deposited on Au (111): A theoretical approach," Langmuir **31**(2), 858–867 (2015).
[249]G. Soldano, E. N. Schulz, D. R. Salinas, E. Santos, and W. Schmickler, "Hydrogen electrocatalysis on overlayers of rhodium over gold and palladium substrates-more active than platinum?," Phys. Chem. Chem. Phys. **13**(36), 16437–16443 (2011).
[250]M. Smiljanić, I. Srejić, B. Grgur, Z. Rakočević, and S. Štrbac, "Hydrogen evolution on Au (111) catalyzed by rhodium nanoislands," Electrochem. Commun. **28**, 37–39 (2013).
[251]S. Štrbac, M. Smiljanić, and Z. Rakočević, "Spontaneously deposited Rh on Au (111) observed by AFM and XPS: Electrocatalysis of hydrogen evolution," J. Electrochem. Soc. **163**(12), D3027 (2016).
[252]M. Smiljanic, Z. Rakocevic, A. Maksic, and S. Strbac, "Hydrogen evolution reaction on platinum catalyzed by palladium and rhodium nanoislands," Electrochim. Acta **117**(20), 336–343 (2014).
[253]S. Štrbac, M. Smiljanić, T. Wakelin, J. Potočnik, and Z. Rakočević, "Hydrogen evolution reaction on bimetallic Ir/Pt (poly) electrodes in alkaline solution," Electrochim. Acta **306**(20), 18–27 (2019).
[254]Y. Zheng, Y. Jiao, Y. Zhu, L. H. Li, Y. Han, Y. Chen, M. Jaroniec, and S.-Z. Qiao, "High electrocatalytic hydrogen evolution activity of an anomalous ruthenium catalyst," J. Am. Chem. Soc. **138**(49), 16174–16181 (2016).
[255]Y. Yao, D. S. He, Y. Lin, X. Feng, X. Wang, P. Yin, X. Hong, G. Zhou, Y. Wu, and Y. Li, "Modulating fcc and hcp ruthenium on the surface of palladium-copper alloy through tunable lattice mismatch," Angew. Chem., Int. Ed. **128**(18), 5591–5595 (2016).
[256]W.-Z. Li, J.-X. Liu, J. Gu, W. Zhou, S.-Y. Yao, R. Si, Y. Guo, H.-Y. Su, C.-H. Yan, and W.-X. Li, "Chemical insights into the design and development of face-centered cubic ruthenium catalysts for Fischer–Tropsch synthesis," J. Am. Chem. Soc. **139**(6), 2267–2276 (2017).
[257]S. Sarkar and S. C. Peter, "An overview on Pd-based electrocatalysts for the hydrogen evolution reaction," Inorg. Chem. Front. **5**(9), 2060–2080 (2018).
[258]A. Zalineeva, S. Baranton, C. Coutanceau, and G. Jerkiewicz, "Octahedral palladium nanoparticles as excellent hosts for electrochemically adsorbed and absorbed hydrogen," Sci. Adv. **3**(2), e1600542 (2017).
[259]X. Huang, S. Li, Y. Huang, S. Wu, X. Zhou, S. Li, C. L. Gan, F. Boey, C. A. Mirkin, and H. Zhang, "Synthesis of hexagonal close-packed gold nanostructures," Nat. Commun. **2**, 292 (2011).
[260]Y. Guo, T. Park, J. W. Yi, J. Henzie, J. Kim, Z. Wang, B. Jiang, Y. Bando, Y. Sugahara, and J. Tang, "Nanoarchitectonics for transition-metal-sulfide-based electrocatalysts for water splitting," Adv. Mater. **31**(17), 1807134 (2019).
[261]J. Yu, Y. Zhong, X. Wu, J. Sunarso, M. Ni, W. Zhou, and Z. Shao, "Bifunctionality from synergy: CoP nanoparticles embedded in amorphous CoOx nanoplates with heterostructures for highly efficient water electrolysis," Adv. Sci. **5**(9), 1800514 (2018).
[262]F. Yang, L. Fu, G. Cheng, S. Chen, and W. Luo, "Ir-oriented nanocrystalline assemblies with high activity for hydrogen oxidation/evolution reactions in an alkaline electrolyte," J. Mater. Chem. A **5**(44), 22959–22963 (2017).
[263]V. Ramalingam, P. Varadhan, H. C. Fu, H. Kim, D. Zhang, S. Chen, L. Song, D. Ma, Y. Wang, and H. N. Alshareef, "Heteroatom-mediated interactions between ruthenium single atoms and an MXene support for efficient hydrogen evolution," Adv. Mater. **31**(48), 1903841 (2019).
[264]H. You, D. Wu, Z.-N. Chen, F. Sun, H. Zhang, Z. Chen, M. Cao, W. Zhuang, and R. Cao, "Highly active and stable water splitting in acidic media using a bifunctional iridium/cucurbit, [6] uril catalyst," ACS Energy Lett. **4**(6), 1301–1307 (2019).
[265]W. H. Lai, L. F. Zhang, W. B. Hua, S. Indris, Z. C. Yan, Z. Hu, B. Zhang, Y. Liu, L. Wang, and M. Liu, "General π-electron-assisted strategy for Ir, Pt, Ru, Pd, Fe, Ni single-atom electrocatalysts with bifunctional active sites for highly efficient water splitting," Angew. Chem., Int. Ed. **131**(34), 11994–11999 (2019).
[266]Y. Zhu, W. Zhou, Y. Zhong, Y. Bu, X. Chen, Q. Zhong, M. Liu, and Z. Shao, "A perovskite nanorod as bifunctional electrocatalyst for overall water splitting," Adv. Energy Mater. **7**(8), 1602122 (2017).
[267]N. Han, K. R. Yang, Z. Lu, Y. Li, W. Xu, T. Gao, Z. Cai, Y. Zhang, V. S. Batista, W. Liu, and X. Sun, "Nitrogen-doped tungsten carbide nanoarray as an efficient bifunctional electrocatalyst for water splitting in acid," Nat. Commun. **9**, 924 (2018).
[268]C. Guan, H. Wu, W. Ren, C. Yang, X. Liu, X. Ouyang, Z. Song, Y. Zhang, S. J. Pennycook, C. Cheng, and J. Wang, "Metal–organic framework-derived integrated nanoarrays for overall water splitting," J. Mater. Chem. A **6**, 9009–9018 (2018).
[269]L. Najafi, S. Bellani, R. Oropesa-Nunez, M. Prato, B. Martín-García, R. Brescia, and F. Bonaccorso, "Carbon nanotube-supported $MoSe_2$ holey flake: Mo_2C ball hybrids for bifunctional pH-universal water splitting," ACS Nano **13**(3), 3162–3176 (2019).
[270]Z. Liu, H. Tan, D. Liu, X. Liu, J. Xin, J. Xie, M. Zhao, L. Song, L. Dai, and H. Liu, "Promotion of overall water splitting activity over a wide pH range by interfacial electrical effects of metallic NiCo-nitrides nanoparticle/$NiCo_2O_4$ nanoflake/graphite fibers," Adv. Sci. **6**(5), 1801829 (2019).
[271]Z.-H. Xue, H. Su, Q.-Y. Yu, B. Zhang, H.-H. Wang, X.-H. Li, and J.-S. Chen, "Janus Co/CoP nanoparticles as efficient Mott–Schottky electrocatalysts for overall water splitting in wide pH range," Adv. Energy Mater. **7**(12), 1602355 (2017).
[272]L. Wang, X. Duan, X. Liu, J. Gu, R. Si, Y. Qiu, Y. Qiu, D. Shi, F. Chen, X. Sun, J. Lin, and J. Sun, "Atomically dispersed Mo supported on metallic Co_9S_8 nanoflakes as an advanced noble-metal-free bifunctional water splitting catalyst working in universal pH conditions," Adv. Energy Mater. **10**(4), 1903137 (2020).
[273]L. J. Yang, Y. Q. Deng, X. F. Zhang, H. Liu, and W. J. Zhou, "$MoSe_2$ nanosheet/MoO_2 nanobelt/carbon nanotube membrane as flexible and multifunctional electrodes for full water splitting in acidic electrolyte," Nanoscale **10**, 9268–9275 (2018).
[274]J. Liu, D. Zhu, T. Ling, A. Vasileff, and S.-Z. Qiao, "S-$NiFe_2O_4$ ultra-small nanoparticle built nanosheets for efficient water splitting in alkaline and neutral pH," Nano Energy **40**, 264–273 (2017).
[275]R.-Q. Li, P. Hu, M. Miao, Y. Li, X.-F. Jiang, Q. Wu, Z. Meng, Z. Hu, Y. Bando, and X.-B. Wang, "CoO-modified Co_4N as a heterostructured electrocatalyst for highly efficient overall water splitting in neutral media," J. Mater. Chem. A **6**, 24767–24772 (2018).
[276]L. Tao, M. Huang, S. Guo, Q. Wang, M. Lia, X. Xiao, G. Cao, Y. Shao, Y. Shen, Y. Fu, and M. Wang, "Surface modification of $NiCo_2Te_4$ nanoclusters: A highly efficient electrocatalyst for overall water-splitting in neutral solution," Appl. Catal. B **254**(5), 424–431 (2019).
[277]C. Xing, Y. Xue, B. Huang, H. Yu, L. Hui, Y. Fang, Y. Liu, Y. Zhao, Z. Li, and Y. Li, "Fluorographdiyne: A metal-free catalyst for applications in water reduction and oxidation," Angew. Chem., Int. Ed. **131**(39), 14035–14041 (2019).
[278]Y. Yang, H. Yao, Z. Yu, S. M. Islam, H. He, M. Yuan, Y. Yue, K. Xu, W. Hao, G. Sun, H. Li, S. Ma, P. Zapol, and M. G. Kanatzidis, "Hierarchical nanoassembly of $MoS_2/Co_9S_8/Ni_3S_2$/Ni as a highly efficient electrocatalyst for overall water splitting in a wide pH range," J. Am. Chem. Soc. **141**(26), 10417–10430 (2019).
[279]L. Yan, B. Zhang, J. Zhu, Y. Li, P. Tsiakaras, and P. K. Shen, "Electronic modulation of cobalt phosphide nanosheet arrays via copper doping for highly efficient neutral-pH overall water splitting," Appl. Catal. B **265**(15), 118555 (2020).